One Space Park
Redondo Beach, CA 90278

TRW

HIGH FREQUENCY PLASMA GENERATORS

FOR ION THRUSTERS

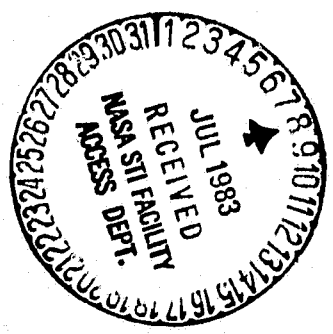

NASA #CR-167957

HIGH FREQUENCY PLASMA GENERATORS FOR ION THRUSTERS

PREPARED FOR

LEWIS RESEARCH CENTER
NATIONAL AERONAUTICS AND SPACE ADMINISTRATION
CONTRACT NO. NAS3-22473

BY

WILLIAM F. DIVERGILIO
HEINZ GOEDE
VERRYL V. FOSNIGHT

INTERIM REPORT
NOVEMBER 1981

TRW
DEFENSE AND SPACE SYSTEMS GROUP

1. Report No.	2. Government Accession No.	3. Recipient's Catalog No.
NASA CR-167957		36208-6031-UT-00

4. Title and Subtitle	5. Report Date
High Frequency Plasma Generators for Ion Thrusters	11/18/81
	6. Performing Organization Code

7. Author(s)	8. Performing Organization Report No.
William F. DiVergilio, Heinz Goede, and Verryl V. Fosnight	
	10. Work Unit No.

9. Performing Organization Name and Address	11. Contract or Grant No.
TRW One Space Park Redondo Beach, California 90278	NAS3-22473
	13. Type of Report and Period Covered
12. Sponsoring Agency Name and Address NASA Lewis Research Center Cleveland, Ohio	Interim, Sep 1980-Nov 1981
	14. Sponsoring Agency Code

15. Supplementary Notes	
NASA Contract Monitor Shigeo Nakanishi NASA Lewis Research Center	TRW Program Manager Gene Komatsu One Space Park Redondo Beach, California 90278

16. Abstract The results of a one year program to experimentally adapt two new types of high frequency plasma generators to Argon ion thrusters and to analytically study a third high frequency source concept are presented. Conventional 30 cm two grid ion extraction was utilized or proposed for all three sources. The two plasma generating methods selected for experimental study were a radio frequency induction (RFI) source, operating at about 1 MHz, and an electron cyclotron heated (ECH) plasma source operating at about 5 GHz. Both sources utilize multi-linecusp permanent magnet configurations for plasma confinement. The plasma characteristics, plasma loading of the rf antenna, and the rf frequency dependence of source efficiency and antenna circuit efficiency are described for the RFI Multi-cusp source. In a series of tests of this source at Lewis Research Center, minumum discharge losses of 220 ± 10 eV/ion were obtained with propellant utilization of .45 at a beam current of 3 amperes. Possible improvement modifications are discussed.

The efficiency and discharge characteristics of the ECH source were examined in several different cusp magnetic confinement geometries, but without beam extraction. The best results obtained corresponds to discharge losses of approximately 185 eV per beam ion, excluding microwave production costs. The ECH source is in an early stage of development, but displays several desirable systems advantages, being electrodeless and promising a very low grid sputtering rate.

17. Key Words (Suggested by Author(s))	18. Distribution Statement
Electrostatic Thruster Radio Frequency Induction Discharge Electron Cyclotron Heating	Unclassified - Unlimited

19. Security Classif. (of this report)	20. Security Classif. (of this page)	21. No. of Pages	22. Price*
Unclassified	Unclassified		

* For sale by the National Technical Information Service, Springfield, Virginia 22161

CONTENTS

1.0 PROGRAM SUMMARY

This report represents the results of a one year program to experimentally adapt two types of high frequency plasma generators for low thrust electrostatic argon ion thrusters. The initial scope of this "High Frequency Plasma Generator" program placed no direct constraints on the method of coupling power to the plasma or on the choice of magnetic field configuration used to enhance the plasma production efficiency. Aside from providing a back-up concept to the more mature, conventional hollow-cathode-based plasma sources, a goal in the present program was to develop a plasma generator which has a high electrical efficiency, a parameter which is of importance for low specific impulse engines.

The two methods selected for coupling electrical power to the plasma generator were (1) Radio Frequency Induction (RFI) which operates in the frequency range of several hundred kilohertz to several megahertz and (2) by Electron Cyclotron Heating (ECH) which operates in the range of several gigahertz. The RFI generator, like the hollow-cathode plasma source, does not fundamentally require the presence of magnetic fields for its operation but the ECH generator by its principle of operation does require that rather strong magnet fields be present inside the engine housing.

The class of magnetic field geometry which was used for both types of high frequency generators is variously know as a "multicusp", "multipole", or "multidipole" configuration and is particularly well suited to thruster applications since permanent magnets are used. Permanent magnets, while adding mass to the thruster, use no electrical power to provide strong particle confinement fields and can be arranged into geometrics which produce very low magnetic field strengths both in the central volume of the plasma generator and at the ion extraction plane. Low fields at these locations are thought to be an aid in the production of a more uniform beam profile and are also required for the ion extraction system (which is a field-free ion optics design) and the beam neutralization process.

Much of the work presented in this report on the RFI source consisted

of experimentation and modeling of the RF power to plasma production coupling physics. Some experimentation was carried out to measure the electron and ion confinement which has a direct impact on the beam production efficiency. One magnetic confinement geometry, namely an axial line cusp, was studied. The results indicate that considerable cross field argon ion transport to the walls occurs and that reduction of this transport is the major mechanism by which the eV/ion value can be improved. A fact worth mentioning here is that doubling the permanent magnet pole face field strength by replacing ceramic magnets (1.5KGauss) with samarium cobalt magnets (3.0KGauss) in the same configuration produced negligible (<5.%) change in the eV/ion. Ceramic magnets which can operate at higher temperatures may therefore be preferred over the more costly rare-earth magnets. With continuous beam testing at NASA-Lewis Research Center the RFI source has produced a 1.KeV, 3.0 ampere beam with minimum discharge losses of 220± 10eV/ion at a propellant utilization of 45.%.

The discharge characteristics and engine efficiency of the ECH plasma generator were experimentally examined in several different cusp magnetic confinement geometrics. Beam extraction was simulated by replacing the two grid acceleration optics with a biased termination plate. The best engine efficiency obtained with this source, which operated with microwave power at 5GHz, was about 185eV/ion assuming a 70% ion transparency extraction system is used. The experiments indicated that the maximum "beam" current that could be extracted from this generator was limited not by the available power, but by the plasma cutoff density condition: $\omega_{pe} = \omega_{\mu}$, where ω_{pe} is the plasma frequency and ω_{μ} the radian frequency of the applied microwave power.

In addition to the above two experimental programs, a third thruster geometry called the Solenoidal B-Field Concept was analytically evaluated. This evaluation consisted primarily of examining past experimental electrostatic thruster geometries in an attempt to define a new geometry for a high frequency thruster that may show improved performance.

1.1 INTRODUCTION

Mercury has until recently been the propellant used in the development of thrusters for primary electric propulsion. Indeed, the 30.cm mercury thruster is the only technology-ready thruster available. However, due to low spacecraft contamination and environmental advantages over mercury, primary propulsion thrusters using inert gases as propellant have been receiving great interest. Of the inert gases the most cost effective propellant is argon and consequently it is receiving the most attention in current research and development.

Studies have shown that the attainment of increased efficiencies for ion thrusters at low (1000 - 2000 second) specific impulse would greatly decrease the overall cost of many proposed geocentric missions which would utilize electric propulsion. The requirement of low specific impulse places more of the emphasis on the electrical efficiency of the plasma generator and its associated power conditioners for attaining high system electrical efficiency. The specific impulse is

$$I_{sp} = \frac{1}{g_o}\left(\frac{2qV}{m}\right)^{\frac{1}{2}}$$

where g_o is the acceleration due to gravity at the earth's surface, V is the net accelerating potential, and q/m is the ion charge to mass ratio. To maintain a high thrust at low I_{sp} requires lowering V and increasing the beam current. For argon with a high q/m (compared to mercury), V must be lowered further. On the other hand, the thruster system power is equal to the product of V and the beam current plus losses that to first order go as the beam current. Hence, the losses that are roughly proportional to beam current must be lowered to take maximum advantage of a lower specific impulse.

The importance of increasing the plasma generator efficiency in order

to increase the total system efficiency can also be seen from the following. For electrostatic thrusters the largest share of electrical power supplied by the system power processor goes to form the thrust producing energetic ion beam. State-of-the-art electrostatic acceleration systems (that is, physical multi-hole grid structures) produce this beam very efficiently; efficiencies of better than 99% (not including power conditioning losses) are not uncommon. The next largest portion of thruster system power is that used to generate the plasma inside the ion chamber. Clearly, the system efficiency will be increased if these plasma ions can be extracted to form the beam before being lost by recombination either in the chamber valume or at the walls. It should be noted, however, that large increases in the plasma production and confinement efficiency may not necessarily have a large impact on the overall system efficiency. For example, let us say that it takes 800 watts to produce a plasma from which a 4 Amp, 1Kvolt beam can be extracted. The total energy efficiency (excluding power conditioning losses) would be 4000/4800 = 83%. Now, if through some means, the plasma production costs could be reduced by a factor of two so that only 400 watts are required to produce a plasma from which a 4 Amp, 1Kvolt beam can be extracted, then the system efficiency increases by only 8%, even though the production costs have been reduced by 50%.

The main goal of the present program was to develop two new plasma generator concepts which showed promise of reducing the energy expenditure for plasma production. Recently, tests with high frequency plasma devices have indicated that plasmas of a few cubic meters volume of various gases can be obtained at ion production costs approaching 50 eV/ion. If such costs could be obtained with ion thrusters, increases in system efficiency of 30 percent or greater could be obtained at low (1400 seconds) specific impulse.

The two argon plasma generating methods selected for experimental

study were a radio frequency induction (RFI) source and an electron cyclotron heated (ECH) plasma source operating at microwave frequencies.

The RFI source is a new approach for production of dense plasmas that was developed at TRW. It offers a number of advantages over hot cathode DC charges. The major advantage is a very large reduction in the average electron current lost from the plasma to electron absorbing elements, because the DC cathode-anode arrangement is replaced by an internal rf antenna. Other advantages include simplicity of operation and control, potentially higher durability, and a startup time of a few seconds. It uses conventional extraction optics and multicusp magnetic plasma confinement.

The ECH or microwave source also uses conventional electrostatic optics and multicusp confinement but is otherwise electrodeless. The plasma is produced by applying microwaves at a frequency equal to the cyclotron frequency of electrons in the confining magnetic field inside the thruster chamber. It offers all of the advantages of the rf source plus very high durability since it has no electrodes.

The analytically studied source was a microwave or rf driven source with a solenoidal magnetic field for confinement. This magnetic configuration is not new, but differs from electron bombardment sources in that it also is electrodeless. The ionizing energy is supplied by electromagnetic waves rather than by ionizing electrons which flow between d.c. electrodes. Hence, higher efficiency is predicted.

One RFI and three ECH sources were built and experimentally investigated. The results are presented in Sections 3 and 4, respectively. A brief introductory theoretical discussion on the principles of operation of the RFI and ECH sources is given in Section 2 together with a cursory evaluation of the possible impact each of these high frequency plasma generators has on the system power processor and other physical thruster parameters. The analytical treatment of the solenoidal magnetic field concept is presented in Section 5.

2.0 PRINCIPLES OF OPERATION

Each of the two selected methods of coupling power to a plasma, namely by Radio Frequency Induction and by Electron Cyclotron Heating has a history of successful application in plasma production. Some of the history, basic theory, and considerations for thruster application of these techniques is given in the following two sections.

The class of magnetic field geometry used for each concept is variously known as "multicusp", "multipole", or "multidipole", and is particularly well suited to thruster applications as it may utilize permanent magnets which require no additional power and provide fields strong enough to confine ions. Additionally, multicusp geometries with very low magnetic fields in the extraction region are possible. Such geometries were first used at Electro Optical Systems[1] for thruster applications, and later adapted with a somewhat different electrical configuration, for laboratory plasma sources[2] and neutral beam applications[3].

2.1 RADIO FREQUENCY INDUCTION MULTICUSP SOURCE

RF induction plasmas generated with a coil antenna surrounding a quartz vessel were first described by Hittorf[4], and have since been used for studies of basic discharge physics [5,6], in electrostatic thruster applications[7], and as light sources for spectroscopic studies.

Adaptation of the rf induction technique to multicusp geometries was first made at TRW in connection with the development of laboratory plasma sources. Simply, a dielectric coated coil antenna is situated in the weak magnetic field region of a multicusp device, and resonated at the desired frequency with external capacitors and inductors. Electrons are collisionally heated in the electric fields induced in the plasma by the circulating

coil current. Since the electron heating takes place in the weak magnetic field region, the confinement properties of the system are very similar to those of a dc discharge (i.e., filament or hollow cathode discharge) in a multicusp geometry. In all applications of this technique to date, including those described in Section 3 of this report, the entire (conducting) wall of the containment vessel, with the exception of the optics, is one common "electrode", with respect to which the plasma assumes a positive potential. The plasma is cusp confined[8] at the magnet pole faces and transport to the walls between magnets is inhibited by the strong magnetic fields.

A complete model of heating in the RFI Multicusp source has not yet been developed, but the basic physics is well described by simple fluid theory. The electron equation of motion in the induced electric field is

$$\frac{d\vec{v}}{dt} = -\frac{e}{m}\vec{E} - \nu\vec{v} \tag{2.1}$$

where ν is the total electron momentum transfer collision frequency. Taking $\vec{E}$ and $\vec{v}$ as complex with time dependence $e^{-i\omega t}$, the solution of (2.1) is

$$\vec{v} = \frac{-e\vec{E}}{m(\nu - i\omega)} \tag{2.2}$$

We may express the plasma response in terms of Ohm's law

$$\vec{j} = -n_e e\vec{v} = \sigma\vec{E} \tag{2.3}$$

with complex conductivity

$$\sigma = \sigma_R + i\sigma_I = \frac{\nu + i\omega}{\nu^2+\omega^2}\ \frac{n_e e^2}{m} \tag{2.4}$$

It may be seen from (2.4) that the plasma response consists of a resistive part and a reactive part.

ORIGINAL PAGE IS
OF POOR QUALITY

The power coupled to the plasma is given by the volume integral

$$P = \int \vec{j} \cdot \vec{E}\, dV = \frac{1}{2}\int \sigma_R\, |E|^2\, dV \tag{2.5}$$

$$P = \int \frac{n_e e^2}{m}\, \frac{\nu}{\nu^2 + \omega^2}\, |E|^2\, dV \tag{2.6}$$

With the assumption that n and ν are spatially uniform in the heating region, this may be written

$$P = \frac{n_e e^2}{m}\, \frac{\nu}{\nu^2 + \omega^2}\, \langle E^2 V\rangle \tag{2.7}$$

where

$$\langle E^2 V\rangle \equiv \int |E|^2\, dV \tag{2.8}$$

In order to sustain a discharge through rf heating, the input power given by (2.7) must balance the discharge power, P_d

$$P_d = n_e n_o (\langle \sigma v_e \rangle_i\, \varepsilon_i + \langle \sigma v_e \rangle_{ex}\, \varepsilon_{ex})\, V_{pp} + \frac{1}{2}\, n_e c_s\, A\, (2kT_e + e\phi_p) \tag{2.9}$$

where ε_i and ε_{ex} are the ionization energy and average excitation energy and $\langle \sigma v \rangle_i$ and $\langle \sigma v_e \rangle_{ex}$ are averages over the electron distribution function of the ionization and excitation cross sections respectively. The electron density and temperature is assumed uniform in the plasma production volume V_{pp}, and the particle loss rate is expressed as the Bohm current over an effective area, A. Expression (2.9) may be written

$$P_D = n_e P_d \tag{2.10}$$

where p_d is the discharge power per unit electron density, and is independent of electron density. Equating (2.7) and (2.10) gives the breakdown requirement

$$\langle E^2 V\rangle = \frac{m}{e^2}\, \frac{\nu^2 + \omega^2}{\nu}\, p_d \tag{2.11}$$

which is independent of density if ν is density independent. If the spatial structure of the electric field is independent of density and frequency, which will be the case for sufficiently low density, then

$$|E|^2 \propto \frac{\nu^2 + \omega^2}{\nu} \tag{2.12}$$

which is familiar as the form of the Paschen high frequency breakdown curve.[8] We may express (2.12) in terms of the antenna current as

$$I_A \propto \frac{|E|}{\omega} \propto \left(1 + \frac{\nu^2}{\omega^2}\right)^{1/2} \nu^{-1/2} \tag{2.13}$$

which result will be referred to in Section 3.

Returning to equation (2.7), it may be seen that if the electric field structure is independent of density, the input power is directly proportional to the electron density. Then, if the plasma loading of the antenna is modeled as an equivalent parallel resistance, that resistance varies inversely with the electron density. More realistically, it is expected that the electric field will be modified by the plasma skin effect. While the rf antennae used in the thruster are mechanically simple, their electric field patterns are not easily modeled analytically. For the purposes of comparison to the case of fields unmodified by the plasma, corresponding to a skin depth much larger than the antenna radius, we consider the case of the skin depth smaller than the inter-turn spacing of the antenna. The fields may then be approximated as those of an infinite straight rod antenna, which case has been treated by one of the authors[9]. From reference 9, the main component of the induced field is along the antenna and is given by

$$E = \frac{2i\omega I_A}{c} K_0(\gamma r) \tag{2.14}$$

where K_0 is the modified Bessel function[10], c is the speed of light, r is measured from the antenna axis and

$$\gamma = \frac{1}{c}(4\pi i\sigma)^{1/2} \tag{2.15}$$

with σ given by (2.4). We have numerically evaluated the volume integral (2.8)

using expression (2.14) with ν/ω as a parameter, and find that, to a good approximation

$$\langle E^2 V \rangle = \frac{4\pi}{c^2} \omega^2 I_A^2 \delta^2 L \qquad (2.16)$$

where L is the antenna length and δ is the skin depth,

$$\delta = (1 + \frac{\nu^2}{\omega^2})^{1/2} \frac{c}{\omega_p} \quad . \qquad (2.17)$$

Expression (2.16) is a good approximation for ν/ω varying from much less than one to much greater than one, as long as the radius of the antenna rod is less than about $\delta/5$. From (2.16), it is apparent that $\langle E^2 V \rangle$ is inversely proportional to density in this extreme case, and therefore, from (2.7), the input power is independent of density. If the plasma is modeled as a parallel resistance to the antenna, the resistance is independent of density.

An experimental determination of the equivalent plasma resistance is described in Section 3.3.2, with a result between the two extreme cases discussed here.

2.3 ELECTRON CYCLOTRON RESONANCE SOURCE

Electron cyclotron heating at microwave frequencies (typically 2 to 30 GHz) has been employed for many years for the production and heating of fusion plasmas[11,12] and occasionally for the production of inert gas plasma sources[13,14]. The most typical magnetic geometry for ECH applications is the magnetic mirror, with field ratios B_{max}/B_{min} = 1.5-3. Microwaves of wavelength much less than the plasma chamber scale size are launched by simple antennae into the chamber which serves as a very high mode Q cavity. The microwave frequency is chosen to match the local electron cyclotron frequency on some surface between the mirror throat (maximum magnetic field region) and midplane (minimum field region). Electrons which pass through the heating zone (which is very narrow in the direction along B) in resonance with the microwave field receive a "kick" in energy. Experimentally, it has been found that this heating method produces a Maxwellian electron distribution, except at very low gas pressures ($<10^{-5}$ torr).

Since the containment vessel dimensions are typically much larger than the wavelength, microwave modes propagating in the plasma are very close to the infinite plasma modes. For any orientation of the wavevector with respect to the magnetic field, there are two modes, only one of which is strongly absorbed at the electron cyclotron resonance. The propagation characteristics as a function of magnetic field and plasma density for the case of the wavevector perpendicular to B are shown schematically in Figure 2.1. Only the extraordinary (E) mode has an electric field component perpendicular to B and is strongly absorbed in the neighborhood of the electron cyclotron resonance. It should also be noted that the ordinary wave is non-propagating for plasma densities above $\omega_p^2 = \omega^2$. In most experiments, a mixture of ordinary and extraordinary waves are launched by the antenna, but very high absorption (>90%) is typically found. It has been shown[15] that the ordinary mode undergoes fairly strong partial conversion to the extraordinary mode upon reflection from the plasma-wall boundary. If the microwave Q of the plasma containment vessel is sufficiently high, all energy input in the ordinary mode will eventually be mode converted and absorbed.

ECH in conventional mirror geometries is not suitable for current thruster technology as superconducting magnets would be required to achieve the necessary field configuration without prohibitively high magnet power. We describe here a concept utilizing ECH in a multi-cusp permanent magnet configuration.

Representative magnetic field lines and lines of constant field for an infinite periodic array of long bar magnets are shown in Figure 2.2. Lines of constant B divide into two topological groups, those which intercept the magnets and those which do not. In considering a plasma in a periodic cusp field, two rather less distinct groups of field lines emerge. The field lines which remain in the high field region form a mirror-like configuration, while field lines extending into sufficiently low field regions are associated with cusp-like plasma behavior.

In conventional multi-cusp sources, such as the multi-cusp hollow cathode discharges and the RFI source described in Section 3 of this report, the source of ionizing electrons is in the low magnetic field region, i.e.,

on cusp-like field lines. In the ECH source described here, the microwave frequency and permanent magnet field strength are such that the resonant heating surface is in the very high field strength region, where most of the magnetic field lines are mirror-like. Electrons are heated and confined to the mirror regions, in direct antithesis to conventional multi-cusp sources. Due to the magnetic field curvature, the plasma produced in the mirror-like regions is unstable to flute or interchange modes and is rapidly transported into the low field region, where the extractor grids are located. In this concept, the screen grid is magnetically insulated from the high temperature regions of the plasma, which should lead to greatly reduced sputtering rates.

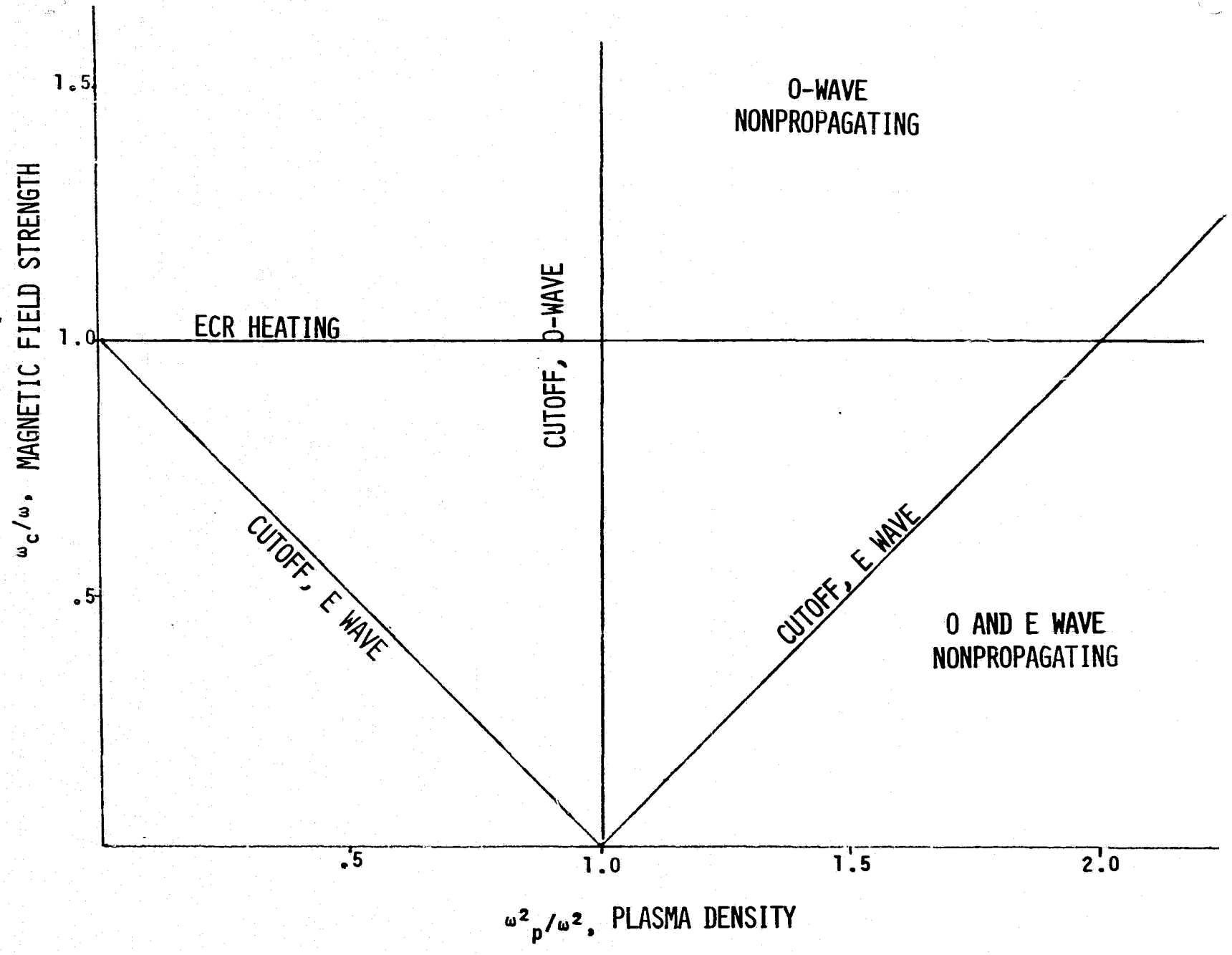

Figure 2.1 Propagation and cutoff regions for ordinary and extraordinary modes for propagation perpendicular to a magnetic field.

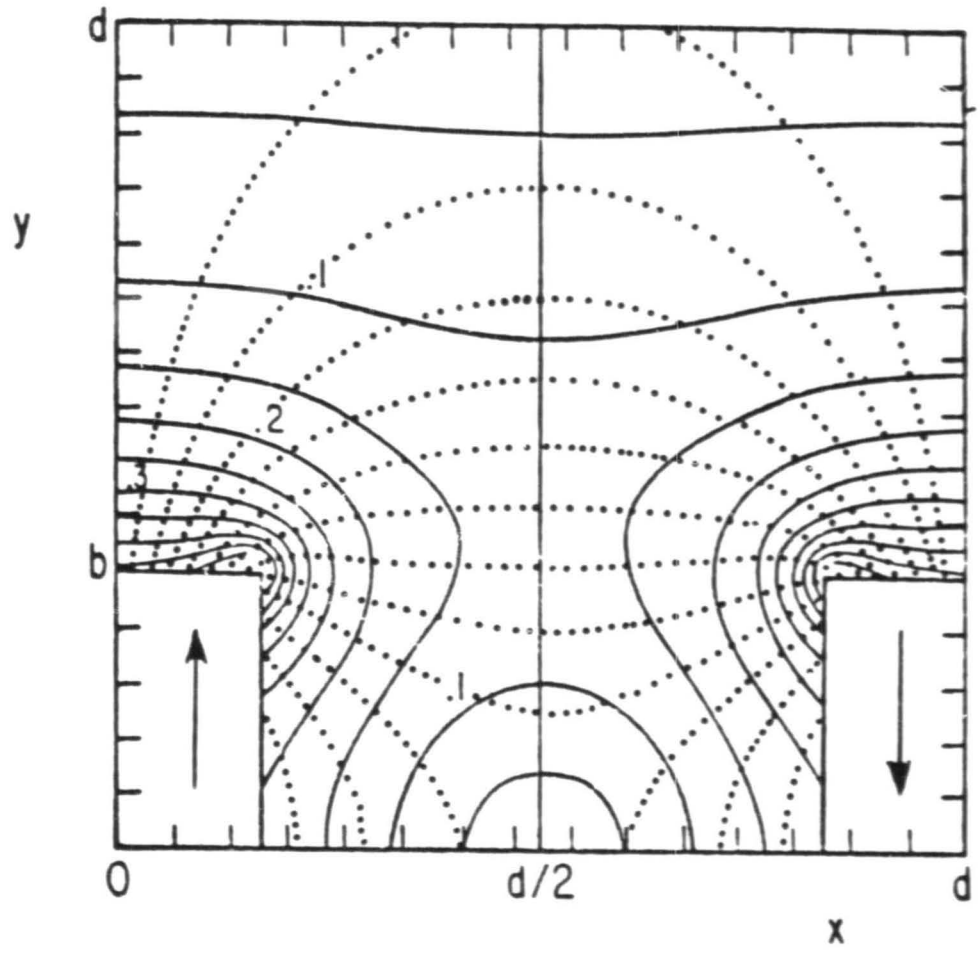

Figure 2.2 Magnetic field lines (dotted) and lines of constant magnetic field (solid) for an infinite periodic array of bar magnets.

2.3 SYSTEM EVALUATION

In developing new concepts for methods of plasma production and confinement for thruster applications, it is important to at least make a cursory examination of the impact these concepts have on the overall design of the thruster, its major components and its associated power conditioners. One may, for example, develop a thruster which is very efficient in terms of eV/ion but which is so complex and delicate that it cannot withstand the g's required to launch it into orbit. Of course, before a new concept is fully developed to a finalized prototype it is all but impossible to state in detail what the total mass or parts count of the new thruster and its power processor will be. The purpose of this section is to relate what major component and electrical changes an RFI and ECH based thruster would have on a baseline 30cm mercury ion thruster whose performance data is referenced to NASA CR-135287 and the results of NASA Contract No. NAS3-21746. A better basis of comparison would have been the hollow cathode, multi-cusp 30cm argon ion thruster, under development at NASA-Lewis Research Center, Hughes Laboratories and (XEROX) EOS, but to our knowledge, no detailed mass, parts count or finalized power processor design for this unit exists.

The major components of the baseline 30cm mercury ion thruster are shown in Fig. 2.3 and a block diagram of its power processor is given in figure 2.4. Note that the largest portion of power supplied by the processor goes to the screen (1100V x 2.1A = 2310 watt) and the second largest portion goes to maintain the plasma discharge (50V x 14A = 700 watt) the reduction of which is one of the goals of the present program. However, with argon as the propellant a 4.4 ampere ion beam must be produced to yield the same thrust with screen and accelerator voltages of 1100V and -500V, respectively; the 4.4 ampere beam current was another design goal under the present High Frequency Plasma Generator program.

A step by step comparison between the baseline system and the RFI

and ECH power conditioning units is made in Table 2.1. Since argon, most likely contained in highly pressurized vessels, replaces mercury as the propellant, all vaporizer supplies would be replaced by an electrically controlled piezo gas valve. The supplies for the hollow cathode used for beam neutralization would remain essentially identical. The screen supply (V11) for an argon thruster would necessarily be required to supply the additional power to maintain the same thrust level as a mercury thruster. RF power in the range of 1MHz used for plasma production can be generated very efficiently (90%) with solid state devices. Microwave power for the ECH unit requires a klystron amplifier or magnetron oscillator to produce the high frequency power; these devices are somewhat less efficient (30 - 70%) in converting dc to high frequency power. From the comparison given in Table 2.1 it is seen that the argon, high frequency RFI or ECH thruster would most likely impact the power conditioner by simplifying it and reducing the parts count.

The power processor is the most massive section of the thruster system and an estimate of the mass of an RFI or ECH power conditioner can be made when a working prototype unit is designed and assembled. The LeRC-TRW J series mercury PPU has a mass of 37.4Kg. The high frequency PPU could have lower mass than this since in general high voltage, low current supplies replace the low voltage, high current supplies.

We forsee no appreciable difference in the mass of the thruster body for a hollow cathode and high frequency thruster. In fact, the present J-series thruster housing could easily be retrofitted from a hollow cathode discharge to an RFI or ECH discharge. Thus, in the final configuration, the most massive components, the thruster shells, magnets and grid set could remain unchanged. Thruster mass estimates are given in Table 2.2.

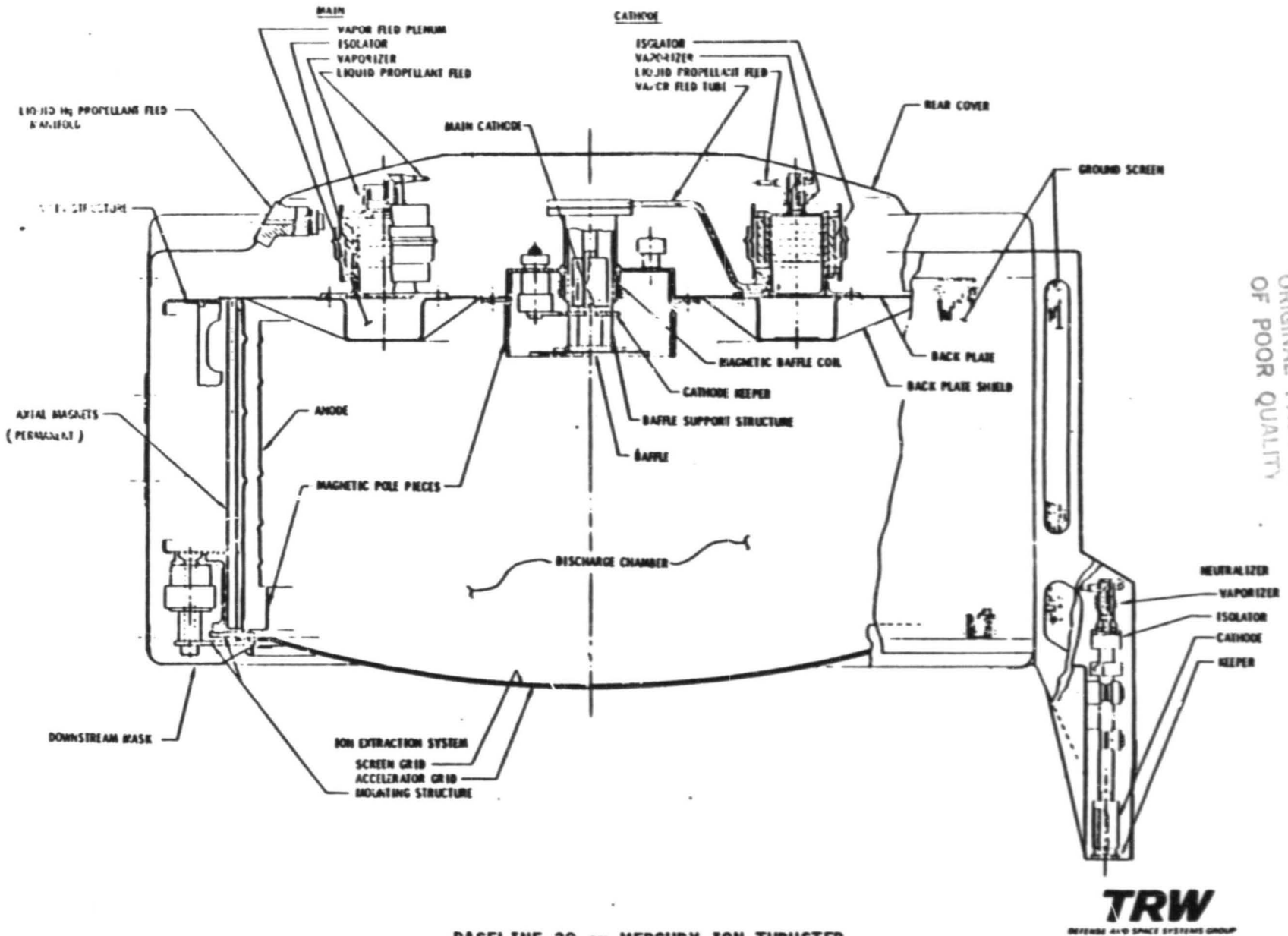

BASELINE 30-cm MERCURY ION THRUSTER

Figure 2.3

PPU BLOCK DIAGRAM

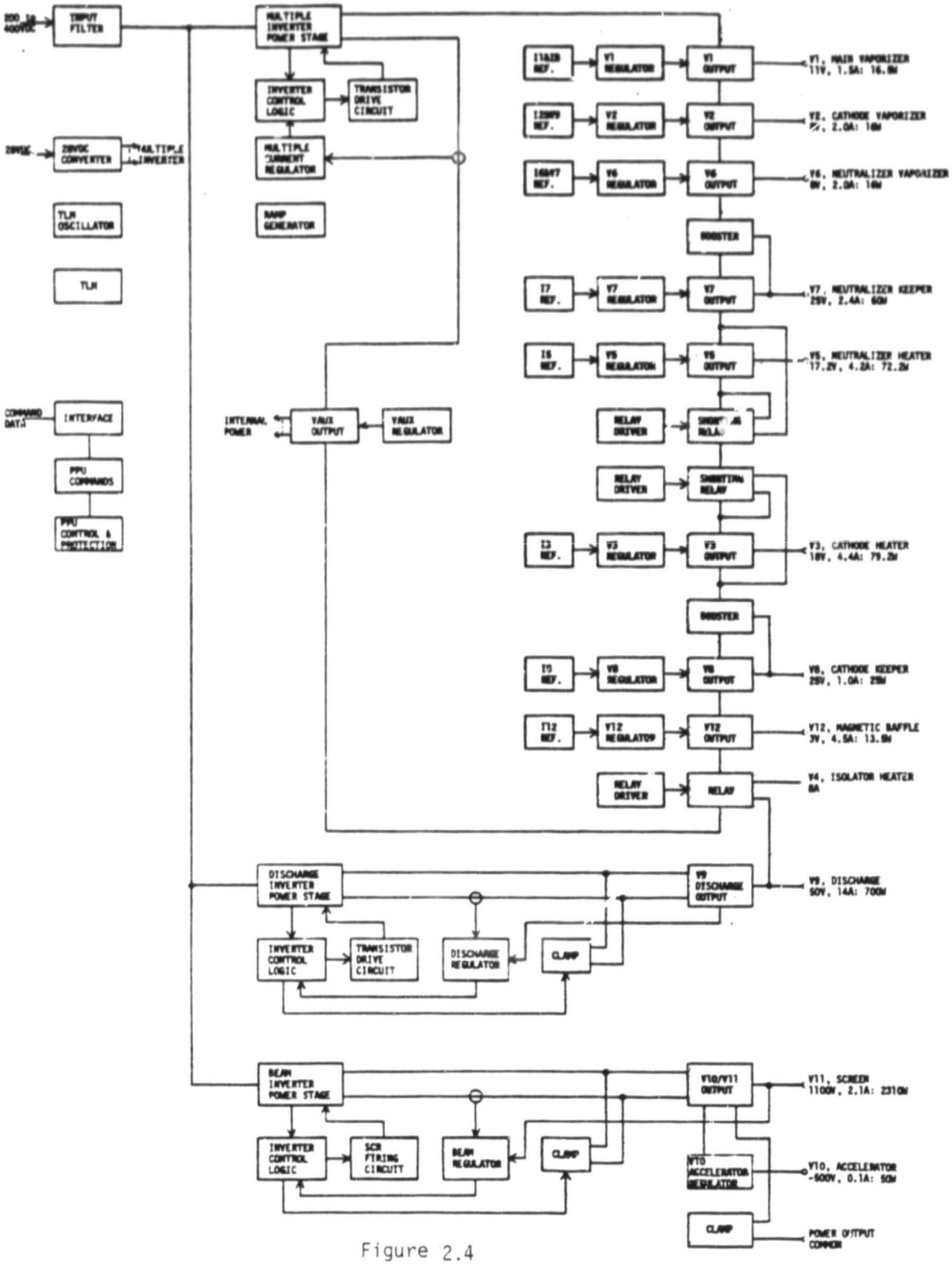

Figure 2.4

TABLE 2.1 COMPARISON OF POWER CONDITIONING

ITEM	BASELINE MERCURY	RFI THRUSTER	ECH THRUSTER
V1 Main Vaporizer	11V, 1.5A: 16.5w	N. R.(1)	N. R.(1)
V2 Cathode Vaporizer	8.V, 2.0A: 16.w	N. R.(1)	N. R.(1)
V3 Cathode Heater	18.V, 4.4A: 79.w	N. R.	5.V,10.A: 50w(2)
V4 Isolator Heater	3V, 8.A: 24w	N. R.	N. R.
V5 Neutralizer Heater	17.V, 4.A: 72w	identical	identical
V6 Neutralizer Vaporizer	8.V, 2.A: 16w	N. R.	N. R.
V7 Neutralizer Keeper	25.V, 2.4A: 60w	identical	identical
V8 Cathode Keeper	25.V, 1.0A: 25w	10.V,2.A: 20w(3)	N. R.
V9 Plasma Production	50.V, 14A: 700w	400.V, 1.8A: 720w(4)	3000.V, 0.3A: 900w(5)
V10 Accelerator	-500.V, 0.1A: 50w	identical	identical
V11 Screen	1100.V, 2.1A: 2310w	1100.V, 4.4A: 4840w	1100.V, 4.4A: 4840w
V12 Magnetic Baffle	18.V, 4.4A: 79.W	N. R.	N. R.

*See Table 2.1 continuation for notes.

TABLE 2.1 COMPARISON OF POWER CONDITIONING, continued

NOTES: (1) N. R. = Not required; merucry vaporizer replaced by pressurized argon feed

(2) Heater supply for magnetron or klystron microwave amplifier

(3) Filament supply for discharge starter

(4) Assumes solid state devices used for RF power production

(5) Beam supply for magnetron or klystron

TABLE 2.2 THRUSTER MASS ESTIMATES

PERMANENT MAGNETS (RARE EARTH COBALT)	4.26kg	
PLASMA GENERATOR BODY (STAINLESS STEEL)	0.09	
SCREEN & ACCEL ELECTRODES[1]	0.47	
NEUTRALIZER ASSEMBLY[1]	0.35	
OUTER SHELL[1]	0.14	
MASK[1]	0.13	
COVER, REAR[1]	0.01	
BRACE, REAR[1]	0.46	
BRACKET, GIMBAL[1]	0.36	
VALVES, SHUT OFF & METERING[2]	1.00	
MISC. HARDWARE (INSULATORS, FASTENERS & WIRES)[2]	1.50	
SUBTOTAL (EXCLUDES HIGH FREQUENCY FEED)		9.65kg
WAVEGUIDE, MICROWAVE[2]	1.00	
TOTAL THRUSTER MASS WITH MICROWAVE PLASMA GEN.		10.65kg
RF ANTENNA & COUPLERS[2]	0.50	
TOTAL THRUSTER MASS WITH RF PLASMA GEN.		10.5kg

[1] J-SERIES THRUSTER COMPONENT MASS DATA FROM HUGHES AIRCRAFT CO. REPORT, 1979

[2] ROM ESTIMATE

3.0 RF THRUSTER TESTING

3.1 GENERAL DESCRIPTIONS

3.1.1 Thruster

For all rf thruster testing a very simple mechanical design was adopted to facilitate the study of different component configurations. The thruster is shown schematically in Figure 3.1 and consisted of a 33cm diameter, 20cm long, cylindrical shell made from 1mm 304 stainless steel welded to front and back mounting rings. SHAG screen and accelerator electrodes were mounted on the exhaust end and insulated with thin sheets of reconstituted mica so that the screen and accelerator could be biased separately with respect to the shell. The other end of the cylinder was formed from 1mm stainless steel sheet. Twelve bar magnets were spaced around the outside of the shell with alternating magnetic polarity to form a line cusp configuration, and five bar magnets continued the line cusps across the backplate. The magnets were ceramic, 1.9cm wide by 2.5cm in the direction of magnetization, with a measured pole face field strength of 1.5kg. A 2.5mm thick iron plate-pole piece completed the magnetic circuit external to the shell for the five backplate magnets. The argon propellant was fed into the thruster through the backplate near the axis. The argon feed line contained a nonconducting section for high voltage isolation of the laboratory gas supply located outside the vacuum chamber. Various copper antennas were suspended axially from a block of insulating material mounted on the outside of the thruster shell. Each antenna was sheathed with a 1mm thick dielectric to shield it from sputtering. Figure 3.2 shows a photograph of the thruster mounted in a one meter by three meter test facility. For ion beam extraction tests, a ground potential screen shielded all of the thruster except the accelerator from backstreaming electrons.

3.1.2 Thruster Electrical Description

The rf power source and matching circuitry for the initial testing is shown in Figure 3.3. Two broadband high gain amplifiers (ENI A-300) were driven by a common oscillator for a maximum power of 600 watts. A multi-tap, ferrite core rf power transformer was used to match the 50Ω

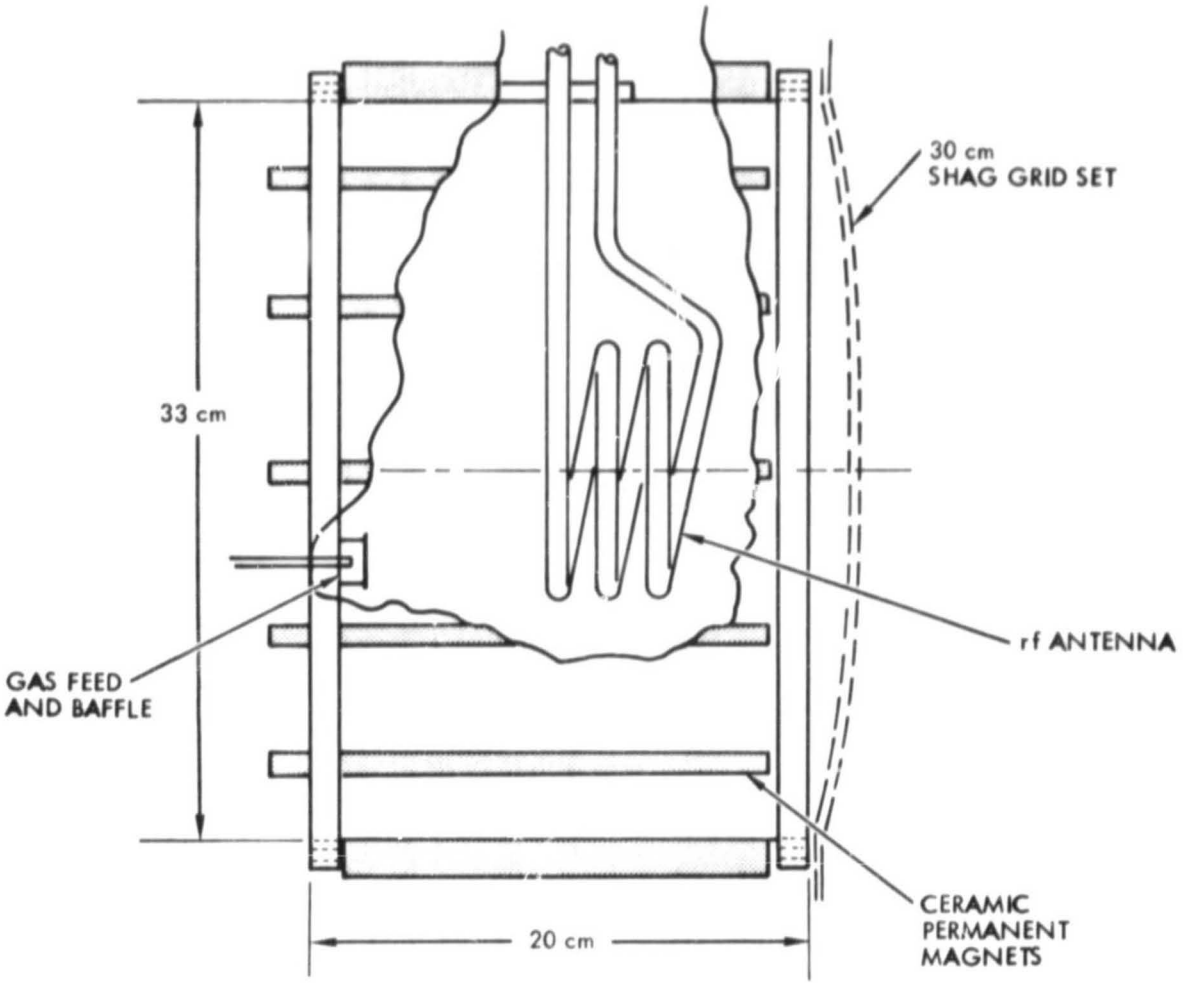

Figure 3.1 Schematic of the RFI Thruster

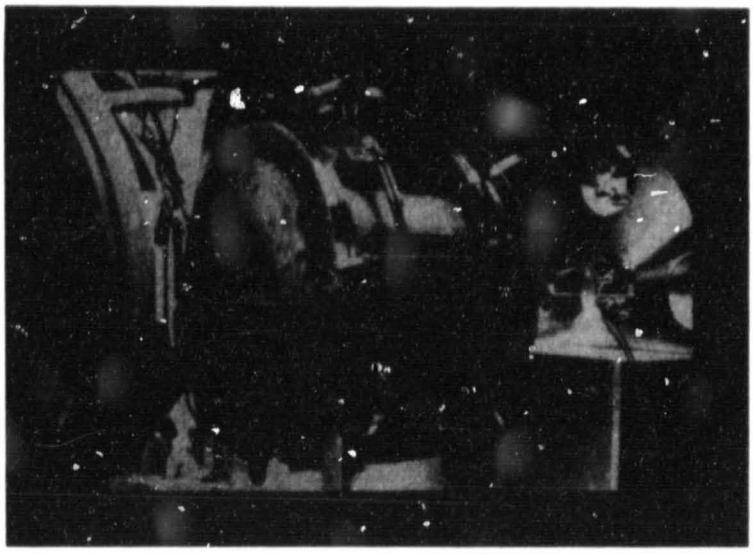

Figure 3.2 RFI Thruster mounted in the TRW test facility

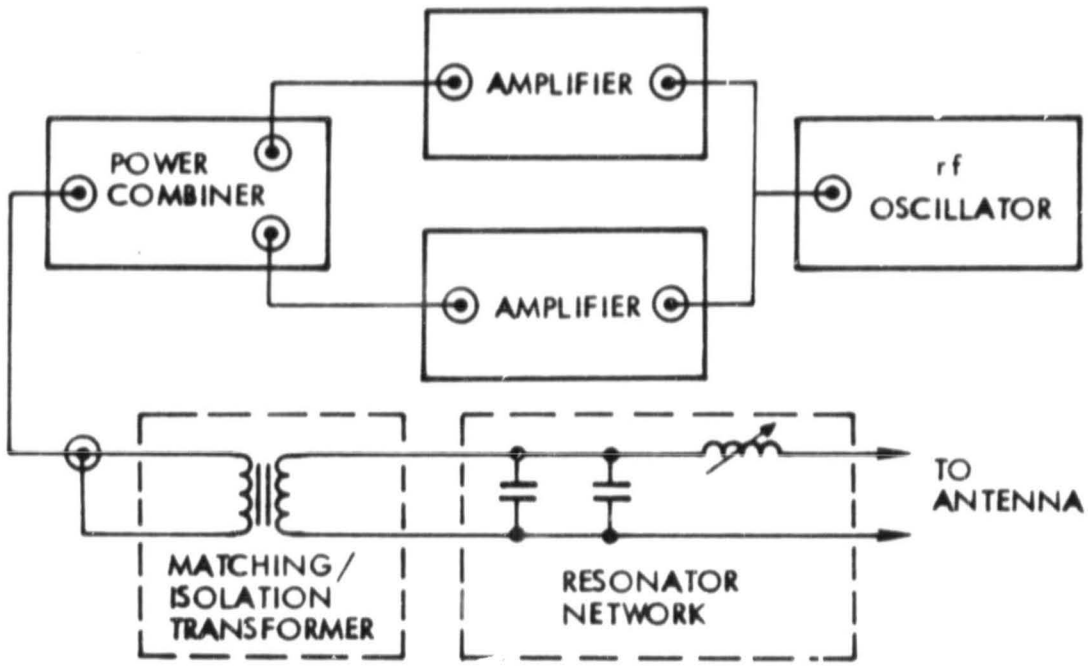

Figure 3.3 RF Circuit Initial Configuration

source impedance to the combined impedance of the resonator network, antenna and plasma. A variable inductance, air core choke in series with the antenna, and strap selectable mica capacitors were used to resonate the system at frequencies between 300kHz and 1MHz. This circuit was able to deliver about 600 watts of rf power at those frequencies. To obtain more power and to test at higher frequencies the apparatus shown in block diagram in Figure 3.4 was used. The class C plate tuned amplifier was driven by a variable frequency oscillator through a broadband rf preamplifier. A one to one ferrite core transformer served to isolate the rf power system from the antenna tank circuit and thruster. The resonator network was a tank circuit whose inductance was the sum of the antenna inductance (.7μh) and the lead inductance (L_{ext} = .47μh). The tank capacitor was a series parallel combination of mica capacitors with a net capacitance of .01μF, giving a resonant frequency of 1.47MHz.

Also shown in Figure 3.4 are the rf voltage and current measurement elements. The rf driving current was detected with a Pearson wideband current transformer with a sensitivity of .100 volt/A whose output was measured on a vector voltmeter (HP8405A). The voltage of the tank circuit was measured from a 500:1 resistive voltage divider with transformer isolation on the second channel of the voltmeter, so the phase angle between the input current and the tank voltage could be measured. This arrangement gave a power measurement corrected for the phase shift between the input current and tank voltage. In the tests at LeRC independent power measurement was obtained with a Byrd rf Power Meter, mounted on the secondary side of the isolation transformer. However, the Byrd meter gave spurious results when the plasma impedance was much different from 50Ω.

Figure 3.5 shows in block diagram the rest of the rf thruster electrical equipment. For rf discharge experiments without the extraction of an ion beam both high voltage power supplies were disconnected and the full ion current was collected on the screen and accelerator connected together by switch S_2 and referenced below ground by S_1 and the screen bias supply. All power supplies were DC, although the two filament heaters could have been AC. The filament neutralizer was optional since the collector and vacuum chamber walls were grounded.

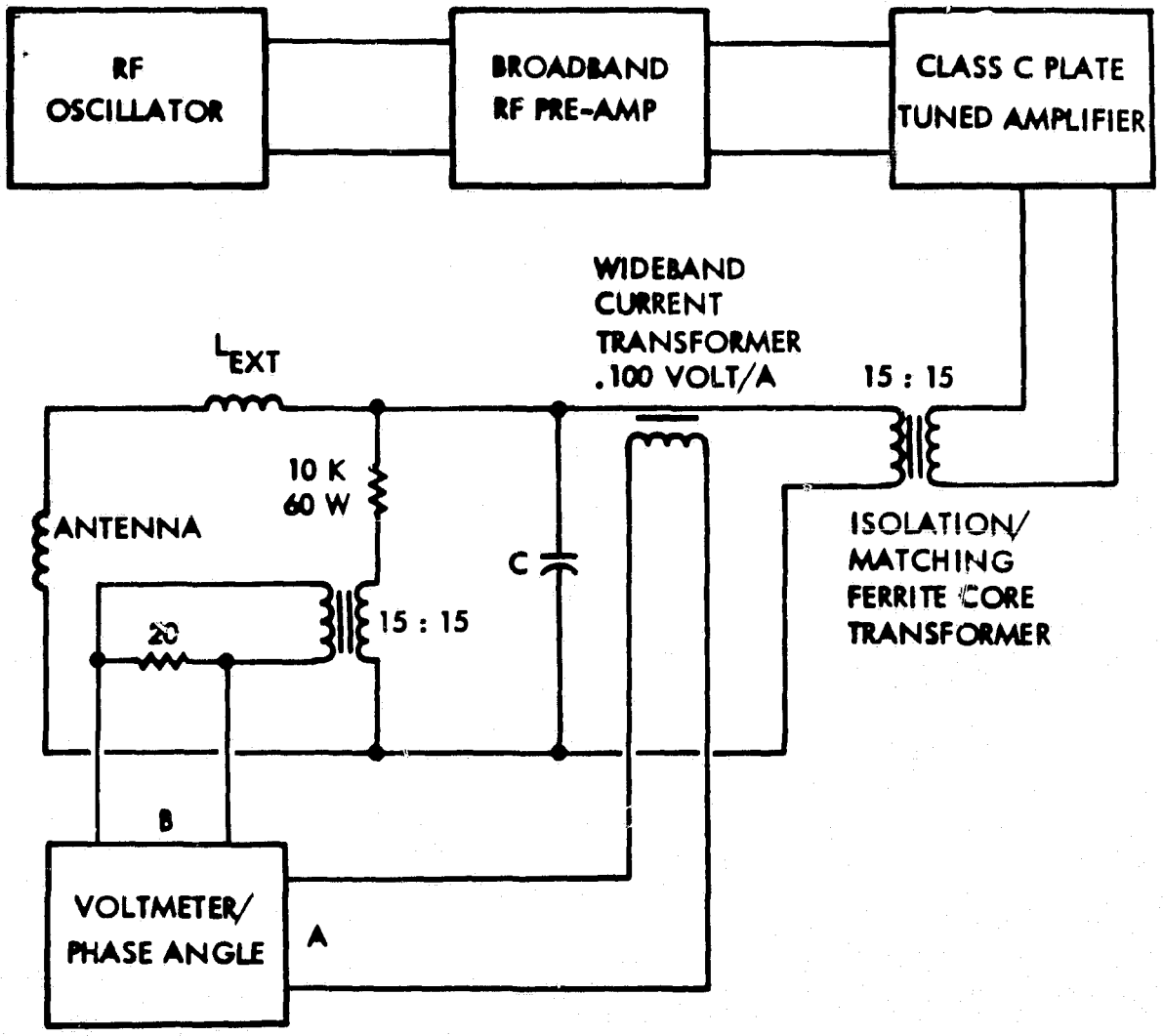

Figure 3.4 Test Setup for RF Drive and Measurement of RF Power

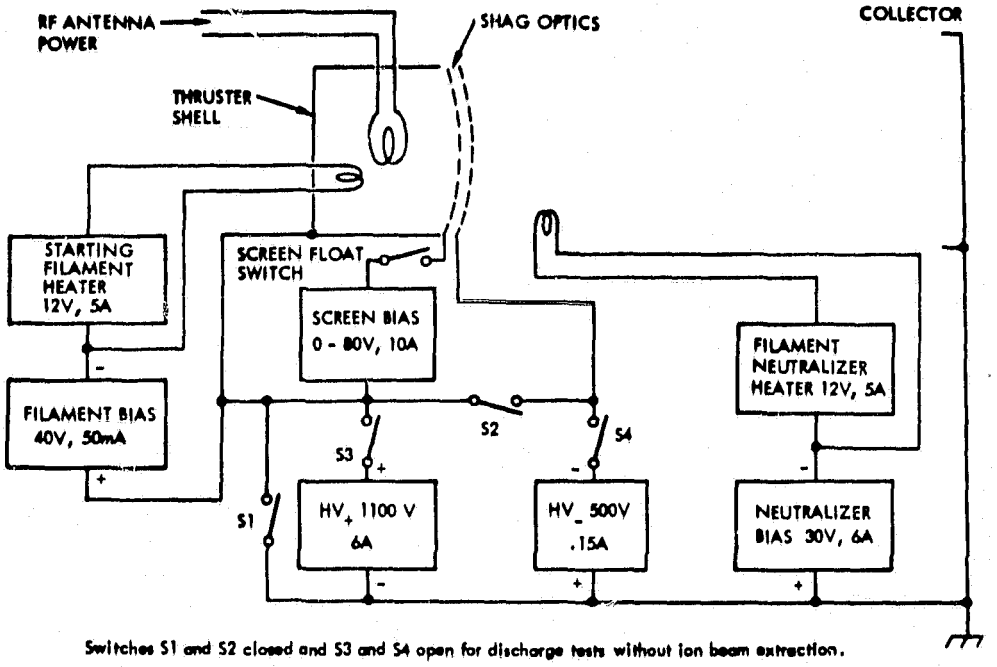

Switches S1 and S2 closed and S3 and S4 open for discharge tests without ion beam extraction.
For ion beam extraction, all four switches reversed.

Figure 3.5 Electrical Block Diagram for RF Thruster Tests

3.1.3 Gas Feed System

The laboratory feed system shown in Figure 3.6 was built to supply the rf thruster with argon gas in either a continuous or pulsed mode. The entire feed system was evacuated by the mechanical pump prior to filling with argon. For a constant flow argon was let into the thruster through either the open constant flow needle valve with the bypass valve closed or from the ballast with those two valves reversed. Pulsed flow was controlled by the valve controller which opens the normally closed solenoid valve. The controller was adjusted to give gas puffs of a varying frequency and varying durations per cycle and was also used to trigger the rf power and beam extraction voltages.

Flowrate measurements were possible for a chamber of large enough pumping speed that a negligible amount of gas re-entered the thruster from the chamber. For such a case the gas was supplied continuously or was pulsed from the ballast. The flowrate through the orifice was thus proportional to the pressure in the ballast which was large enough to maintain a nearly constant flow for several minutes of continuous operation and for longer periods for pulsed operation.

3.1.4 Test Facility

The vacuum chamber for all testing at TRW was 1.2 meter diameter by 2.1 meter long pumped by a single 40cm oil diffusion pump. The pumping speed was inadequate to allow accurate gas flowrate measurements, because the amount of gas backstreaming into the thruster from the chamber was not insignificant. Therefore, in all tests at TRW the gas pressure in the thruster was measured as an operating level parameter. The gas pressure was measured by the chamber ion gauge, and those measurements were corrected for argon gas.

3.1.5 Description of Antennas

Four antennas were tested covering a range of geometries. The tests, though by no means exhaustive, served to illuminate some of the basic parametric dependence of the rf coupling to the plasma on antenna geometry. Table 3.1 summarizes the four antennas, all of which were cylindrical coils made from standard copper tubing.

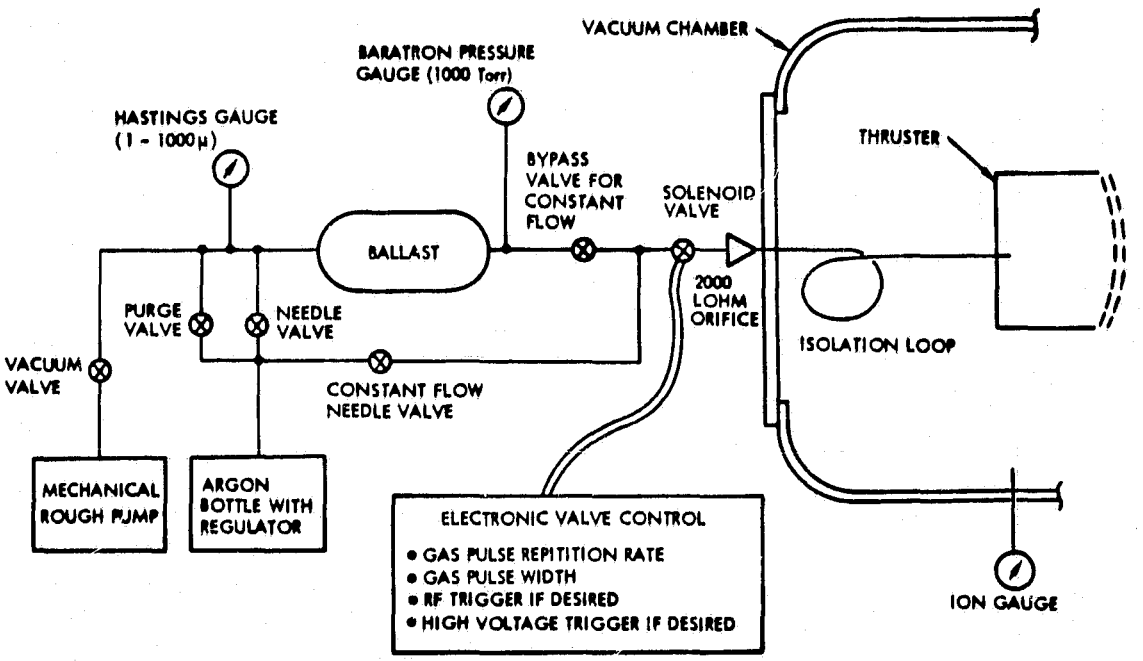

Figure 3.6 Laboratory Feed System

Table 3.1. Antenna Geometries

Antenna	Number of Turns	Turn Diameter (cm)	Axial Length (cm)	Tube Diameter (cm)	Dielectric Shield Diameter (cm)	Total Length (cm)
1	2	18	4	.64	.9	127
2	3	10.5	12	.64	.9	100
3	2	8.5	6	.32	.45	50
4	2	8.5	6	.64	.9	50

Each antenna total length includes the length of the tubing between the coil ends and the wall of the thruster shell. This entire length was sheathed with glass fiber sleeving of about 1mm thickness (about .5 mm in the case of antenna 3) to reduce antenna damage from sputtering by plasma ions. With the coil axis on the thruster axis, the antennas were suspended from an insulating block mounted on the thruster shell.

The first attempts to obtain a plasma were made with antenna 1 and without beam extraction and without the filament. They were unsuccessful for all argon pressures practical for a thruster application (10^{-3} to 10^{-5} torr) even after the addition of a hot filament neutralizer to provide a source of seed electrons. With these failures it was suspected that the diameter of the antenna was too large, so that it extended into regions of too high a magnetic field. The radial field strength was measured to be 50 to 70 Gauss at the location of the 18cm diameter antenna coils.

The smaller antenna 2 was then installed along with the internal tungsten filament as shown in Figure 3.1. The filament was installed because high frequency discharges usually require a seed electron population for startup, the required density being a function of the electron heating rate and confinement time. With antenna 2 the source was not self starting with antenna currents as high as 90 A_{rms} at a frequency of .36MHz and argon pressures as high as 10^{-2} torr. With the filament hot and biased greater than 20 volts negative, a faint discharge between it and the shell could be seen and measured as a few tens

of milliamp of emission current. Under this condition, at pressures in the range 10^{-4} - 10^{-3} torr, the rf discharge could be initiated instantly and repeatedly at a coil current of approximately $60A_{rms}$. After startup the filament was not required to sustain the discharge. Figure 3.2 is a photograph of the discharge in the thruster with the filament off.

Most of the results presented in the rest of this report, including those obtained at the Lewis Research Center Facility, were obtained with antenna 2. Results obtained with antenna 3 and 4 are pertinent to the understanding of rf coupling to the plasma and to possible future work in antenna optimization, and are described in section 3.3.

3.2 RFI THRUSTER TESTS AT LEWIS RESEARCH CENTER

3.2.1 Purpose

In a two week series of tests the Radio Frequency Induction Multicusp Thruster was operated at Tank 5 of the NASA Lewis Research Center Advanced Electric Propulsion Laboratory. The purpose of these tests was to demonstrate and characterize the operation of the first experimental model of a multicusp rf thruster under conditions of continuous ion beam extraction. An important goal of the tests was to determine to what degree test results obtained without beam extraction and with pulsed beam extraction could be extrapolated to thruster operation with continuous extraction.

3.2.2 Test Configuration

In section 3.1, the thruster chamber, magnet configuration, rf antennas and drive circuitries, and diagnostic instrumentation were described. For the LeRC tests antenna 2 powered by the instrumented rf circuit of Figure 3.4 was used. Initial testing was done with the ceramic magnets described in section 3.1.1. They were 1.9 cm wide by 2.5 cm in the direction of magnetization, with a measured pole face field strength of 1.5 kG. After initial testing, the original magnets were replaced with samarium cobalt magnets, furnished by NASA/LeRC. The $SmCo_5$ magnets, which were 1.25 cm x 1.9 cm x approximately .75 cm in the direction of magnetization, were arranged on mild steel plates with the 1.9 cm dimension along the azimuthal direction of the thruster chamber,

to simulate the original ceramic bar magnet geometry. The peak magnetic field strength was thereby increased from 1.5 kG to 3 kG, while holding the magnetic field geometry nearly constant. At the time of the magnet change, the electrodes were changed to another set similar to the original except for the larger accel grid holes in a central hexagonal section approximately 15 cm across.

A power measurement independent of that given by the rf voltage, current, and phase angle, shown in Figure 3.4 was obtained with a Byrd RF Power Meter, mounted on the secondary side of the isolation transformer. However, the Byrd meter gave spurious results when the plasma impedance was much different from 50Ω.

For ion beam extraction the thruster shell was biased to a positive high voltage of about 1100 volts and the SHAG accelerator was held at 300 to 500 volts negative with respect to vacuum tank ground. The screen grid could be biased up to 60 volts negative with respect to the thruster shell, but was usually left floating.

The argon gas feed could be maintained at a constant amount through a piezoelectric valve and was measured by two NASA LeRC furnished Hastings flowmeters in parallel. The output reading of the flow meters was converted to equivalent amperes of argon ion current by a calibration curve furnished by NASA LeRC. The gas flow could also be pulsed to correlate the former TRW pulsed mode thruster test results to the LeRC continuous tests. In the pulsed mode the pulse width and magnitude could be varied, and the pulse could also be delayed or advanced with respect to the rf power, which also could be pulsed.

A small tungsten filament inside the thruster was heated with DC power and biased negative to act as a source of seed electrons to enable the initiation of the rf discharge. For pulsed operation with pulses every few seconds the filament was left on continuously; for continuous operation the filament was required only for initiation of the discharge. The voltage on a cylindrical Langmuir probe inside the thruster could be swept (-30 volts to +30 volts with respect to the thruster shell) using a sawtooth generator and isolation transformer, and the collected current detected with a current probe.

3.2.3 Results

Presented here are results on the RFI thruster operating efficiency over an extracted beam current range of .4 to 3 amperes, and an equivalent mass flow range of 3.9 to 6.6 amperes, with both ceramic and Samarium Cobalt magnets. Also presented is a comparison of thruster operation with and without beam extraction.

In the ultimate design of an rf thruster discharge power system, consideration must be made of power processor losses, rf amplifier or oscillator losses, rf circuit losses, and finally plasma discharge losses. In this study, only the last two elements are considered, and, for the purpose of improving the understanding of discharge operation, the circuit and plasma losses were separated by the following method. The gas flow, beam and accelerator grid voltages were set to the desired values, and the rf power was increased until the beam current reached the desired value. RF input current, tank voltage, and relative phase angle were recorded and used to compute the total rf input power, including circuit losses. In order to obtain the circuit losses alone, gas flow was set to zero and the rf drive was set to reproduce the same value of the tank voltage as with a discharge. The actual rf discharge losses were obtained by subtracting the circuit losses from the total input power. A typical application of this procedure is illustrated in Figure 3.7 which shows total rf input power, circuit losses, and their difference for beam currents from .4 to 3 amperes. The data was obtained with ceramic magnets and a mass flow of 6.6 amperes equivalent. The circuit losses are a weakly increasing function of beam current, and are well approximated by the linear fit for P_c in watts and I_B in Amperes,

$$P_c = 21 + 6I_B \qquad (6)$$

For these data, the discharge losses (total rf input power minus circuit losses) correspond to 230eV/ion independent of beam current from .4 to 3 amperes, within experimental error. The remainder of this section reports only discharge losses with rf circuit losses subtracted out. For all data presented, the inclusion of circuit losses raises the eV/ion figure by 10 to 15 for beam currents above 2 amperes.

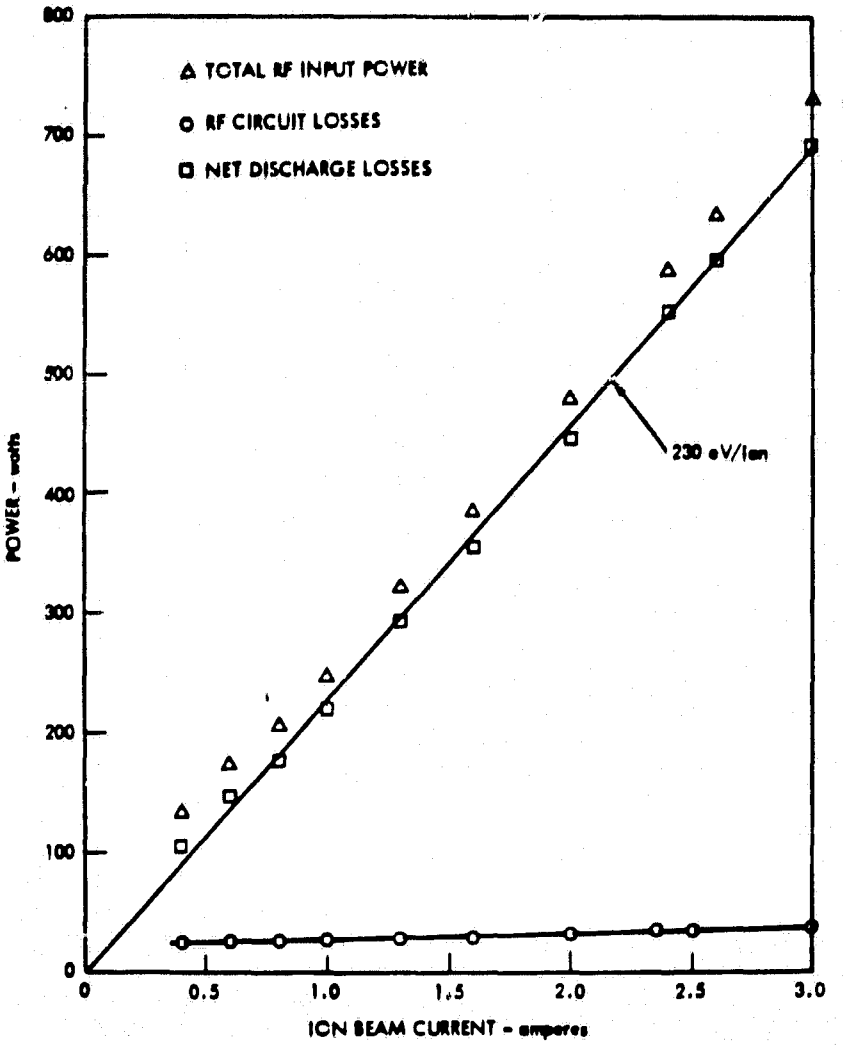

Figure 3.7 Total rf input power, circuit losses, and their difference (net discharge losses) as a function of ion beam current. Argon flow rate was 6.6 ampere equivalent.

Performance of the thruster with ceramic magnets is summarized in Figure 3.8, which shows discharge losses as a function of propellant utilization for mass flows of 4.2, 5.3, and 6.6 amperes equivalent. For mass flows above about 5 amperes, the minimum discharge losses were independent of mass flow to within experimental error, with a value of 220 $\pm$ 10 eV. Since the design beam current level for the 30cm Argon thruster is 4.4 amperes, performance is best characterized at a mass flow rate of approximately 5.3 amperes, which would yield a utilization of .83. Unfortunately, it was not possible to obtain beam currents in excess of 3 amperes due to power supply and grid arcing problems, so that the "knee" of the performance curve is not obtained in these data.

Thruster performance curves with Samarium Cobalt magnets are illustrated in Figures 3.9 and 3.10 at mass flow rates for 6.6 and 3.9 amperes equivalent, respectively. Also shown for comparison are the ceramic magnet performance curves at similar flow rates. At a flow rate of 6.6 amperes, thruster performance with ceramic and Samarium Cobalt magnets was identical within experimental error. At the lower flow rate, the $SmCo_5$ magnets resulted in very slightly (10 to 15%) better performance. Some possible interpretations of these results are discussed in section 3.5.

A comparison was made of the determination of discharge losses with and without beam extraction, utilizing the Samarium Cobalt configuration. For measurements without beam extraction, the screen and accel grids were electrically connected and biased at -40 volts with respect to the thruster walls, which were held at ground potential. It was found that when the ion current collected by the screen plus accel combination was multiplied by a factor of .7 to adjust for ion losses to the screen during normal beam extraction, the discharge losses with and without extraction were the same to within experimental error for propellant utilizations of less than about .4. At high utilizations, as expected, the discharge loss figures obtained without beam extraction were significantly lower than with extraction, due to recycling of ions recombining on the screen. Indeed, without extraction apparent utilization of greater than one could easily be obtained. Comparison results at flow rates of 6.6 amp and 3.9 amp equivalent are illustrated in Figure 3.11.

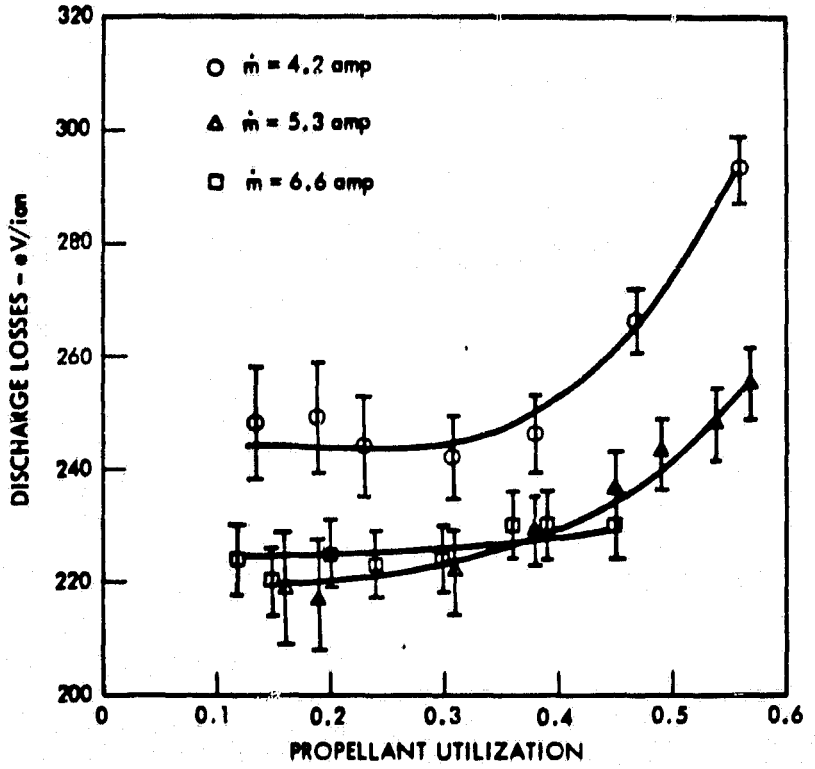

Figure 3.8 Performance of RFI Multicusp Thruster with ceramic magnets (1.5 kG) at flow rates of 4.2, 5.3, and 6.6 ampere equivalent Argon flow rates.

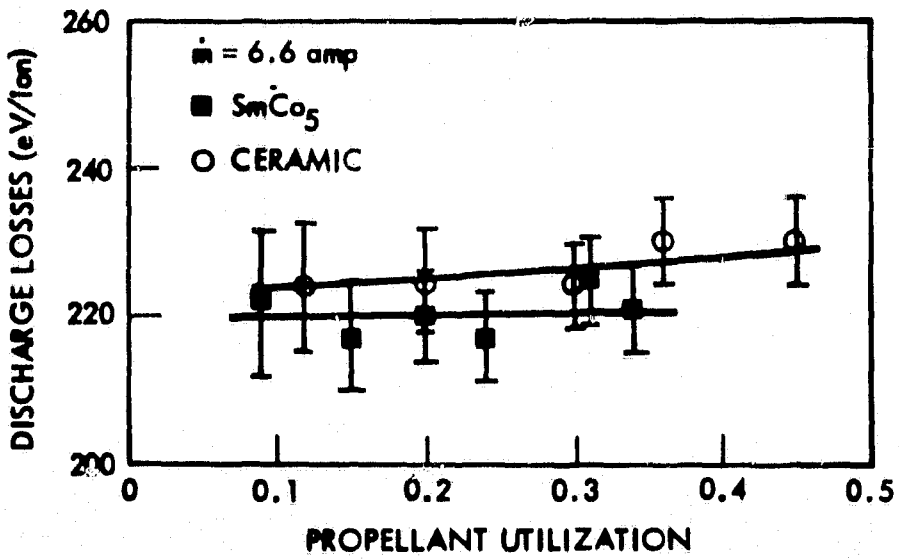

Figure 3.9 Comparison of thruster performance with Samarium Cobalt (3 kG) and ceramic (1.5 kG) magnets and mass flow rate of 6.6 ampere equivalent.

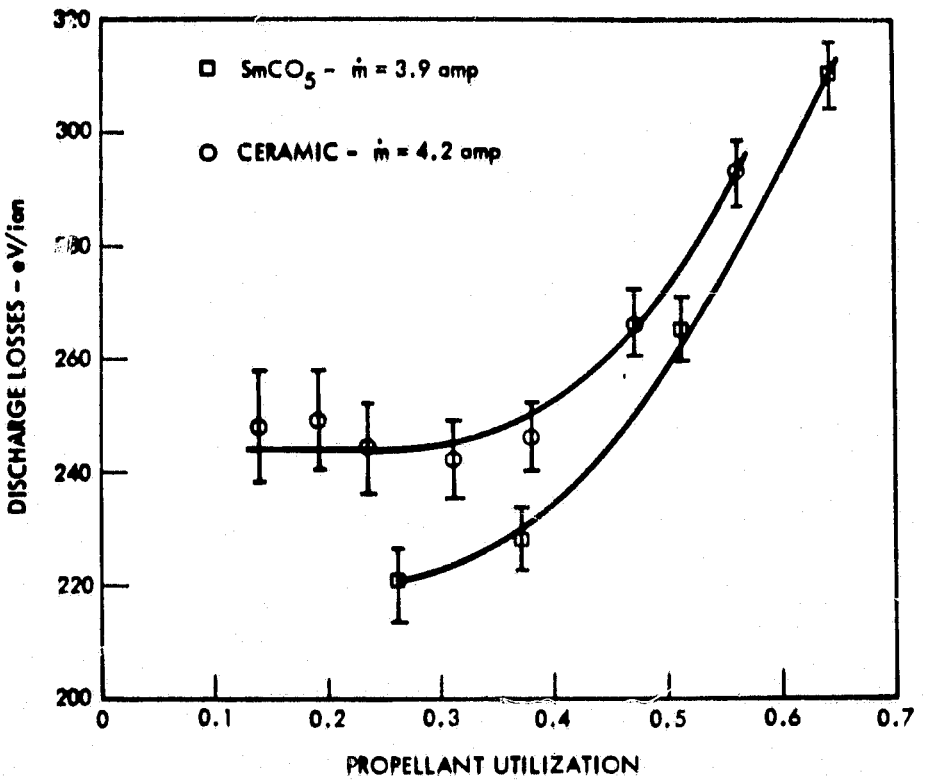

Figure 3.10 Comparison of thruster performance with Samarium Cobalt and ceramic magnets at mass flow rate of 4.2 ampere equivalent. Slightly improved low pressure performance with $SmCo_5$ magnets is probably a result of improved confinement of energetic electrons rather than ions.

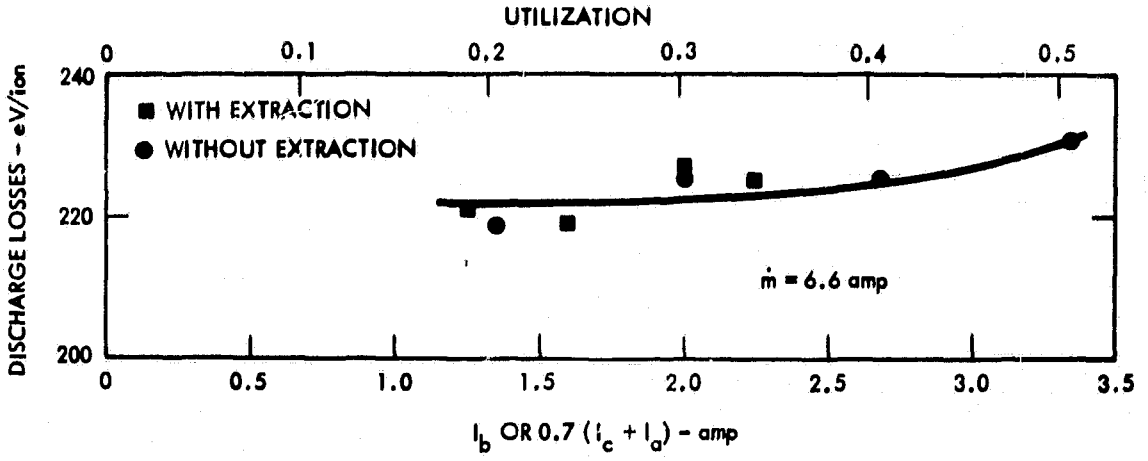

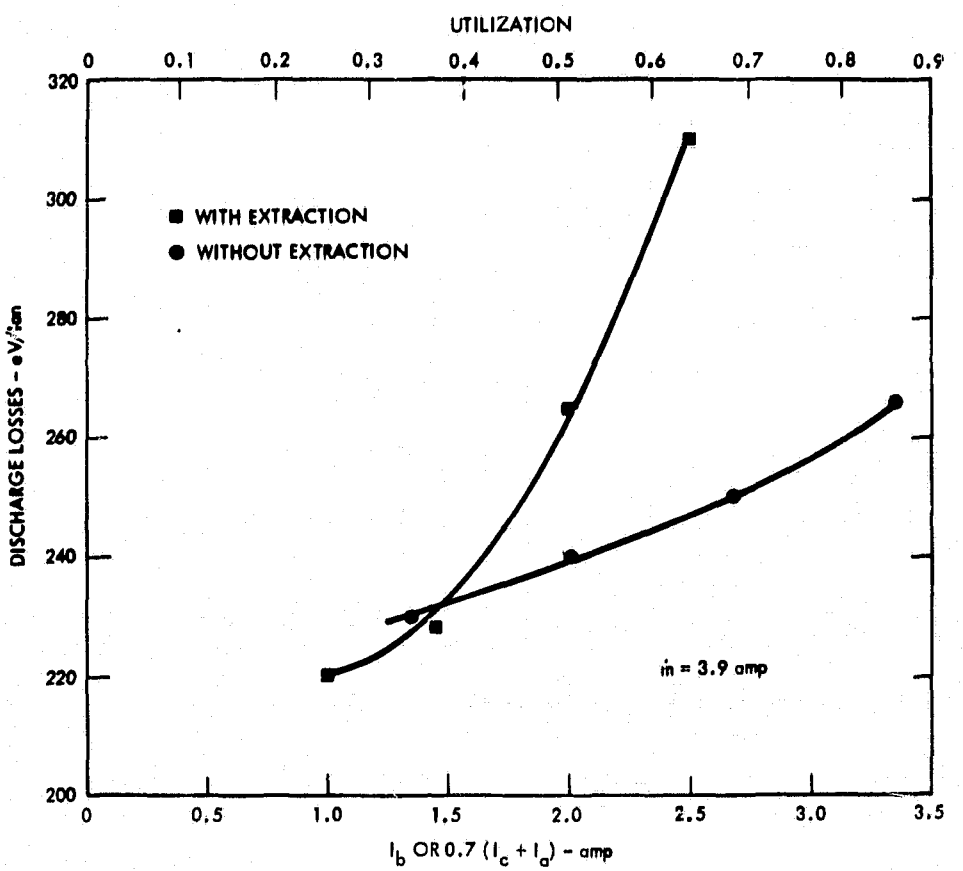

Figure 3.11 Comparison of discharge losses measured with and without beam extraction, as a function of beam current or equivalent beam current, obtained by correcting the collected screen plus and current by the factor .7. Actual screen transparency was approximately .67, but correction factor of .7 was chosen as best fit.

Discussion of these results and conclusions are presented in the next two sections.

3.3 RF COUPLING PHYSICS

3.3.1 Frequency Dependence of Discharge Efficiency

To examine the dependence of discharge and rf circuit efficiency on frequency, a series of experiments was performed without beam extraction but with plasma ions collected on the screen and accel biased together at -40 volts. The antenna circuit resonant frequency was varied by changing the capacitance and/or the inductance in the resonator network of Figure 3.4. The rf oscillator was then adjusted to the resonant frequency and the source operated at a given gas pressure to measure the rf power coupled to the plasma, the rf antenna ohmic losses, and the discharge efficiency measured in eV/ion. To allow direct comparison of the many results, the antenna ohmic losses were not included in the discharge efficiency. The results for antenna 2 are shown in Table 3.2 and plotted in Figure 3.12. To within experimental error the discharge efficiency is approximately independent of frequency over the range tested. This behavior is as expected for a non-resonant electron heating process, and leaves us free to choose the frequency so as to minimize rf circuit losses.

The two main areas for circuit losses are the conversion losses of the rf oscillation (or power amplifier) and resistive losses in the antenna, which depend on both antenna current and frequency. From (2.13), the antenna current required to sustain an rf discharge has the frequency dependence

$$I_A \propto \left(1 + \frac{\nu^2}{\omega^2}\right)^{1/2} \qquad (3.3.1)$$

under the assumption that the spatial dependence of the induced electric field is independent of frequency. The measured frequency dependence of the antenna current is illustrated in Figure 3.13, which shows the product of antenna current and frequency, versus frequency. Also shown in Figure 3.13 are plots of $I_A f$ with I_A given by equation (3.3.1) for assumed collision frequencies of 10^7, 1.5×10^7 and 3×10^7 s^{-1}. The theoretical curves are normalized to $I_A f = 21.5$ amp-MHz at

Table 3.2 RF Thruster Discharge Data for Different Frequencies

(No Beam Extraction)

FREQUENCY (kHz)	ARGON PRESSURE ($x10^{-4}$ torr)	SCREEN+ ACCEL CURRENT (A)	ANTENNA VOLTAGE (rms volt)	ANTENNA CURRENT (rms A)	RF CURRENT (rms A)	PHASE (deg)	RF POWER (watts)	ANTENNA LOSSES (watts)	DISCHARGE POWER (watts)	DISCHARGE EFFICIENCY (eV/ion)
361	2.6	2.0	337	62.9	1.50	~0	506	248	258	129
718	2.6	2.0	325	30.5	1.16	~0	377	99	278	139
1065	2.6	2.0	308	24.7	1.16	~0	357	67	290	145
1458	2.6	2.0	214	19.7	1.44	1	308	30	278	139
718	2.6	3.6	338	32.0	1.84	~0	622	109	513	142
1070	2.6	3.6	333	27.0	1.82	~0	606	80	526	146
1469	2.6	3.5	226	~20	2.29	0	518	33	485	138
361	5.3	3.0	311	60.3	1.97	~0	613	218	395	132
718	5.3	3.6	310	29.8	1.86	~0	577	88	489	136
1070	5.4	3.6	303	24.2	2.07	~0	627	69	558	155
1500	5.3	3.0	193	~17	2.57	0	496	24	472	157

Notes: 1. RF Power = (Antenna Voltage) (RF Current) (cos phase)

2. Screen and Accelerator Electrodes biased together at -40 volts

3. Discharge Efficiency = (RF Power - Antenna Losses)/Screen+Accelerator Current

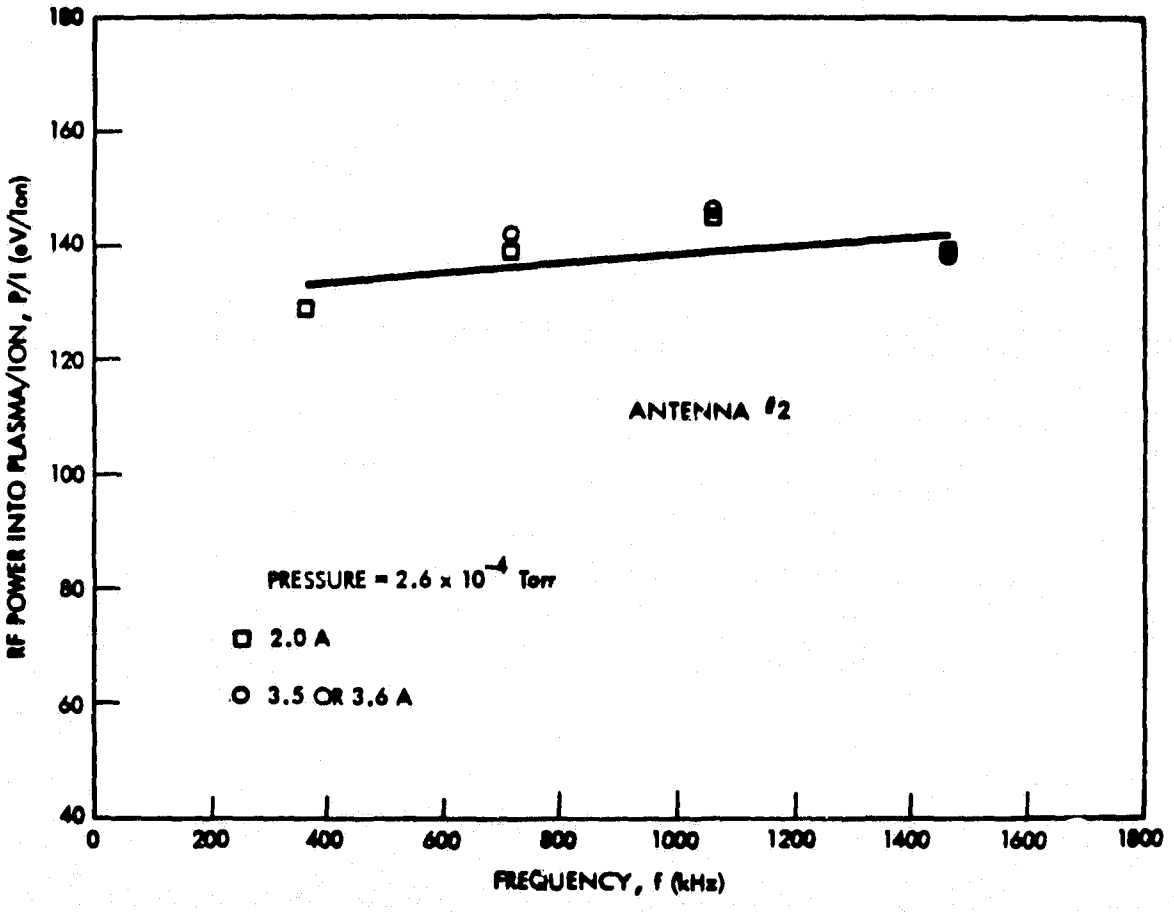

Figure 3.12 RF Power into Plasma (Antenna Losses Deducted) Versus Frequency

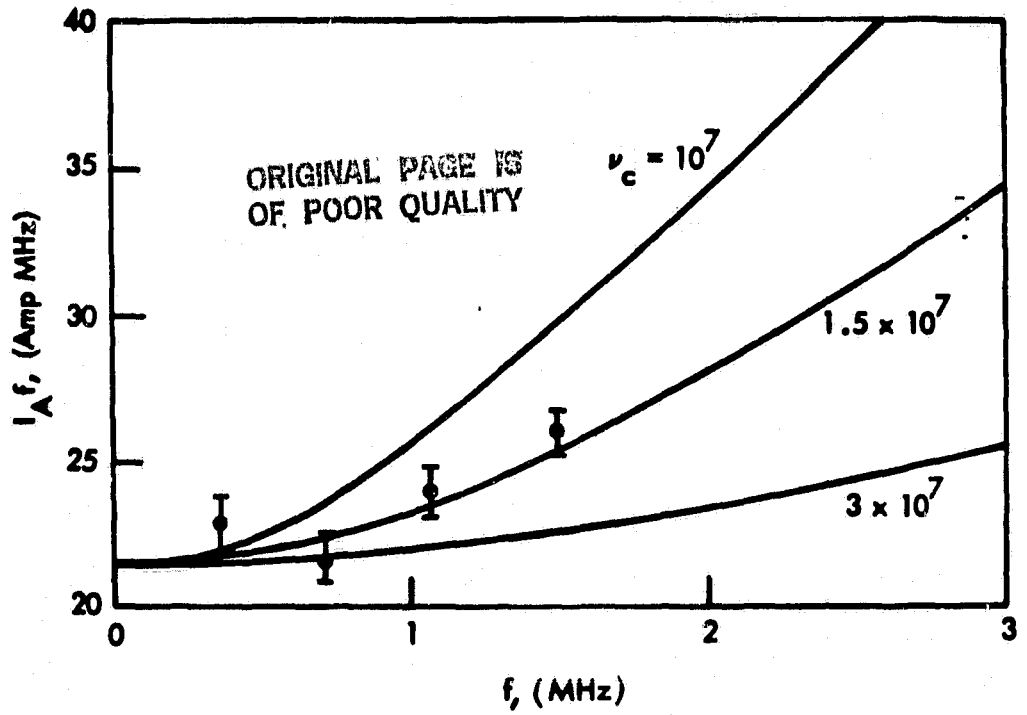

Figure 3.13 Antenna Current Times Frequency versus Frequency

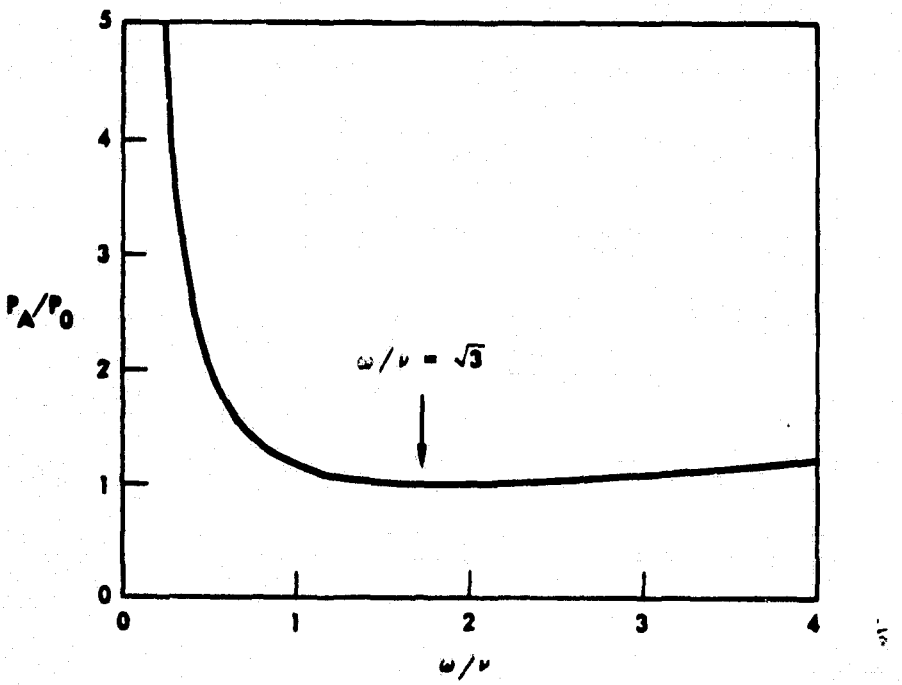

Figure 3.14 Normalized Antenna Power versus Quotient of Driving and Collision Frequencies

f = 0 in order to obtain the best fit to the data at the low frequency end. The observed frequency dependence of the antenna current is seen to agree reasonably well with the theoretical form given by (3.3.1) with an effective collision frequency of $\nu = 1.5 \times 10^7\ s^{-1}$.

Combining (3.3.1) and the frequency dependency of the antenna resistivity (i.e., the skin effect), the frequency dependence of the antenna resistive power is

$$P_A = I_A^2 R_A \propto \left(\frac{\nu}{\omega}\right)^{3/2} + \left(\frac{\nu}{\omega}\right)^{1/2} \qquad (3.3.2)$$

which has a minimum at a frequency

$$\omega = \sqrt{3}\,\nu \qquad (3.3.3)$$

Figure 3.14 is a plot of P_A normalized to the minimum value, and shows that the minimum is very broad, allowing a considerable range over which the rf frequency may be chosen to optimize some other aspect of the total system. Since rf oscillator (or amplifier) efficiency tends to decrease with increasing frequency, it is to be expected that the optimum frequency will be considerably lower than that given by (3.3.3). For the experimentally determined value of $\nu \approx 1.5 \times 10^7\ s^{-1}$, (3.3.3) predicts a frequency of approximately 4.1 MHz for minimum antenna loss. For our typical operating frequency of 1.5 MHz, (3.3.2) predicts antenna losses about 60% higher than the minimum. Measured antenna losses at an operating frequency of 1.5 MHz represent only about 5% of total discharge power, and the slight improvement which might be obtained at higher frequencies would most likely be offset by increased rf conversion losses.

3.3.2 Antenna Loading

The study and analysis of plasma loading of the rf antenna impacts several facets of thruster design. Knowledge of the effective impedance presented to the antenna, and its dependence on thruster operating parameters, in particular beam current and propellant flow rate, is of course critical to the design of the rf power and matching system. Study of the dependence of loading on antenna geometry (e.g. wire diameter, length, coil diameter, etc.) provides input data for optimization of antenna design. In addition, the loading characteristics provide some insight into the details of the interaction between the rf fields and the plasma.

An equivalent circuit analysis of the plasma loading of the antenna was performed for one rather complete set of data obtained at the Lewis Research Center tests. The data, which was obtained with the Samarium cobalt magnet configuration at flow rates of 60,100 and 150 SCCM and beam currents from .4 to 2.6 amperes, is summarized in Table 3.3. At each beam current and flow rate, the rf frequency was adjusted for $0 \pm 2^{\circ}$ phase difference between the antenna tank circuit voltage and input rf current, and voltage, current and frequency were recorded.

An interactive terminal version of the IBM Electronic Circuit Analysis Program (ECAP) was used to analyze the data in terms of a single equivalent circuit model of the plasma load. In that model the plasma is replaced by an inductor and resistor in series with each other and in parallel with the antenna, as shown in Figure 3.15. This is the simplest equivalent circuit which retains both the resistive and reactive plasma response, as described in Section 2. For each pair of values I_{rf} and frequency, with the measured values of tank capacitance C, lead inductance, L, and antenna inductance, L_A, the inductance L_p, and resistance, R_p, were varied to obtain a best fit to the measured tank voltage, V_T, and 0° phase angle between V_T and I_{rf}. In each case, the voltage was fit to within .4 volts rms and the phase to within $.2^{\circ}$, well within the experimental error.

The values of R_p and L_p are given in Table 3.3 and illustrated in Figures 3.16 and 3.17 as a function of beam current, with Argon flow rate as a parameter. Each set of values of

Table 3.3 Results of Equivalent Circuit Analysis

MEASURED VALUES					FIT RESULTS	
FLOWRATE (SCCM)	FREQUENCY f (kHz)	BEAM CURRENT I_b (A)	RF DRIVE CURRENT I_{rf} (rms A)	TANK VOLTAGE V_T (rms volt)	PLASMA RESISTANCE R_p (ohms)	PLASMA INDUCTANCE L_p (μh)
150	1542	2.6	2.92	210	19.13	.883
(9.9 A	1540	2.5	2.88	210	19.2	.91
equiv.)	1535	2.4	2.70	206	20.4	.95
	1530	2.25	2.58	204	21.7	.97
	1520	1.8	2.10	195	25.3	1.20
	1510	1.6	1.90	190	29.5	1.15
	1502	1.3	1.60	185	35.5	1.25
	1492	1.0	1.34	180	42.5	1.36
	1485	.7	.93	175	61.1	1.82
100	1523	2.25	2.48	214	24.05	1.06
(6.55 A	1520	2.0	2.30	209	25.4	1.10
equiv.)	1509	1.6	1.88	200	31.0	1.28
	1500	1.28	1.60	194	37.2	1.35
	1495	1.0	1.30	187	45.3	1.51
	1489	.75	1.08	183	54.5	1.68
	1485	.60	.87	180	67.4	2.0
	1480	.40	.68	177	87.9	2.05
60	1520	2.5	3.02	275	24.7	1.18
(3.9 A	1520	2.0	2.40	240	29.2	1.20
equiv.)	1500	1.45	1.70	215	38.2	1.47
	1490	1.0	1.23	200	51.5	1.70
	1480	.50	.66	188	99.3	1.72

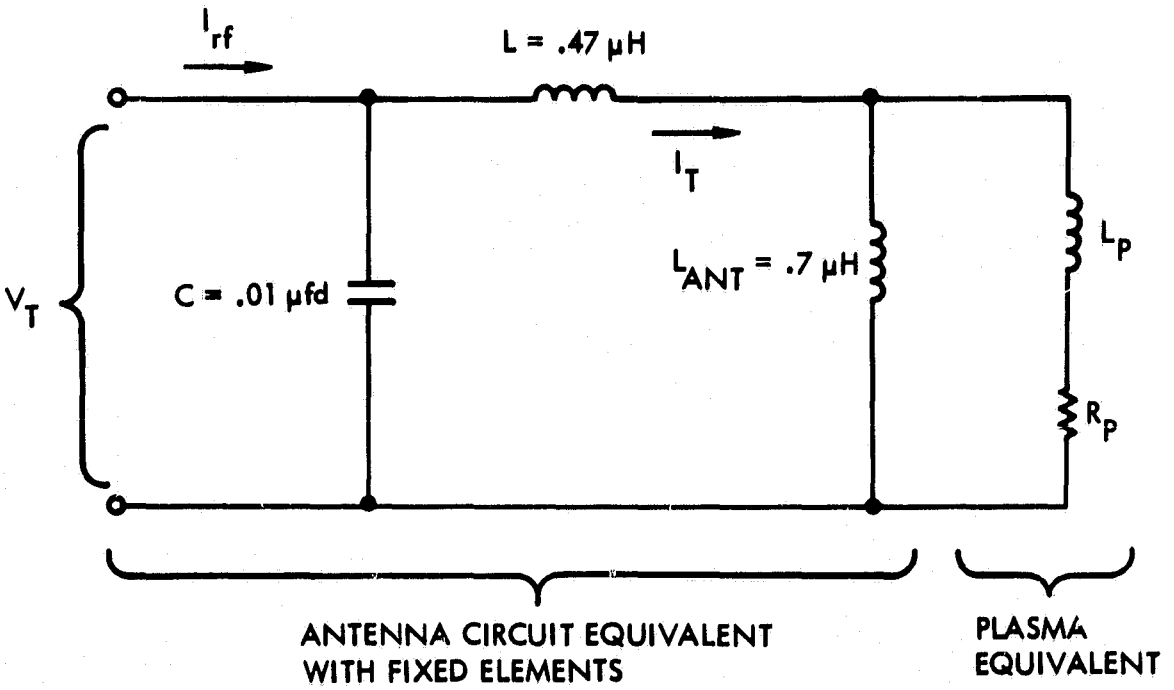

Figure 3.15 Equivalent Circuit Used for Analysis

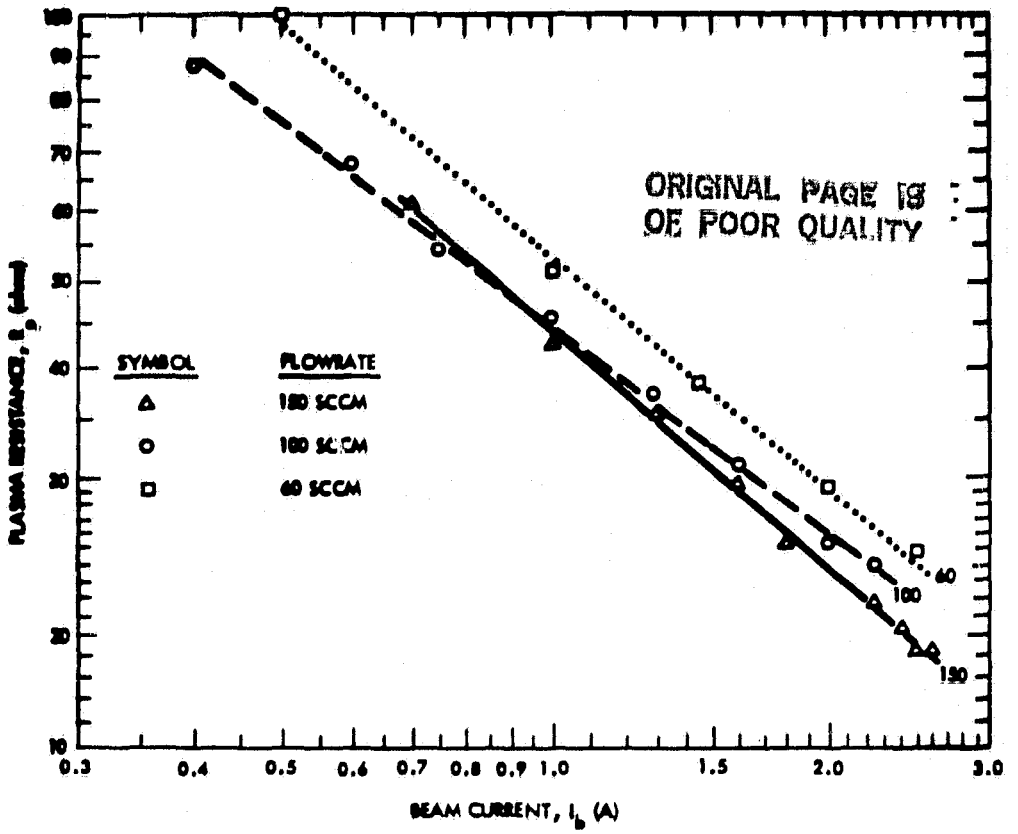

Figure 3.16 Plasma Resistance versus Beam Current

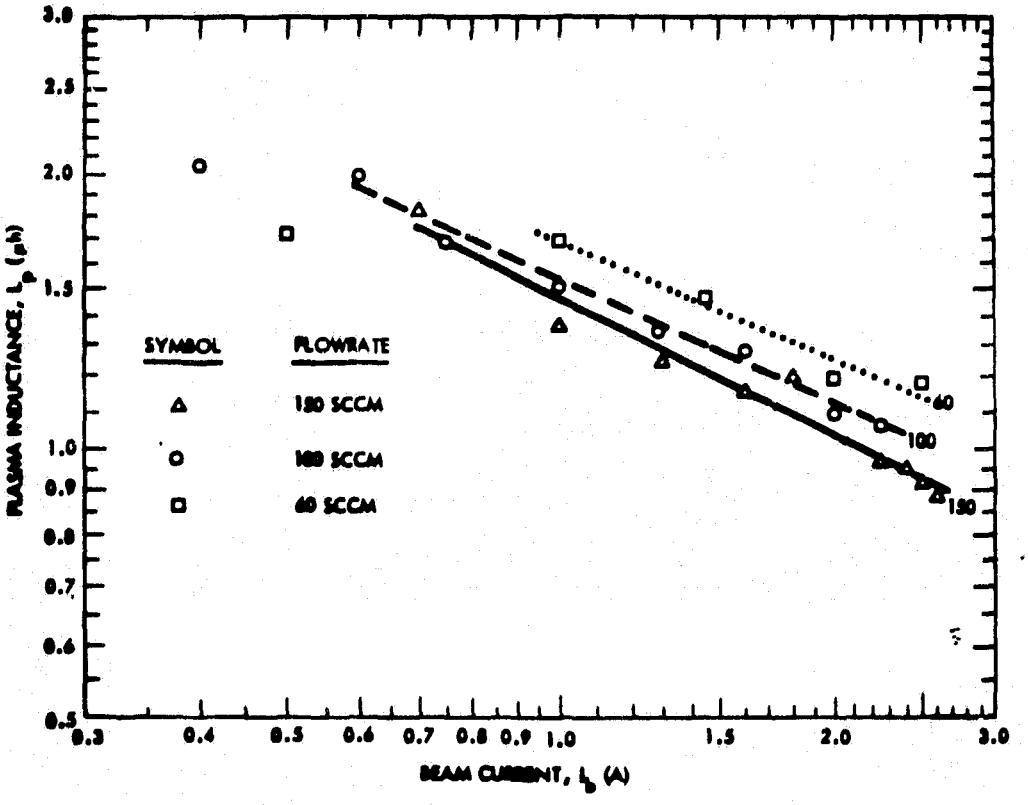

Figure 3.17 Plasma Inductance versus Beam Current

R_p and of L_p was fit to a power equation dependence on beam current by linear regression on the logarithms of the data. The resulting fits are shown by the solid lines in the figures and are explicitly:

$R_p = 44\ I_B^{-.88}\Omega$ at 150 SCCM

$R_p = 44\ I_B^{-.77}\Omega$ at 100 SCCM .

$R_p = 53\ I_B^{-.86}\Omega$ at 60 SCCM

$L_p = 1.5\ I_B^{-.50}\mu H$ at 150 SCCM

$L_p = 1.5\ I_B^{-.41}\mu H$ at 100 SCCM

$L_p = 1.7\ I_B^{-.43}\mu H$ at 60 SCCM

An interesting result here is that both the plasma resistance and inductance are nearly independent of neutral pressure (which is proportional to flow rate) over the range examined. Since the plasma resistivity is proportional to the electron momentum transfer collision frequency, these results provide rather strong evidence that electron neutral collisions are not the dominant sources of plasma resistivity. This is in agreement with the results of the study of the frequency dependence of the antenna current, described in section 3.3.1. The effective collision frequency of $1.5 \times 10^7 s^{-1}$ was approximately six times the electron neutral collision frequency at the operating pressure of 2.7×10^{-4} torr.

Langmuir probe measurements indicate that, for fixed neutral pressure (or flow rate), the electron temperature is independent of electron density over the range examined in these data. Therefore, the functional dependence on electron density of the equivalent plasma resistance and inductance is the same as the functional dependence on beam current. As discussed in section 2, the dependence of R_p on electron density is expected to be between n^{-1}, when the rf fields are unaffected by the presence of the plasma, and n^0 (i.e. independent of density), when the rf fields are confined to a skin depth less than the turn to turn spacing of the antenna. Thus, the experimental values indicate that the fields are not greatly perturbed by the plasma.

A series of tests was conducted to examine the dependence of rf circuit losses and discharge losses on antenna geometry, using antennas

2, 3 and 4, the geometries of which are described in section 3.1.5. The antenna current required to sustain a discharge, and therefore the rf tank circuit losses, was strongly dependent on antenna geometry. Antenna designs 3 and 4 each resulted in approximately a factor of two increases in circuit losses over antenna 2. As expected, the required antenna current decreased with increasing total antenna length and with decreasing antenna wire diameter, though quantitative characterization will require more extensive testing. Discharge losses (i.e. neglecting circuit losses) depended only weakly on antenna geometry, and appeared to depend only on the relative surface area of the antenna. Antenna 4, with 1/4 the surface area of antenna 2, gave an improvement of approximately 15 watts per ampere of screen plus accelerator current in tests without beam extraction. This corresponds to an improvement of about 21eV/ion with beam extraction.

3.4 PLASMA CHARACTERISTICS

Following tests of the RFI Multicusp Thruster at Lewis Research Center, a series of detailed measurements of the plasma characteristics was made at the TRW facility. The purpose of these tests was to obtain additional data to aid in the interpretation of the discharge loss characteristics of the thruster.

The thruster configuration and operating rf frequency were identical to those used in the first series of Lewis tests (i.e., ceramic magnets). A Langmuir probe was inserted through the side wall of the thruster, so that it could be moved across the thruster diameter. The probe shaft had a 90^{o} bend, so that rotation of the probe support shaft would allow measurements at other locations in the thruster as shown in Figure 3-18.

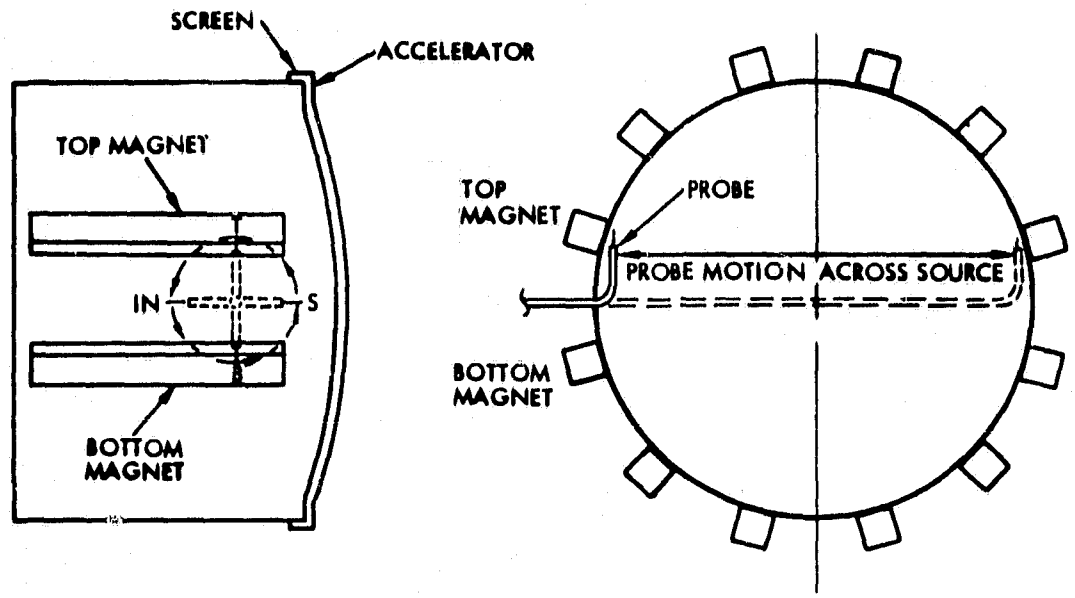

SIDE VIEW SHOWING PROBE ORIENTATIONS

S - NEAR SCREEN ELECTRODE

T - AT TOP MAGNET

B - AT BOTTOM MAGENT

IN - BETWEEN MAGNETS

(PROBE SHOWN AT "S" POSITION)

NOTE: PROBE IN "S" POSITION EXTENDS BEYOND END OF MAGNETS

EXHAUST VIEW SHOWING PROBE MOTION ACROSS SOURCE DIAMETER

(PROBE SHOWN AT "T" POSITION)

Figure 3.18 Experimental Setup for Movable Probe Inside RF Thruster

For measurements across the source diameter the probe was placed in the "S" position with its tip within 2 mm of the screen electrode at the edge of the source. With the probe biased about 60 volts negative, only ions were collected, and the ion current collected was recorded versus position in the source. Two traces are shown in Figure 3.19. For these traces the argon gas pressure as measured by the vacuum chamber ion gauge was 2.6×10^{-4} and the screen currents (no beam extraction) were 2.0 and 3.0 A. The right hand half of each curve is slightly lower than the left half due to the reduced plasma density from recombination on the probe lead as its area inside the source increased as it was pushed further inside the thruster. This explanation for the skew was demonstrated in two other ways. A drop in screen current, I_s, was seen as the probe was extended. Second, similar results but with much more skew were seen for a much larger diameter probe shaft. The flatness parameter, F, defined by Kaufman as the average source current density divided by the maximum current density, for these two curves are .58 and .63.

The probe was then used as a Langmuir probe to determine the electron temperature, plasma potential, and electron density in different locations. In particular, comparisons of these parameters for the "T" and "B" positions (in the magnetic cusps near the wall) versus the "IN" or the "S" positions were made. The "IN" and "S" positions were not equivalent, since in the "S" position the probe extended beyond the end of the magnets.

The results are shown in Figures 3.20 and 3.21. A single curve has been drawn for the T and B probe positions since there seems to be little difference between them except at the 3 1/2 cm point. At that position the probe in the T orientation was close to the antenna, and the local density may well have been lowered by recombination on it. In the next Figure separate curves have been drawn for the screen and the IN data although they are nearly identical from about 10 cm out to the wall. But near the center the IN density may be lower as indicated because of the presence of the antenna. The single data point at the center was taken with the probe rotated into the center of the antenna coil.

Comparing Figures 3.20 and 3.21 shows that the density varies only with radial position, and that there is no significant difference in

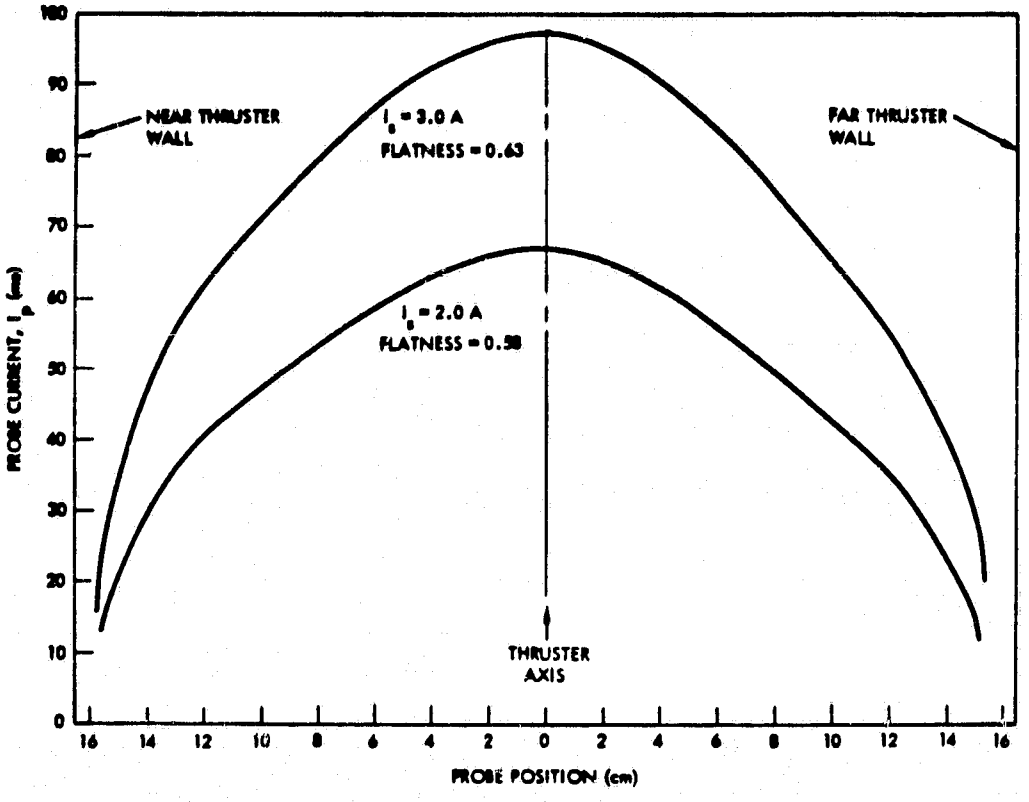

Figure 3.19 Probe Ion Current Traces Near Screen Electrode Inside RF Source

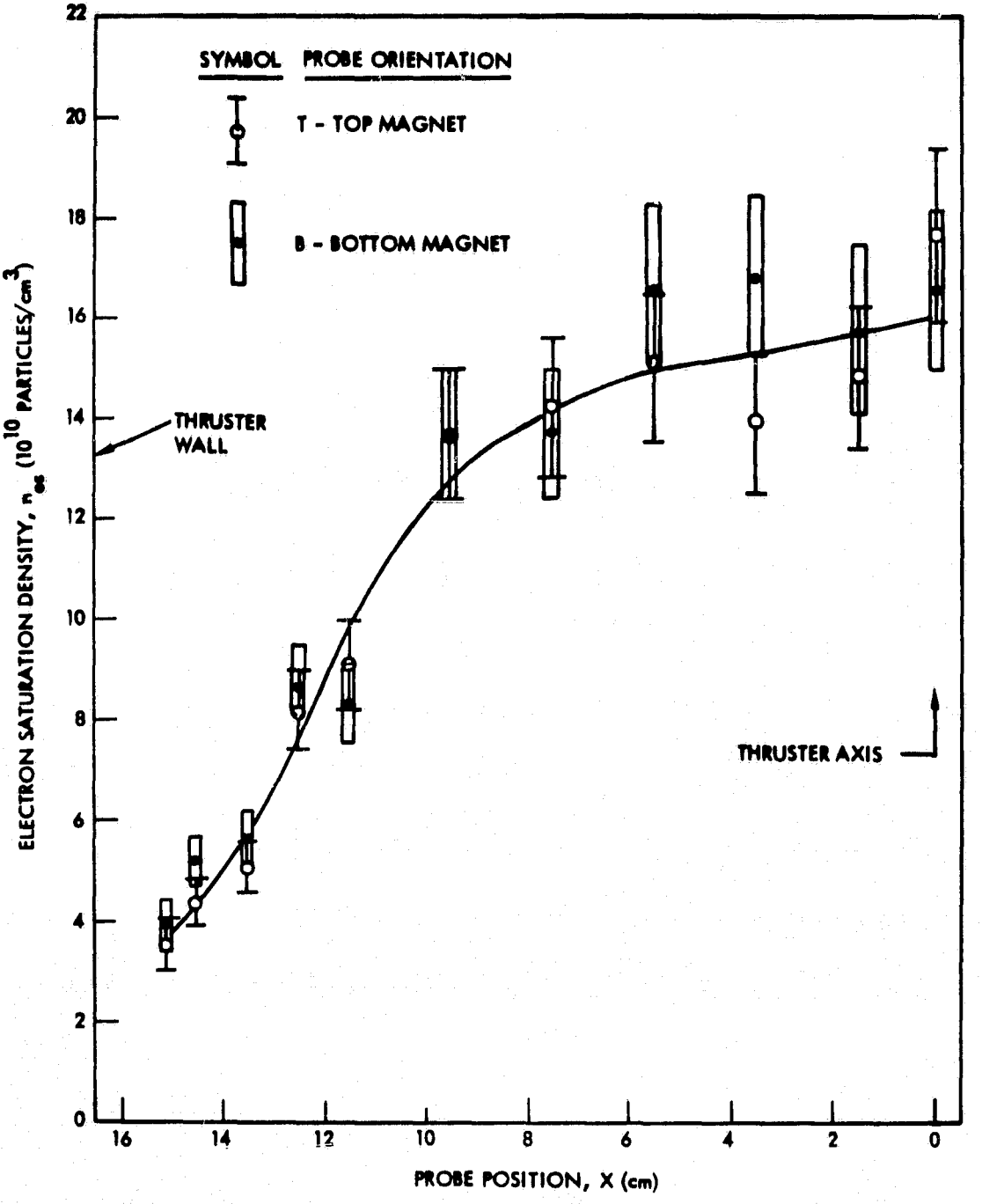

Figure 3.20 Electron Saturation Density Inside RF Thruster

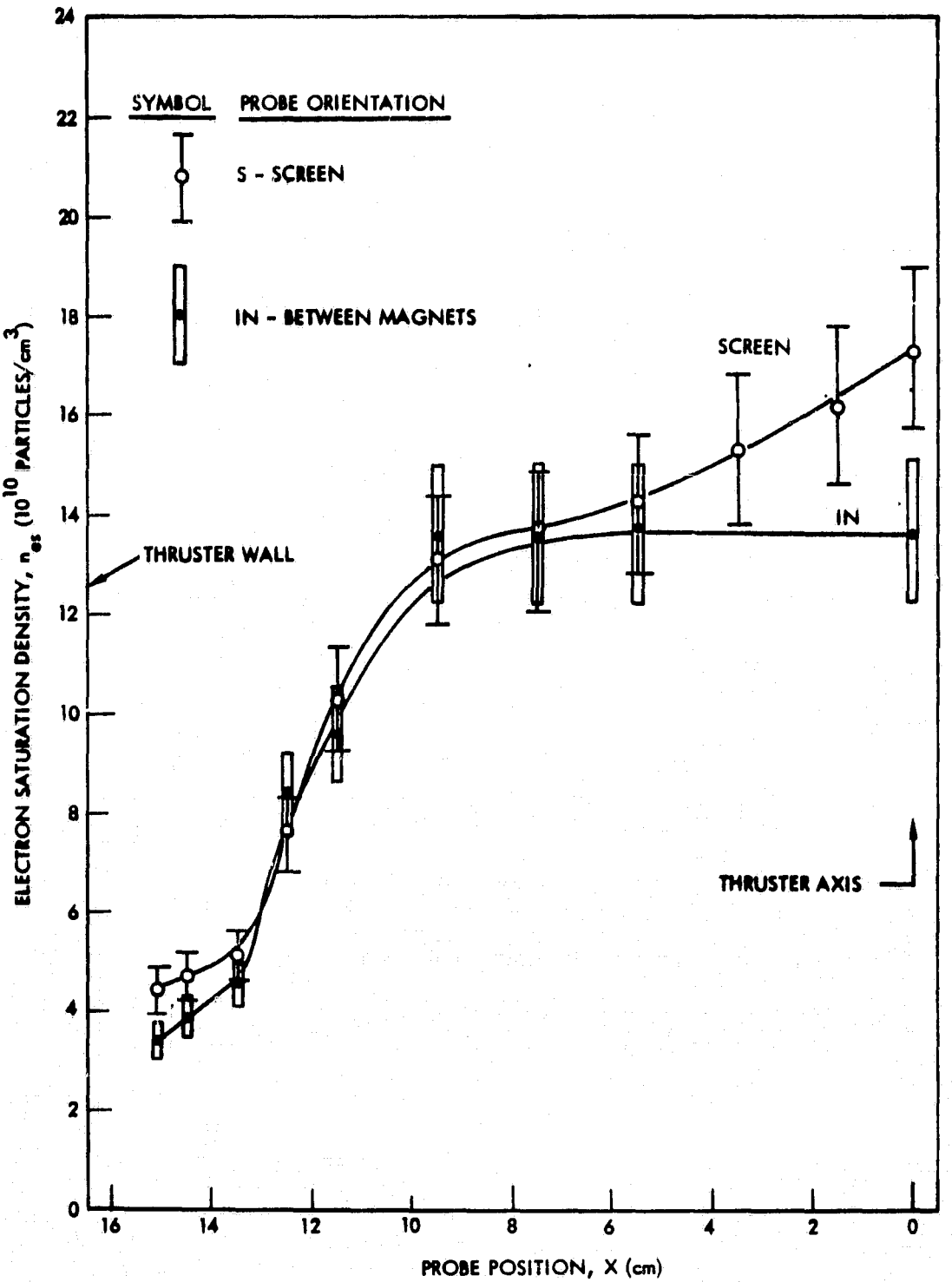

Figure 3.21 Electron Saturation Density Inside RF Source

density in the cusps (T and B near the wall) and in the spaces between cusps (IN) or beyond the ends of the magnets (S). The density does fall off rapidly, however, near the walls, and probably near the antenna, each of which is a surface where ion-electron recombinations can occur.

The electron temperatures determined from these Langmuir traces are plotted in Figures 3.22 and 3.23. The four probe orientations all gave electron temperatures of about 6 eV from the center out to about 8 cm. From 8 cm to the walls all electron temperatures dropped, with a much larger drop for the IN position, that is between the magnets. The sharp drop in electron temperatures between magnets started as the probe entered the dark region bounded by the cusps similar to those in the photograph of Figure 3.2.

An estimate of the total ion loss rate to the thruster walls may be made from a measurement of the change in plasma potential under various screen bias conditions, subject to the validity of certain assumptions concerning particle loss rates. In the electrical configuration for this experiment, the screen and accelerator grids are electrically connected and can be biased at any desired voltage, V_S with respect to the thruster walls. Assume that the ion current to the screen/accelerator combination is independent of bias. This assumption will be valid as long as

$$V_p - V_S \simeq kT_e \qquad (3.4.1)$$

where V_p is the plasma potential, and in so far as the plasma density near the screen is unaffected by change in bias. The same assumptions are made for the ion flux to the wall. Furthermore, we assume that the electron loss rate to the screen/accel combination and to the walls follows the Boltzmann relation

$$F_e \propto e^{-eV/kT_e} \qquad (3.4.2)$$

and that the electron temperature is uniform and independent of the bias conditions. When the screen/accelerator combination floats with respect to the walls, the electron and ion fluxes are equal

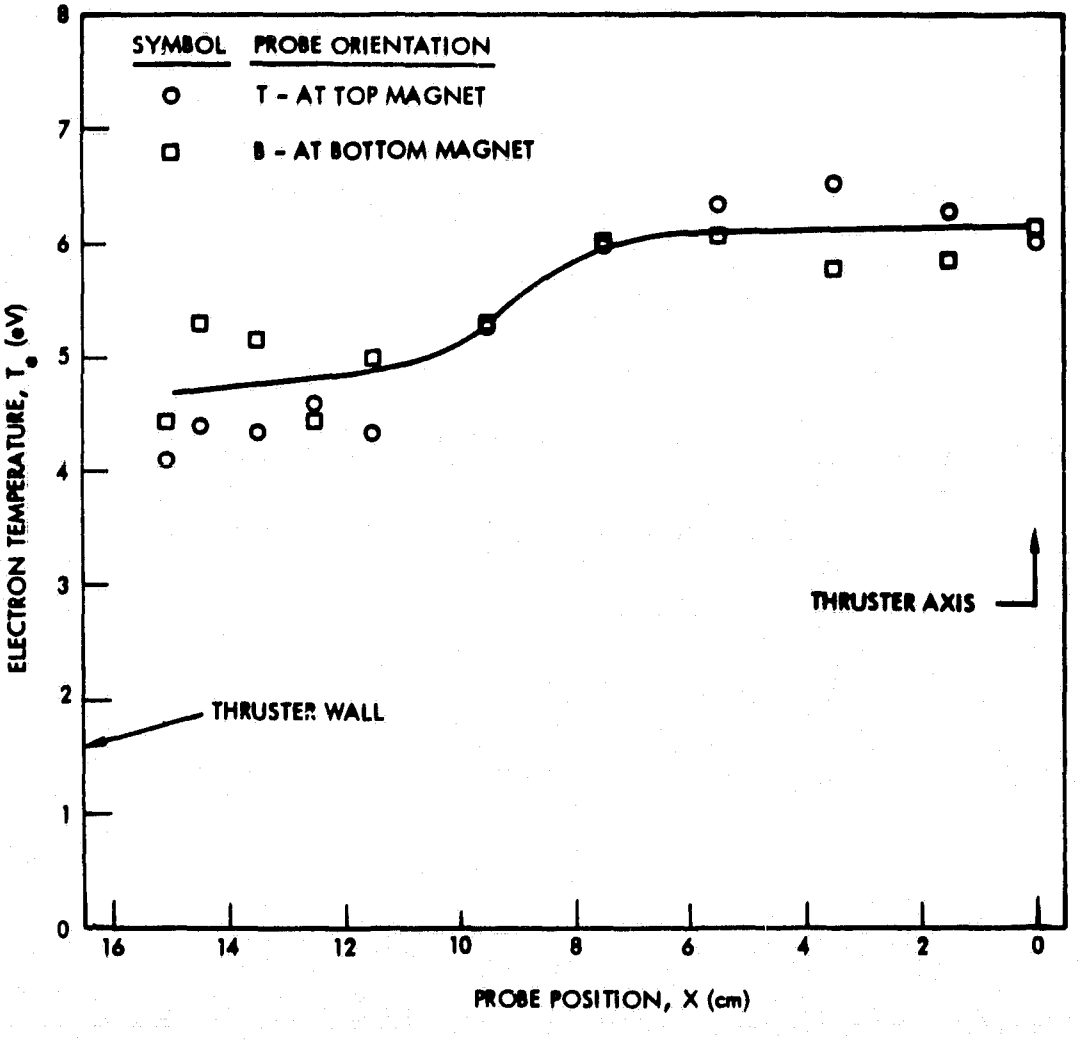

Figure 3.22 Electron Temperature Inside RF Source

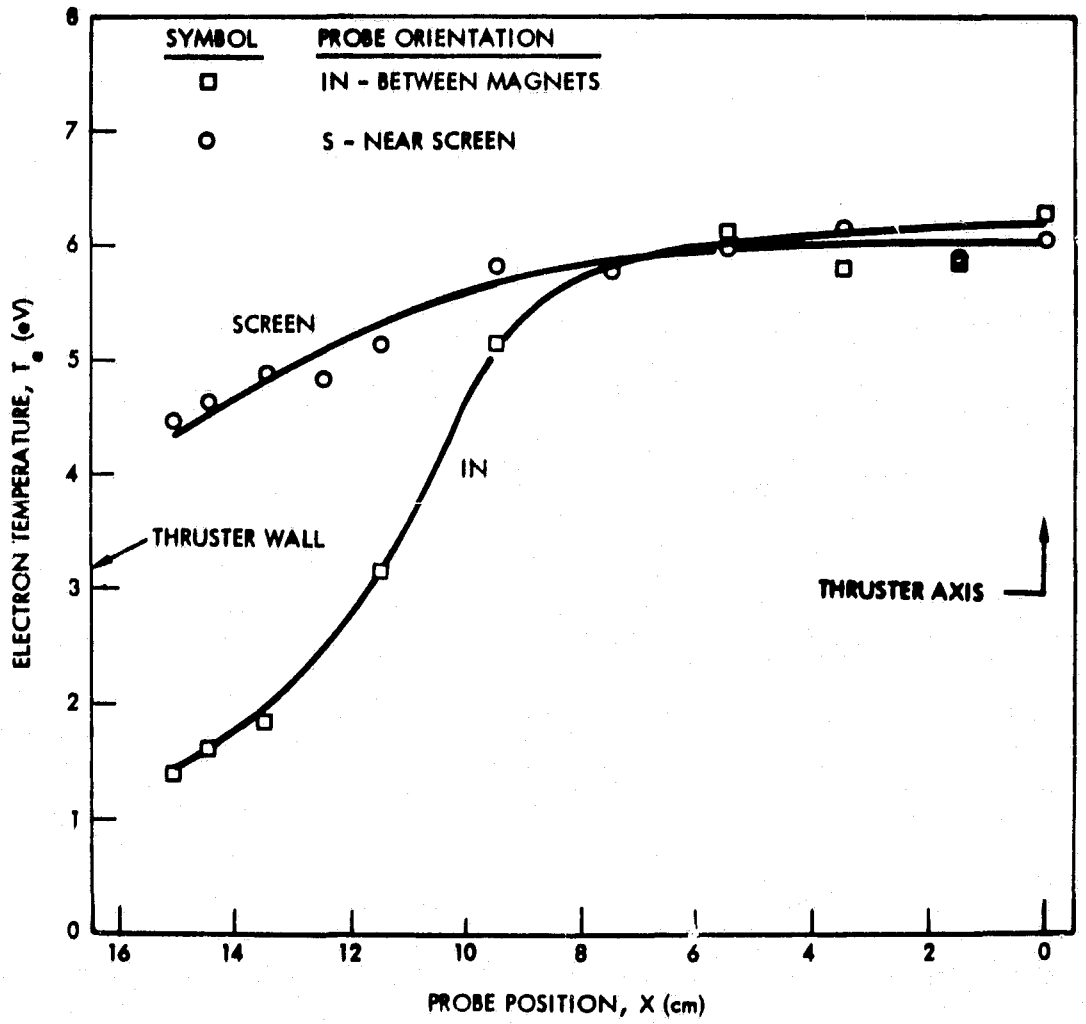

Figure 3.23 Electron Temperature Inside RF Source

$$F_{es} = F_{iw} \tag{3.4.3}$$

$$F_{ew} = F_{Iw}. \tag{3.4.4}$$

If the difference between the screen/accelerator potential and wall potential is increased by δV_s, a fraction of the electron flux $I_e = F_{es}$ is reflected from the screen and must be collected by the wall. As a result, the plasma potential shifts by δV_p such that

$$I_e = F_{ew} (e^{-\delta V_p/kT} - 1) \tag{3.4.5}$$

Using relation (3.4.4) and rearranging yields

$$F_{iw} = \frac{I_e}{e^{-\delta V_p/kT} - 1} \tag{3.4.6}$$

where I_e is the bias supply current and δV_p is measured with a Langmuir probe. The value of interest for computation of discharge losses is the ratio of the ion wall current to the beam current. The equivalent beam current is obtained by multiplying the screen/accelerator combination ion current, measured at a bias of -40V, by a transparency factor of .7. Values for the wall ion current normalized to the beam current obtained by this method are plotted in Figure 3.24, as a function of the change in screen potential. By performing the measurement at a number of different screen potentials, a check is provided on the validity of the Boltzmann assumption for electron losses. For the data of Figure 3.24,

$$\frac{I_w}{I_b} = .82 \pm .1 \tag{3.4.7}$$

for changes in screen potential up to 7 volts, indicating that the Boltzmann relationship holds. For larger changes in screen potential, the values obtained for Iw/I_b fall monotonically with increasing δV_s. At the larger values of δV_s, some, if not all, the assumptions made in the interpretation are probably invalid. Indeed, the Langmuir probe measurement show significant changes in the electron temperature profiles for large δV_s.

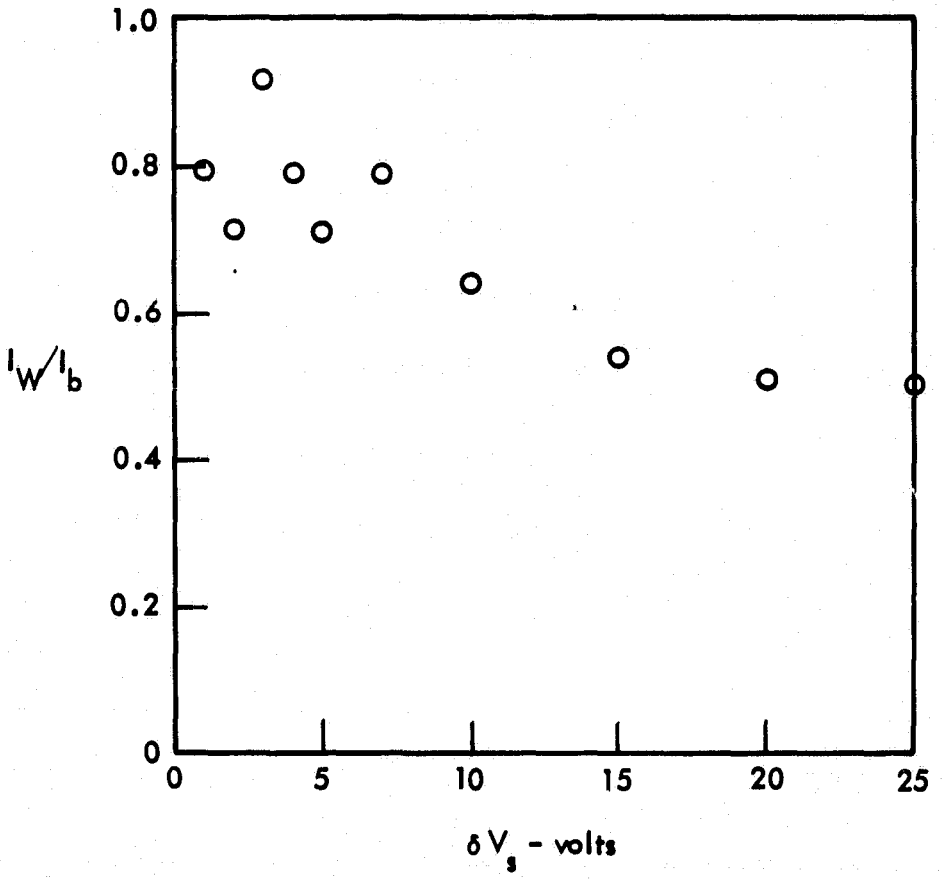

Figure 3.24 Normalized Wall Current versus Potential Change

This technique, with appropriate modifications to the interpretation was used to analyze data obtained at the Lewis Research Center tests with and without beam extraction, with the result

$$I_w/I_b \simeq 2.1 \pm .6$$

The large discrepancy between this result and the result (3.4.7) is not understood at this time.

The technique described here is a potentially powerful tool for estimating wall losses, but may be subject to significant error due to differences in particle loss dynamics to the cusp regions and between the cusps. The technique could be improved substantially, and tested more thoroughly, in a geometry where the cusp surfaces and surfaces between cusps could be separately biased.

3.5 INTERPRETATION OF DISCHARGE LOSSES

In this section we attempt to interpret the experimentally measured discharge losses in the RFI Multicusp Thruster in terms of fundamental plasma production and loss mechanisms and identify areas where improvements may be made.

In analyses of ion sources, it has proven useful[1] to express the discharge losses per beam ion as

$$\varepsilon_b = \varepsilon \frac{I_t}{I_b} \tag{3.5.1}$$

where ε is the energy expenditure per ion created, I_t is the total production rate (in units of electrical current) and I_b is the ion beam current. ε includes ionization and excitation losses and electron and ion convective energy losses. Recognizing that the ion convective energy loss is negligible and that the electron convective energy loss is a strong function of the potential of the loss surface and the temperature of the electrons lost to the surface, we may more accurately replace (3.5.1) with

$$\varepsilon_b = \frac{\sum_j \varepsilon_j I_{ej}}{I_b} \tag{3.5.2}$$

where

$$\varepsilon = \varepsilon_i + \varepsilon_{ex} + \varepsilon_{ec} \tag{3.5.3}$$

and we have used the fact that the total electron loss rate equals the total ion loss rate.* ε_i is the ionization energy, ε_{ex} the excitation energy, ε_{ec} the electron convective energy loss, and the summation is over the thruster electron loss surfaces, j. For Argon, ε_i = 15.7 eV and we will approximate ε_{ex} as equal to ε_i. As shown in appendix A, the average electron convective loss energy for a Maxwellian distribution is

*For a DC discharge, the discharge electron current would have to be included as a separate term without ε_i and ε_{ex}.

$$\varepsilon_{ec} = 2kT_e + e\phi \qquad (3.5.4)$$

where ϕ is the potential of the plasma with respect to the surface.

The loss surfaces to be included in the summation are the thruster walls, the screen, and the antenna. In the electrical configuration used at the Lewis beam extraction tests, the screen and antenna were allowed to float with respect to the thruster walls, and the beam voltage was applied between the vacuum tank ground and the thruster walls. Under these conditions the currents

$$I_{es} = I_{is} \qquad (3.5.5)$$

$$I_{eA} = I_{iA} \qquad (3.5.6)$$

$$I_{ew} = I_{iw} + I_b \qquad (3.5.7)$$

where e and i refer to electron and ion currents, and s, A, w and b refer to screen, antenna wall, and beam areas respectively.

For typical thruster operating conditions, the electron temperature in the field free region, which includes the antenna and the screen, is about 6eV. The plasma potential is typically + 12 volts and the (floating) screen potential is -16 volts. Since most of the antenna electrostatic potential is dropped in the dielectric sheath, we will assume the same value for the antenna floating potential as for the screen. For the screen and antenna then, (3.5.3) and (3.5.4) give

$$\varepsilon_A = \varepsilon_s \simeq 71eV \qquad (3.5.8)$$

For the wall losses, distinction should be made between losses to the cusps and losses between the cusps, as T_e along cusp field lines is about 6eV, while T_e between cusps is as low as 2.5eV. We will, however, ignore this difference and simply take T_e = 5eV, giving

$$\varepsilon_w \simeq 55 \text{ eV} \tag{3.5.9}$$

From the comparison of measured discharge losses with and without extraction, described in section 3.1, we have for the screen

$$I_{is}/I_b = I_{es}/I_b \simeq .43 \tag{3.5.10}$$

We approximate the antenna current by two methods. If we assume that the ratio of antenna and screen currents is equal to the ratio of their areas, then

$$I_A/I_b \simeq .5 \tag{3.5.11}$$

The second method is to compare the discharge losses obtained with antennas 2 and 3, assuming that the reduction in discharge losses with the smaller antenna is due to the reduction in effective areas. This method yields

$$I_A/I_b \simeq .4 \tag{3.5.12}$$

in fair agreement with 3.5.11.

An experimental method for determining the ion loss current to the walls was described in section 3.4, however, a sizable discrepancy was found between results in beam extraction experiments and in experiments without extraction, and we do not consider the technique well proven. Rather than employing this estimate, we use the measured value of

$$\varepsilon_b = 220 \pm 10\text{eV}$$

in (3.5.2) along with the estimates of (3.5.8) through (3.5.12) to obtain an estimate for the wall ion current of

$$I_{iw}/I_b \simeq 1.9 \pm .3$$

We believe this estimate to represent approximately a maximum for ion wall losses. The largest potential source of error in this analysis is in the estimate $\varepsilon_{ex} = \varepsilon_i$. Some extreme estimates of excitation losses yield a value of $\varepsilon_{ex} \simeq 31$ eV, which gives

$$I_{iw}/I_b \simeq 1.1 \pm .2$$

We may subdivide the wall losses into three types:

1. I_c - Cusp losses, i.e., ion losses along field lines which extend into the "field free" region of the device.
2. I_d - Cross field losses, i.e., plasma transport across the mirror like field regions between the magnets.
3. I_e - End effect and error field losses, which includes any losses due to departure from an ideal cusp configuration.

Theoretical estimates for cusp losses range from loss through a "hole size" of a hybrid gyroradius, which would yield $I_c/I_b \simeq .3$ at a peak cusp field strength of 1.5 kG, to an upper bound[2] of a "hole size" of $(T_e/T_i)^{1/2} r_{ci}$, which would yield $I_c/I_b \simeq 4$. All theoretical estimates for ion loss rates to a cusp predict a 1/B dependence. If cusp loss rates are close to the upper bound in the RFI Multicusp Thruster, the 1/B dependence would have resulted in approximately a 25% reduction in discharge losses for the increase of B_{max} from 1.5 kG to 3 kG as effected during the Lewis Research Center series of tests. The observed change in discharge losses of less than about 5% strongly indicates that cusp ion losses are near the low estimate of $I_c/I_b \simeq .3$, and thus that cross field and/or end effect losses are dominant. The probe measurements of section 3.4 showed that the density profiles in the region between the cusps were essentially identical to those in the cusps, indicating a high cross field transport rate. The large magnet spacing employed in the thruster may not have provided sufficient flux to inhibit cross field ion transport. Experiments with a geometry providing much more flux between the cusps, though not necessarily higher B_{max} are indicated.

With wall ion current in the range of .9 to 2.2 times the beam current, reduction in ion wall loss area remains the primary area for potential thruster efficiency improvement. The next stage of research on the RFI Multicusp thruster will therefore concentrate on improvement of multicusp ion confinement. A reduction in wall ion current by a factor of three would reduce discharge losses to the range of 150 to 170 eV/ion, and bring the energy expenditure associated with wall losses down to approximately the value associated with antenna and with screen losses. We have demonstrated the feasibility and effectiveness of smaller loss area antennas. Though further design study is necessary, it seems likely that a factor of three reduction in antenna area can be made. Sovey has found an ion transparency factor of .82 with improved SHAG optics, the incorporation of which would further reduce discharge losses by about 16 eV. With improvements in the optics and antenna design, and fairly modest reduction in wall losses, discharge losses on the order of 120 eV/ion appear likely for the RFI Multicusp thruster.

3.6 SUMMARY AND CONCLUSIONS

The first experimental Radio Frequency Induction Multicusp Argon ion thruster was designed and fabricated, and tested in a series of experiments at both a TRW test facility and at Tank 5 of the NASA/Lewis Research Center Electric Propulsion Laboratory. The source utilizes standard 30 cm two grid SHAG optics, with a design goal beam current of 4.4 ampere at a beam of 1100 volts.

The first series of tests, performed at the TRW test facility, without beam extraction, concentrated on general characterization of the rf discharge and discharge and rf circuit losses as a function of frequency and antenna configuration. Discharge losses were found to be independent of rf frequency over the range examined (.35 to 1.5 MHz), while antenna tank circuit losses varied approximately as the inverse of the frequency to the 3/2 power. At a frequency of 1.5 MHz, antenna tank circuit losses were only about 5% of total rf power.

Following a preliminary system checkout, including pulsed beam extraction, the RFI thruster was brought to NASA/Lewis Research Center for a two week series of tests with continuous ion beam extraction.

Minimum discharge losses of 220 ± 10 eV/ion were obtained with propellant flow rates in the design goal range (5.3-6.5 amp), for propellant utilizations less than about .45. Discharge loss figures at high utilizations were not obtained at these flow rates because of grid arcing and power supply problems.

Discharge loss figures obtained without extraction (by collecting ion current on the screen and correcting for screen transparency) were compared with the results of tests with extraction. Excellent agreement was found in the flat portion of the discharge loss-utilization curve (i.e., utilizations of less than about .4).

The effect of permanent magnet strength on discharge losses was examined by replacing the original ceramic magnets (B_{max} = 1.5 kG) with Samarium Cobalt magnets (B_{max} = 3 kG), reproducing as nearly as possible the original magnet configuration. Rather unexpectedly, at the increased field strength discharge losses were unchanged at a flow rate of 6.6 ampere equivalent and at most 15% lower at a flow rate of about 4 ampere.

Following the Lewis series of tests, additional experiments were performed at the TRW facility to aid in the interpretation of discharge losses. It was concluded that the ion current to the walls was between .9 and 2.2 times the beam current, and represents between 25% and 50% of the total discharge losses. We interpret the data to indicate that the ion losses to the wall regions between the magnets dominate cusp losses. Directions for modification of the field geometry to reduce the wall losses have been identified, along with possible improvements associated with modification of the antenna and optics.

4.0 ELECTRON CYCLOTRON RESONANCE THRUSTER

4.1 EXPERIMENTAL ARRANGEMENT

4.1.1 Microwave Source and Circuit

All data on the electron cyclotron resonance ion source presented in this report was obtained with the use of 4.9 GHz microwave power delivered from a Varian (VA888) klystron amplifier. This amplifier has a maximum rated CW power output of 1.4 k watt; although the amplifier may be tuned over a frequency range of 4.4 to 5.0 GHz, we were limited to an operating frequency of 4.9 to 5.0 GHz by the acceptance bandwidth of the available circulator. The microwave circuit configuration is shown in Figure 4.1. An oscillator (HP 8690) with variable attenuation output drives the amplifier. The function of the circulator is to protect the amplifier from excessive reflected power which can occur due to load impedance variations. Microwave power is delivered to the thruster chamber via fundamental mode rectangular wave guide. This guide has an attenuation of approximately 8.dB per 100 meters; we therefore lose about 7% of the forward power over the 4 meters of wave guide used in the circuit.

A known fraction of the forward and reflected power is coupled to thermistors which serve as forward and reflected power monitors. The thermistor readings were compared to absolute power measurements by calorimetry. This was accomplished by replacing the thruster chamber with a matched high power dummy load which was immersed in a water filled plexiglass beaker. The known quantity of water (10.35 liters) was stirred continuously while 500. watts, as read by the forward power monitor, was delivered to the load. The reflected power monitor read 8. watts. The measured temperature rise of the water as a function of time is shown in Figure 4.2. After an equilibration time, the absolute power may be obtained from the slope, dT/dt, and is given by

$$P(\text{watt}) = 69.8\ V(1)\ \frac{dT}{dt}\ \left(\frac{^{o}C}{\text{min.}}\right)$$

where V is the volume of water in liters. In this case the calorimetric power was 436. watts indicating that the power, as monitored by the

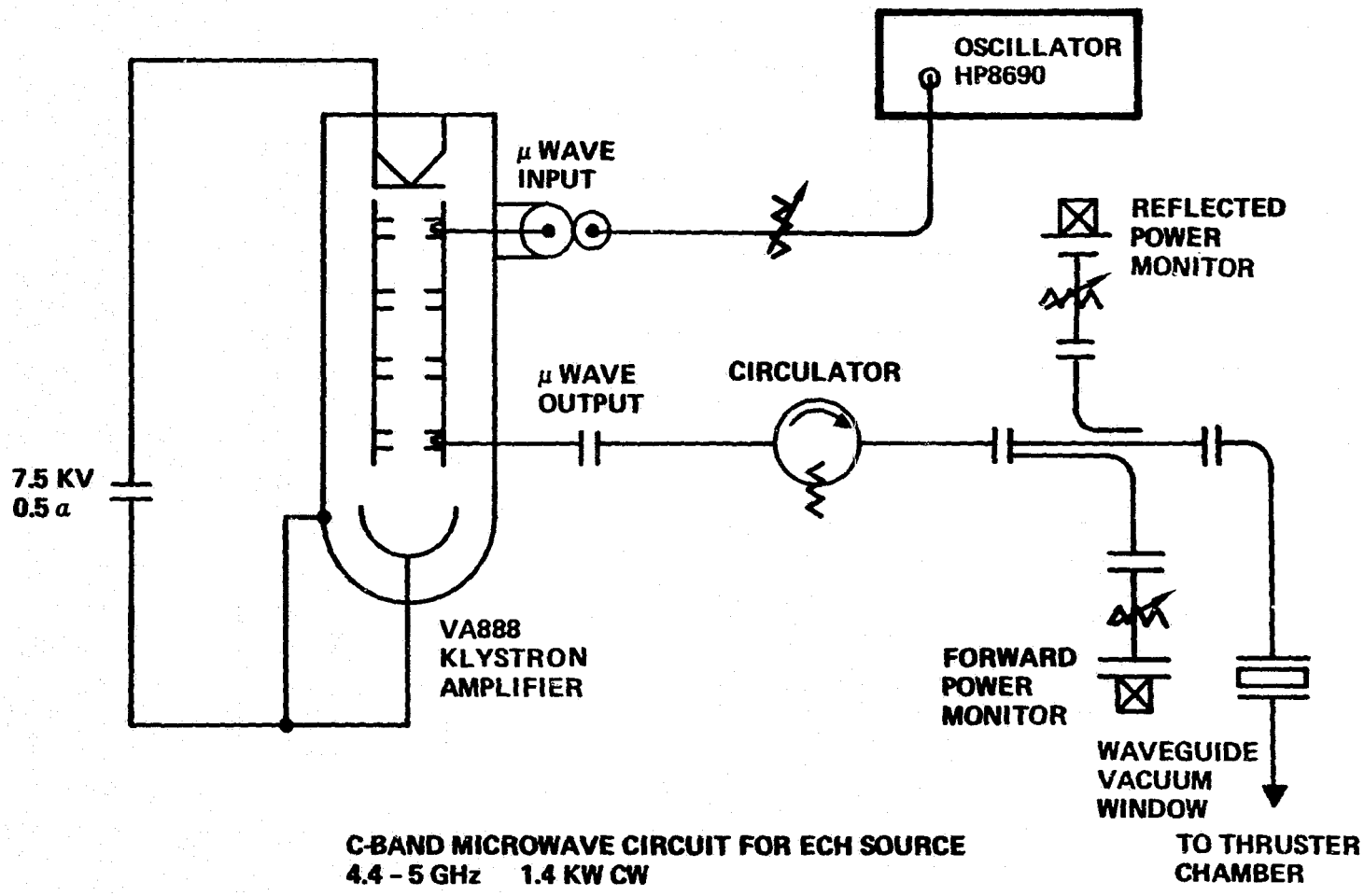

C-BAND MICROWAVE CIRCUIT FOR ECH SOURCE
4.4 - 5 GHz 1.4 KW CW

Figure 4.1

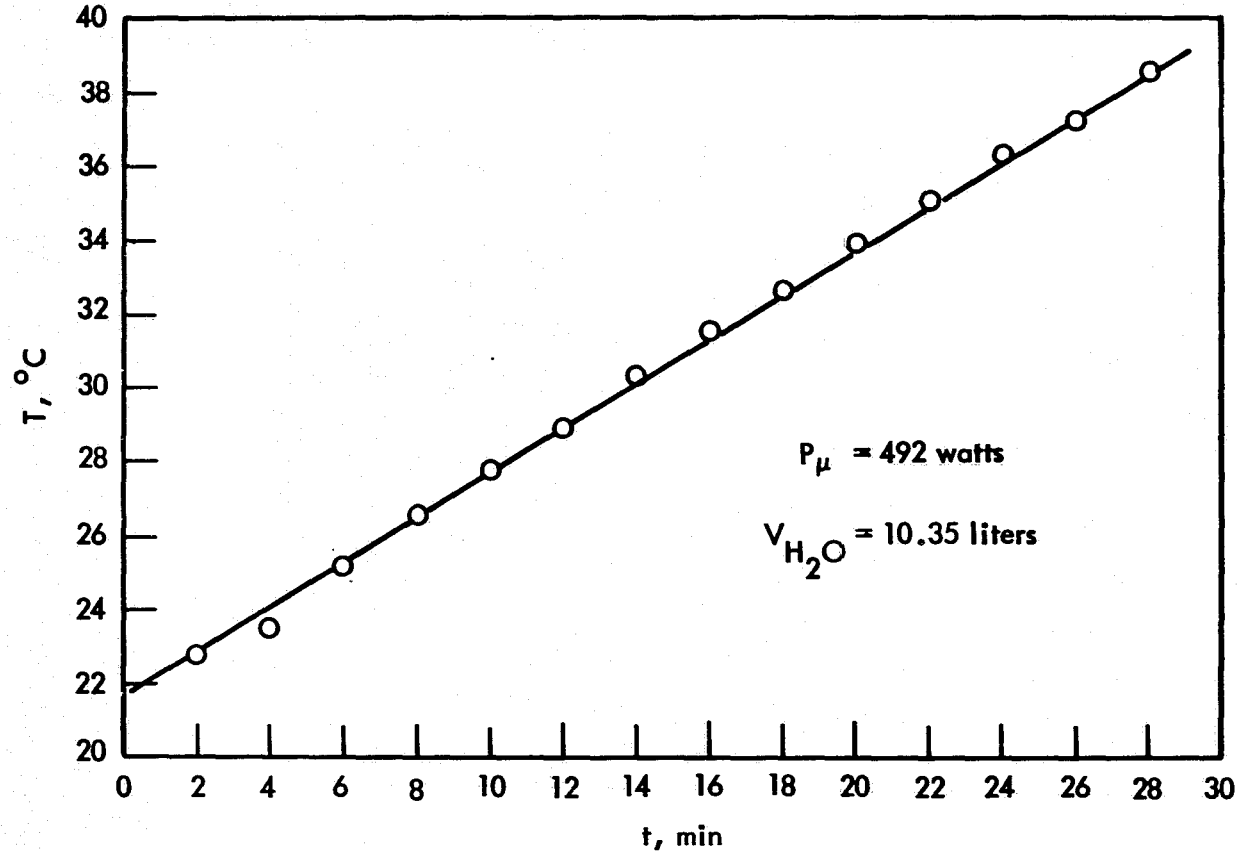

Figure 4.2 The temperature rise of a fixed quantity of water absorbing a constant amount of microwave power.

thermistor, is about 13.% higher than the actual power being delivered. Due to the infancy of the ECH thruster program this power correction factor is not included in any of the data to be presented. All quoted power measurements are as read by the thermistor monitors. To obtain the actual forward power the reader may multiply the quoted values by 0.88 or in the case of a quoted eV/ion value he may multiply by this factor to obtain the actual value.

Since the thruster chamber was mounted inside a larger vacuum chamber while the klystron amplifier and associated circuitry was outside the vacuum, a microwave pressure window was required. Although high power windows are commercially available they are quite expensive and generally have long lead time for delivery. We experimented with thin windows using several different materials. For some time we used one eighth inch thick teflon windows but these burst due to power absorption and atmospheric pressure after four or five hours of continuous operation at 700 watt power levels. The final successful design incorporated a 1/16 inch thick quartz window having dimensions of 1/16 inch greater than the inside dimensions of the wave guide; this quartz plate was mounted with Torr Seal™ to a standard milled flange. This window, which has a VSWR of 1.4 at the 4.9 GHz operating frequency, was mounted about 30. cm away from the thruster housing and is still in use after many hours of operation.

4.1.2 Thruster Chamber Diagnostics

The ECH thruster housing serves as a microwave cavity. The cylindrical section (length 30. cm, diameter 30. cm) of this cavity as well as one end plates are fabricated of 0.040" thick 304-SS. The other end of the cylinder consists of a 0.20" thick copper plate (hereafter referred to as the grid) uniformly perforated with 0.094" diameter holes to allow visual observation of the plasma as well as gas pumping. This copper plate, which is electrically insulated and thus biasable with respect to the cylindrical section, simulates the ion extraction area. The thruster housing is contained within a larger vacuum chamber with argon gas feed and pressure sensing occurring in the larger vacuum volume. The gas presently enters the thruster through the perforated copper plate. The thruster chamber is designed to allow a variety of magnet configurations

and chamber lengths to be tested without major refabrication. As no cooling provisions were made for the housing a thermocouple was put in contact with the chamber wall to monitor its temperature. Experiments were discontinued when the housing temperature reached 200°C in order to protect the samarium cobalt magnets. This allowed about four hours of continuous operation at 700. watts input power due to the reasonable high heat capacity of the chamber.

The plasma density, electron temperature, space potentials and their spatial variations were all obtained from standard Langmuir probe traces. The Langmuir probe usually consisted of a 0.0229 cm diameter, 0.50 cm long cylinder of tungsten. Special care had to be taken in the construction of this probe as the intense microwave fields that exist in the thruster chamber have a tendency to destroy most insulating materials (e.g. glass weaving and aluminum oxide) and at times can cause the tungsten probe to glow white hot. Needless to say it was not necessary to draw excessive electron current to the probe to clean it. The local plasma densities quoted in this report were obtained from probe electron saturation current measurements using the formula

$$n_e(cm^{-3}) = \frac{3.74 \times 10^8 \, I_{es}(ma)}{A(cm^2)\sqrt{T_e(eV)}}$$

where I_{es} is the electron saturation current in milliamperes, A is the probe area in square centimeters and T_e is the maxwellian electron temperature in electron volts.

As mentioned previously the perforated copper dish was biased to collect ions from the discharge chamber. The measured argon ion current and the thermistor microwave power measurements were used to obtain eV per non-extracted ion values. No beam ions have been extracted from the ECH source to date.

4.2 AXIAL LINE CUSP CONFIGURATION

The initial operation of the ECH source utilized 12 rows of uniformly spaced, alternating polarity RCo_5 magnets mounted to the outside cylindrical walls of the 30.cm long chamber as sketched in Figure 4.3. The multidipole line cusps were continued on the back plate with 5 rows of

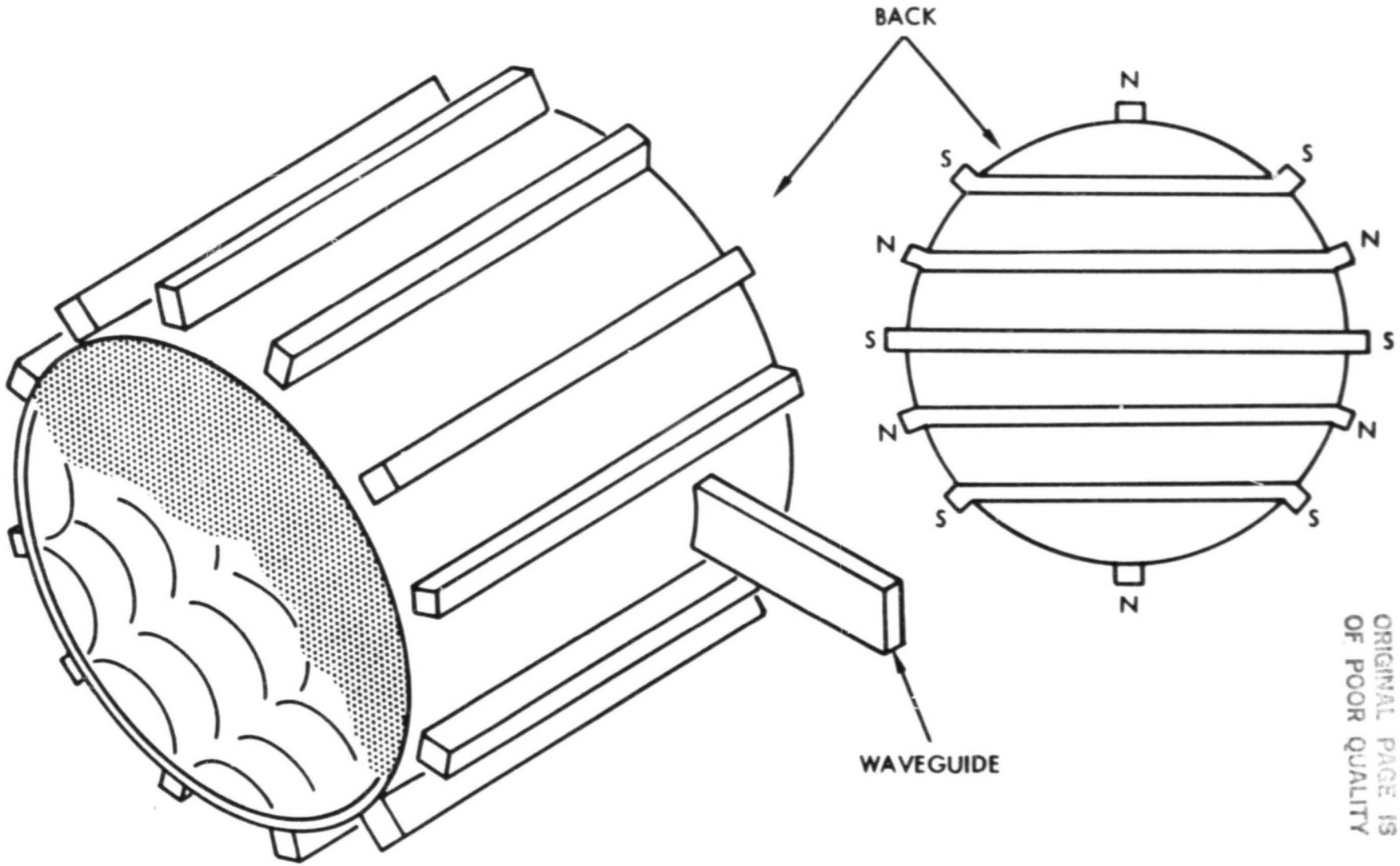

Figure 4.3 Sketch of the ECH source with the axial line cusp magnet configuration.

magnets. The magnet rows were assembled from magnets with dimensions 1.27 ↑x 1.27 x 2.54 cm and cubes of 1.27 cm. (↑ indicates the direction of magnetization). These magnets were mounted on 0.318 cm thick cold rolled steel strips to double their effective aspect ratio and produce measured pole face magnetic fields of about 4.5 kG. This ensures that the electron heating zone, which is B = 1.75 kG at f_μ = 4.9 GHz, is about one-half centimeter (minus the stainless steel wall thickness of 0.10 cm) from the housing surface.

The microwave feed configuration (Figure 4.3) consists of a standard C-band waveguide silver soldered to the perimeter of a hole cut out of the cylindrical wall of the chamber. This feed and magnet arrangement is approximately such that an extraordinary mode is launched from the guide.

Although a startup electron source was initially included in the design, it proved to be unnecessary as the discharge was self initiating at power levels above 75. watts at neutral pressures above $1.x10^{-4}$ torr. This easy startup is a result of the reasonably high Q of the thruster chamber which allows the microwave fields to build up to breakdown levels even at modest input powers. Figure 4.4 is a photograph of the discharge at a microwave input power of 100. watts.

The bright regions of plasma at the periphery are zones of high electron energy where most of the plasma production occurs. As hypothesized these zones are the mirror-like magnetic field regions where electrons are confined. Each of the bright regions appear to terminate at the very edges of the magnets while the majority of the field lines emanating from the central portions of the magnet pole faces appear dark indicating low electron temperature and little plasma production. Between adjacent magnets at the cylindrical walls we note that the bright regions dip toward and touch the walls. This behavior, which should not occur if the electron guiding centers strictly follow the magnetic field lines, is the result an interchange (or flute) like instability which occurs in regions where magnetic field lines have average unfavorable curvature. This instability would clearly adversely affect particle confinement and reduce the engine efficiency.

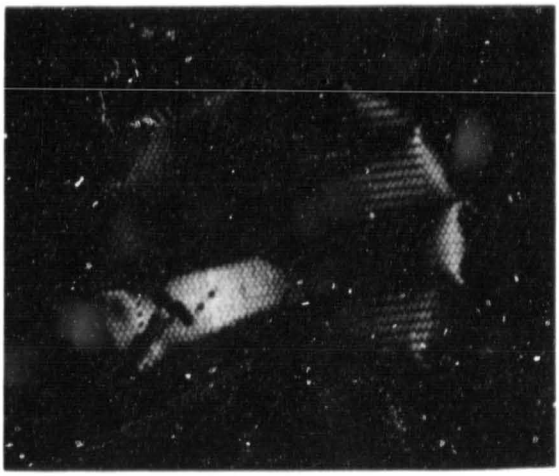

Figure 4.4 Front view of the ECH source. Bright regions are zones of plasma production.

Another thing to notice from figure 4.4 is that the bright regions on the back plate alternate from right to left. For example the lowest strip of plasma at the back plate is brightest on the right side while the next strip up is brightest on the left side of the chamber. This effect is due to the ∇B drift of electron guiding centers which causes electrons to drift across the field lines and build up at the edges thus resulting in bright regions there.

4.2.1 Radial Plasma Profile

Figure 4.5 shows the inverted radial temperature profile obtained from measurements with a Langmuir probe positioned 5. cm from the copper grid and centrally located between two magnet rows. The central portions of the discharge chamber contains maxwellian electrons (figure 4.6) of temperature 3.1 eV. Near the periphery where most of the plasma production occurs the temperature reaches 6. to 7. eV. Probe measurents in the high magnetic field regions should only be interpreted as indicative of the temperature as the probe considerably perturbs the plasma in this region. Non-perturbing optical measurement of line intensities have indicated that temperatures as high as 20. eV exist in this ECH source.

The plasma density profile, also illustrated in figure 4.5, is peaked in the central region of the chamber, indicating that the plasma is rapidly transported from the high magnetic field to the low field region. The plasma density does not peak where most of the production takes place. The plasma potential with respect to the thruster walls was 20 $\pm$ 1. volts positive independent of radial position. The floating potential (i.e. the probe voltage at which equal electron and ion currents are collected), on the other hand, was measured to be 4.5 volts positive of the wall in the central regions and decreased, starting at r = 10. cm, to a negative 5. volts near the thruster housing. The copper grid which simulates the extraction grids had a floating potential of positive 10. volts with respect to the chamber walls, or negative 10. volts with respect to the plasma, a result of the low electron temperature in the vicinity of the grid.

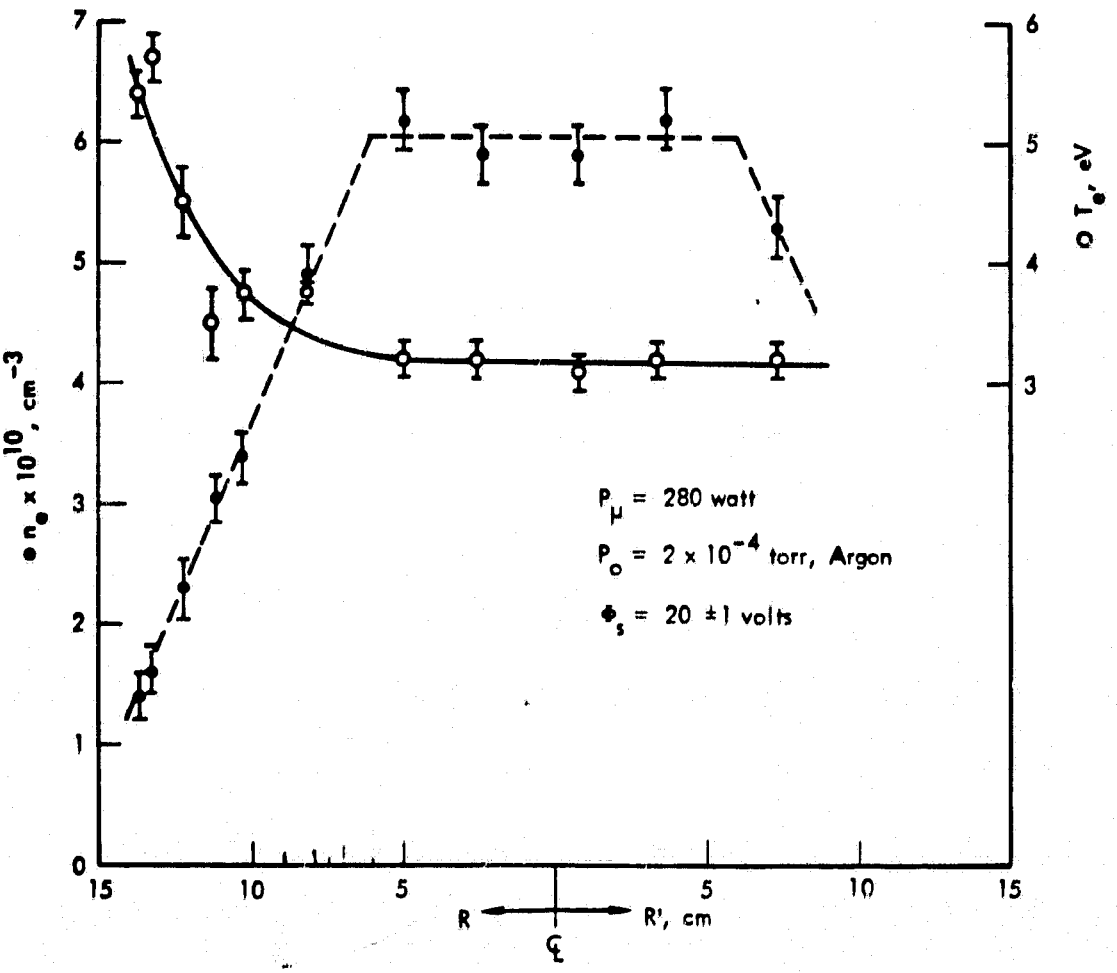

Figure 4.5 ECH source radial electron density and temperature profiles for the axial line cusp configuration.

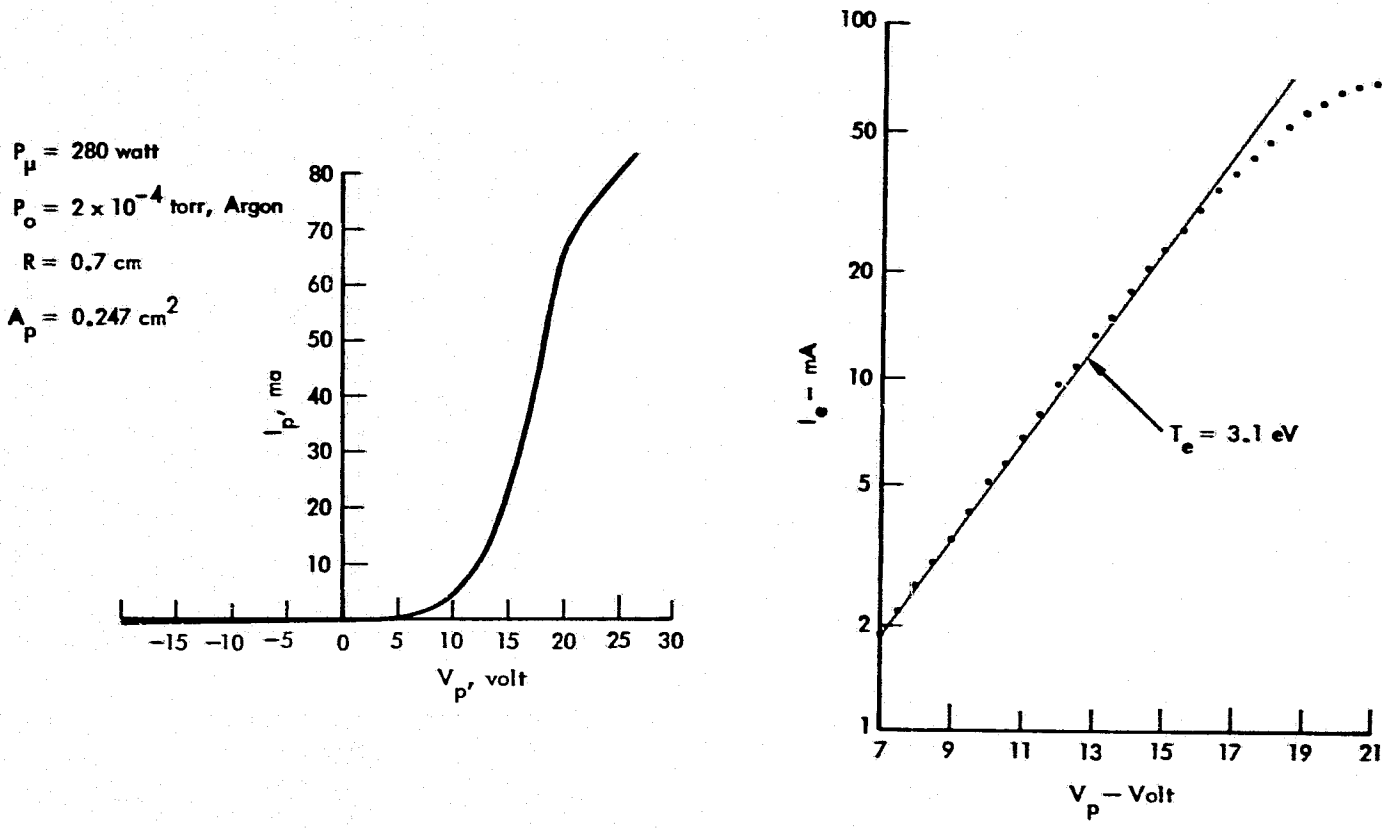

Figure 4.6 Current-voltage characteristic of a Langmuir probe in the central region of the ECH source. The semi-log plot indicates a one-temperature Maxwellian electron distribution.

4.2.2 Density and Grid Current as a Function of Power

Although the discharge cavity, in vacuum, is large enough that theoretically a particular, discreet mode should not exist (i.e. there should be mode overlap), the discharge does exhibit a number of discreet "modes" especially at applied microwave powers of less than 300 watts. Some of the moding characteristics are illustrated in figure 4.7a which shows electron density and reflected microwave power as a function of applied microwave power. A particular discharge mode, characterized by breakdown in an isolated location of the chamber, forms at an applied power of 100 watts with a plasma density in the central low B field region of 1.5×10^9 cm^{-3} and a reflected power of 20 watts. As the applied power is increased up to a value of approximately 300. watts, the plasma density remains unchanged with the additional power merely being reflected back toward the microwave source. At an applied power slightly greater than 300. watts, the discharge jumps into a mode characterized by plasma formation in all peripheral mirror regions. In this mode the central plasma density increases fairly linearly with applied power up to the maximum power of 700. watts. The general characteristics of the high power modes depended sensitively on the neutral pressure.

The electron density and ion current to the copper grid as a function of net input power (applied minus reflected power) is illustrated in figure 4.7b. The electron temperature in the central regions of the chamber is independent of applied power at fixed neutral pressure. Ion current collected by the 700. cm^2 grid biased at -60. volts is linear with net input power and corresponds to discharge chamber losses of about 280. eV/ion assuming all net power is absorbed by plasma electrons. The measured reflected power, in the region where collected ion current is linearly proportional to applied power, represents about 30.% of the forward power. In the low power "mode" characterized by a very localized plasma production volume the eV/ion (calculated from net power) is approximately 550 to 600 volts. This suggests that the efficiency could be improved by increasing the production volume perhaps through the use of microwave power at a lower frequency.

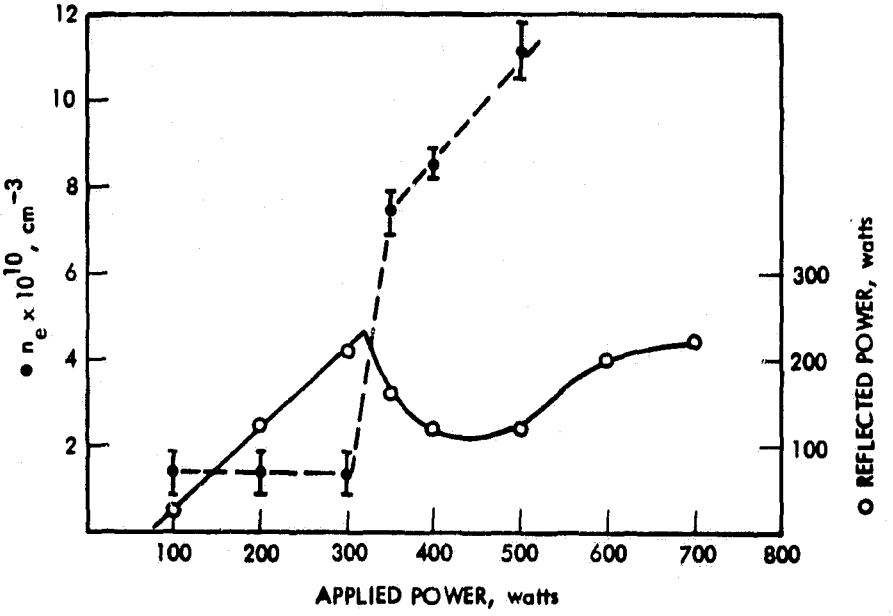

Figure 4.7a Plasma density in the central region of the ECH source as a function of the applied microwave power. Also indicated is the microwave power reflected back into the feed guide.

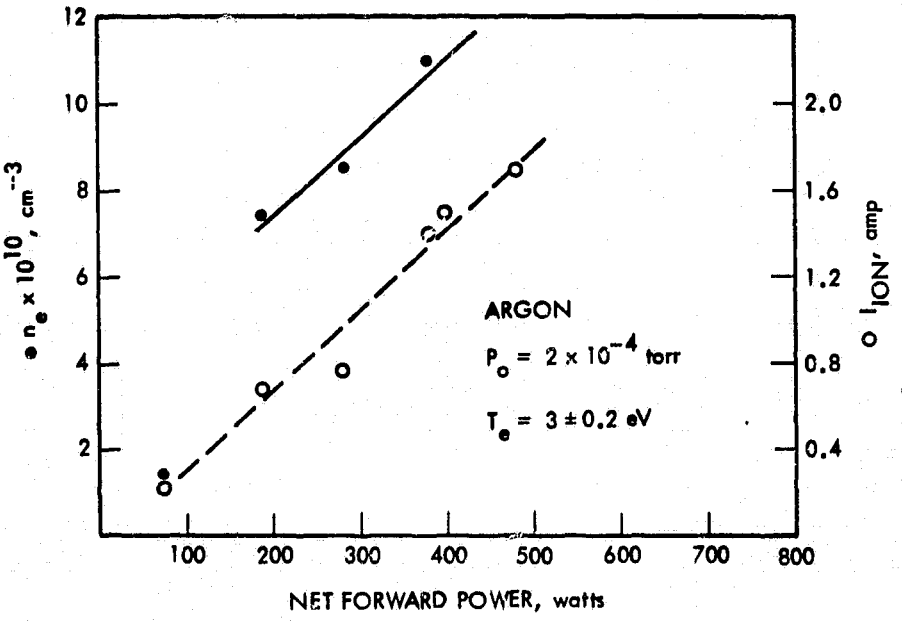

Figure 4.7b Plasma density and ion current collected by the grid as a function of total microwave power absorbed by the plasma electrons.

4.2.3 Attempt to Produce an Overdense Plasma

Although the design of the ECH thruster is to operate with an underdense plasma (i.e. $\omega_\mu > \omega_{pe}$) it would be advantageous to remove this requirement for at least the following reasons. First, higher efficiency microwave sources are available at lower frequencies. Second, the use of lower microwave frequencies would allow greater freedom in magnet design by possibly reducing the magnet mass or by improving the thruster performance since heating surfaces could be moved further from the magnet pole faces.

We have attempted here to produce an overdense ($\omega_{pe} > \omega_\mu$) plasma using the magnet and microwave feed configuration shown in figure 4.3 The only change was to replace the copper grid with a plate identical to the back plate already attached to the housing. Therefore, with all chamber walls covered with magnetic line "cusps", the loss area would be reduced and the maximum achieved density would not be a consequence of microwave power limitations.

The results of the measured plasma density in the central regions of the chamber as a function applied power is shown in figure 4.8. The density saturates with increased power and asymptotically approaches a density that is about 75% of the cutoff density of the ordinary mode for 4.9 GHz. These Langmuir probe density measurements are estimated to be accurate to about $\pm$ 20.%. Since the measurements were made in the central volume of the chamber where the density has been shown to be a maximum (see figure 4.5), we conjecture that the density at the resonance zones near the magnet pole faces must be about the same as in the central volume. If this were not the case it would be difficult to imagine why the density saturates very near the cutoff density. We had hoped that an overdense plasma could be achieved since the resonance zones are very near the low density regions between magnet rows. As seen from figure 4.5 the density between the magnets and near the walls is about one order of magnitude lower than the density in the central region. The microwaves therefore would propagate in this underdense plasma until they reach the cutoff near the resonance zone. Since the collisionless skin depth, c/ω_{pe}, is roughly 1. cm for a 3. x 10^{11} cm^{-3}

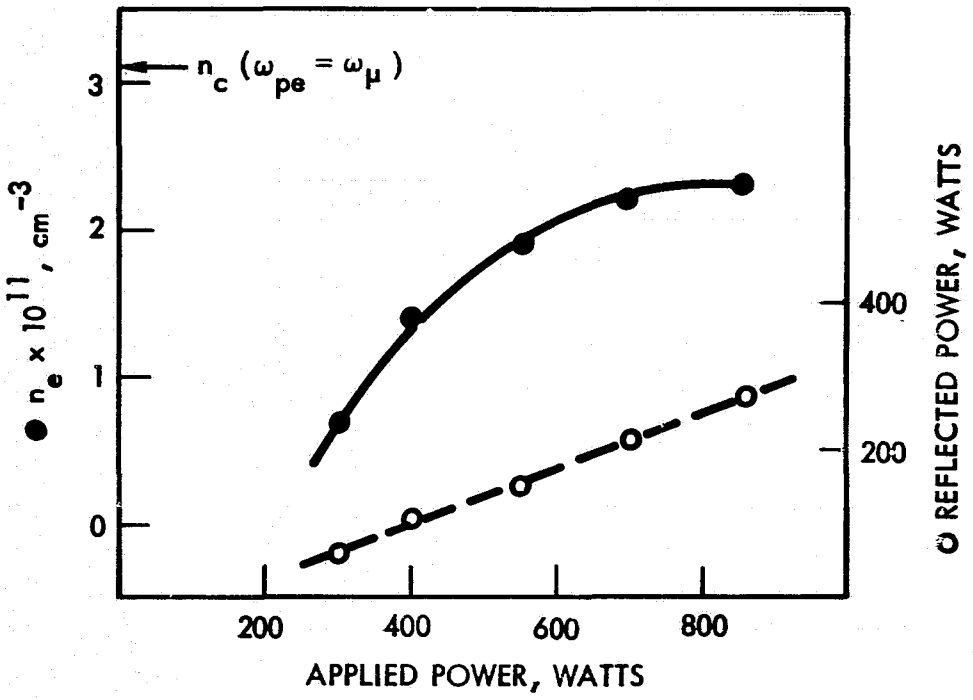

Figure 4.8 Central volume plasma density as a function of applied power in an attempt to achieve an over-dense plasma.

density plasma, they could penetrate with sufficient amplitude to maintain electron heating. However it would appear from these results that this does not occur.

The reflected microwave power measurements shown in figure 4.8 do not increase sufficiently as the plasma density approaches saturation. At the cutoff density the microwaves should be totally reflected if the absorption mechanism, mentioned in the last paragraph, does not occur, as seems to be the case. Therefore, at the cutoff density, when the applied power is increased the reflected power should increase by a corresponding amount. This, however, does not occur. For example, in Table 4.1 when the applied power was 700. watts a plasma density of 2.2×10^{11} cm^{-3} was obtained with 214. watts of reflected power. When the applied power was increased to 860. watts the density changed very little to a value of 2.3×10^{11} cm^{-3} but the reflected power was only 277. watts. One must ask what has happened to the almost 100. watts of applied power that does not show up in reflected power? Either plasma losses have increased, or the power measurement is suspected or something else within the chamber (possibly the chamber itself) has absorbed this power. We had observed on some occasions that, in a particular "mode", microwave power could be coupled to the four stainless steel screw heads that exist at the chamber cavity walls for they would glow red hot. Future development of an ECH thruster should incorporate cooled aluminum or copper walls in order to be more confident that the net forward power is being transferred first to the plasma electrons. That is, the vacuum cavity should be designed to have a higher Q than the present one.

Table 4.1 summarizes and compares the central volume density and electron temperature as a function of applied microwave power for the case (1) when the chamber is terminated with the copper grid and case (2) when the grid is replaced with a wall of line cusp magnets. With magnets on all walls the electron temperature is lower. This is a result of the fact that the ratio of plasma production volume to ion loss area, V_{pp}/A_{il}, is larger for the case with magnets on all walls than for that with the grid termination. As shown in figure 5.2 devices with larger effective length $L \equiv V_{pp}/A_{il}$ can be expected to operate at lower

Table 4.1

PARAMETER COMPARISON OF A DISCHARGE TERMINATED WITH A COPPER GRID AND ONE TERMINATED WITH A WALL OF MAGNETS

$P_{\mu F}$(Watt)	$P_{\mu R}$(Watt)	$P_{\mu N}$(Watt)	$n_e \times 10^{10}(cm^{-3})$	T_e(eV)	$n_e/P_{\mu N} \times 10^8$	
100.	16.	84.	1.4	3.1	1.6	CASE 1 WITH GRID (BIAS = -60.v)
200	79.	121.	1.45	3.1	1.2	
300.	132.	168.	1.35	3.2	0.8	
350.	100.	250.	7.4	3.0	3.0	
400.	76.	324.	8.5	3.0	2.6	
500.	76.	424.	11.0	2.8	2.6	
300.	63.	237.	6.9	3.1	2.9	CASE 2 WITHOUT GRID (MAGNETS ON ALL WALLS)
400.	107.	293.	14.	2.0	4.8	
550.	151.	400.	19.	2.4	4.8	
700	214.	486.	22.	2.1	4.5	
860.	277.	583.	23.	2.1	3.9	

ARGON, $P_o = 2.0 \times 10^{-4}$ Torr

$P_{\mu N} \equiv P_{\mu F} - P_{\mu R}$

electron temperatures at a given neutral gas pressure. Also indicated in Table 4.1 is that the plasma density per net watt of input power is approximately a factor of 2 higher with magnets on all walls. Since the fractional increase in production volume of case (2) over case (1) is too small to account for the factor of 2 increase in $n_e/P_{\mu N}$ it must be that the surface magnetic (or electric) fields do provide some ion confinement. However, systematic comparisons of different configurations with this ECH source for the purpose of examining ion confinement, have been annoyingly difficult because of the various plasma "modes" that exist. Such difficulty may be seen, for example, in Table 4.1 by comparing $n_e/P_{\mu N}$ values for $P_{\mu F}$ = 350 watts and $P_{\mu F}$ = 300 watts in case (1) and case (2), respectively. Approximately the same net power is measured in each case and the values of $n_e/P_{\mu N}$ are nearly identical, a result that could be interpreted as showing that there is absolutely no ion confinement.

4.3 VARIATION IN MAGNET SPACING

With the axial line "cusp" configuration described in section 4.2.2 the magnets formed continuous line cusps with center-to-center magnet spacing of 7.85 cm on the cylindrical walls. It was noted with that configuration that a considerable amount of plasma intercepted the thruster wall between each of the magnets; this would reduce the efficiency and could possibly account for the rather high eV/ion values quoted in that section. As noted previously, the plasma streaming to the walls between the magnets most likely is the result of the magnetohydrodynamic interchange instability which occurs when $\bar{\nabla}B \cdot \bar{\nabla}p > 1$. (Here p is the plasma pressure and $\bar{\nabla}B$ the magnetic field gradient.) To determine if this plasma-wall interception can be suppressed we tested the line "cusp" configuration with a variety of magnet center-to-center spacings ranging from 0.0 cm to 7.6 cm in 1.27 cm steps; it was hoped that simple visual observation would allow us to determine which particular spacing would be more favorable in keeping plasma from the walls.

The magnetic line configuration used in this test is sketched in figure 4.9a. Ceramic magnets of dimensions 2.5† x 1.9 cm were used

at the location where the microwave feed is connected to the chamber housing. These magnets have a pole face field of 1.5 kG which is below the resonance field for the 4.9 GHz power used. As a consequence the field lines by the power feed should contain no hot electrons and little or no plasma production should occur directly in front of the feed. (This arrangement with two non-resonance field magnets by the feed was also used in the ECH test results described in the previous sections; with resonance field magnets at the power feed the gas would break down at the feed location and the reflected power would be considerably higher than the values already mentioned.) The samarium cobalt magnets, shown in Figure 4.9a, were of dimensions 1.27 x 1.27 cm with 4.5 kG pole face fields.

Figure 4.9b is a photograph of the discharge with the magnet arrangement sketched in Figure 4.9a. As expected the plasma forms the usual cusp shape, similar to that in an RF or hollow cathode discharge, on the field lines terminating at the ceramic magnets. The plasma on the field lines of the $SmCo_5$ magnets with a spacing of 6.4 cm appears to intercept the wall between the magnets. In fact on close inspection all spacings down to 2.5 cm showed this wall interception. Although it is difficult to determine with certainty, due to the high brightness and diffuse nature of plasma, the 1.3 cm spacing did appear to show no plasma wall interception of the same character as the 6.4 cm spacing.

All considered, this test of a variety of magnet spacings was rather inconclusive from the point of view of determining the efficiency of a full scale ion source. That is, even though the 1.3 cm spacing showed no wall interception one cannot be certain that a thruster uniformly surrounded by magnets with this spacing, would guarantee better performance. It may be, for example, that transport of plasma toward the interior of the thruster chamber is hindered with the 1.3 cm spacing due to the higher field strengths that exist at the plasma production region; or it may be that the efficiency would be reduced over, for example, the 6.4 cm spacing simply because of a reduction in plasma production volume. At the time of these tests we were not in possession of a sufficient quantity of $SmCo_5$ magnets to allow us to experiment with each magnet spacing surrounding the thruster chamber.

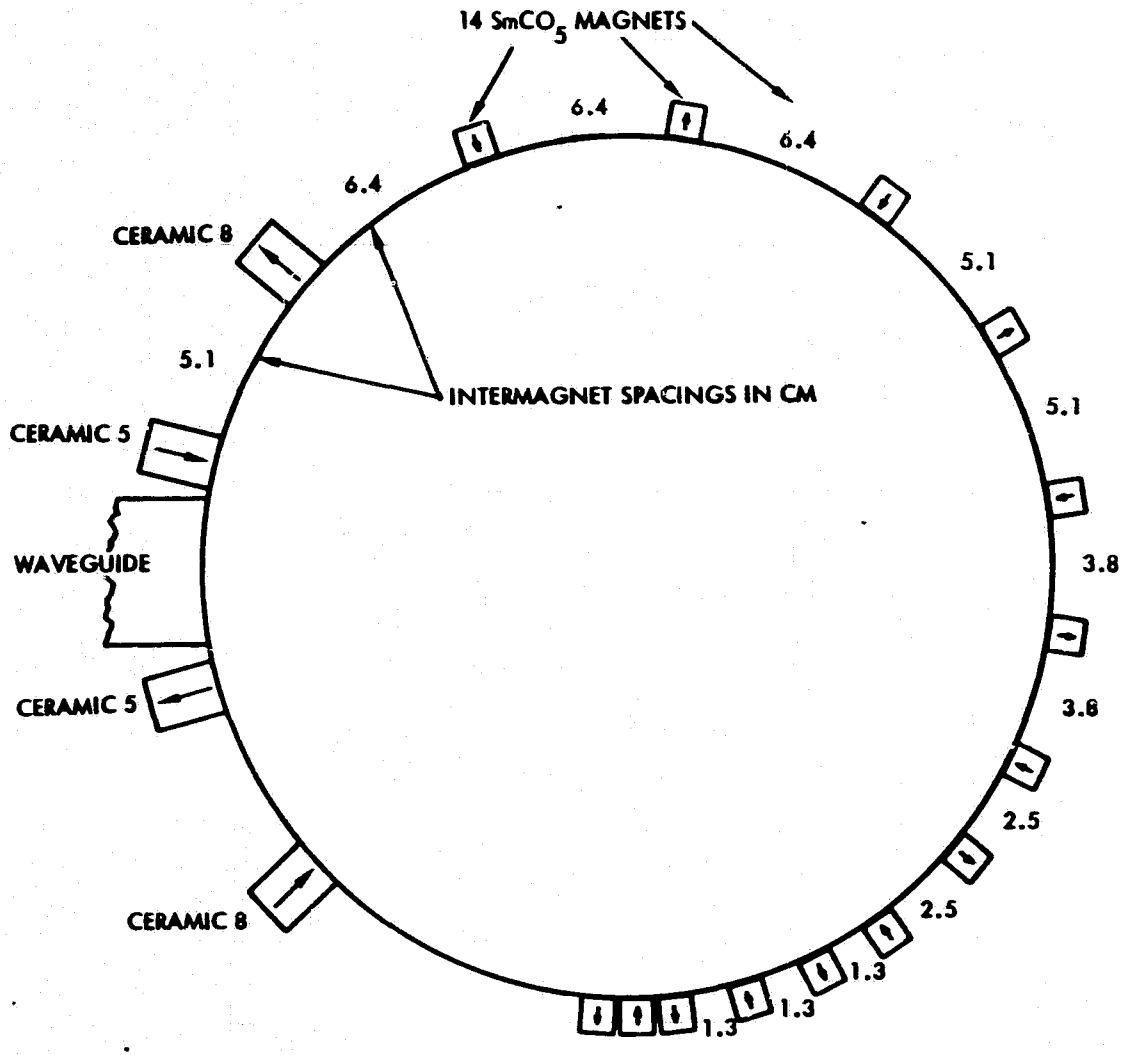

Figure 4.9a Magnet arrangement and power feed for the discharge shown in Figure 4.9b and 4.9c.

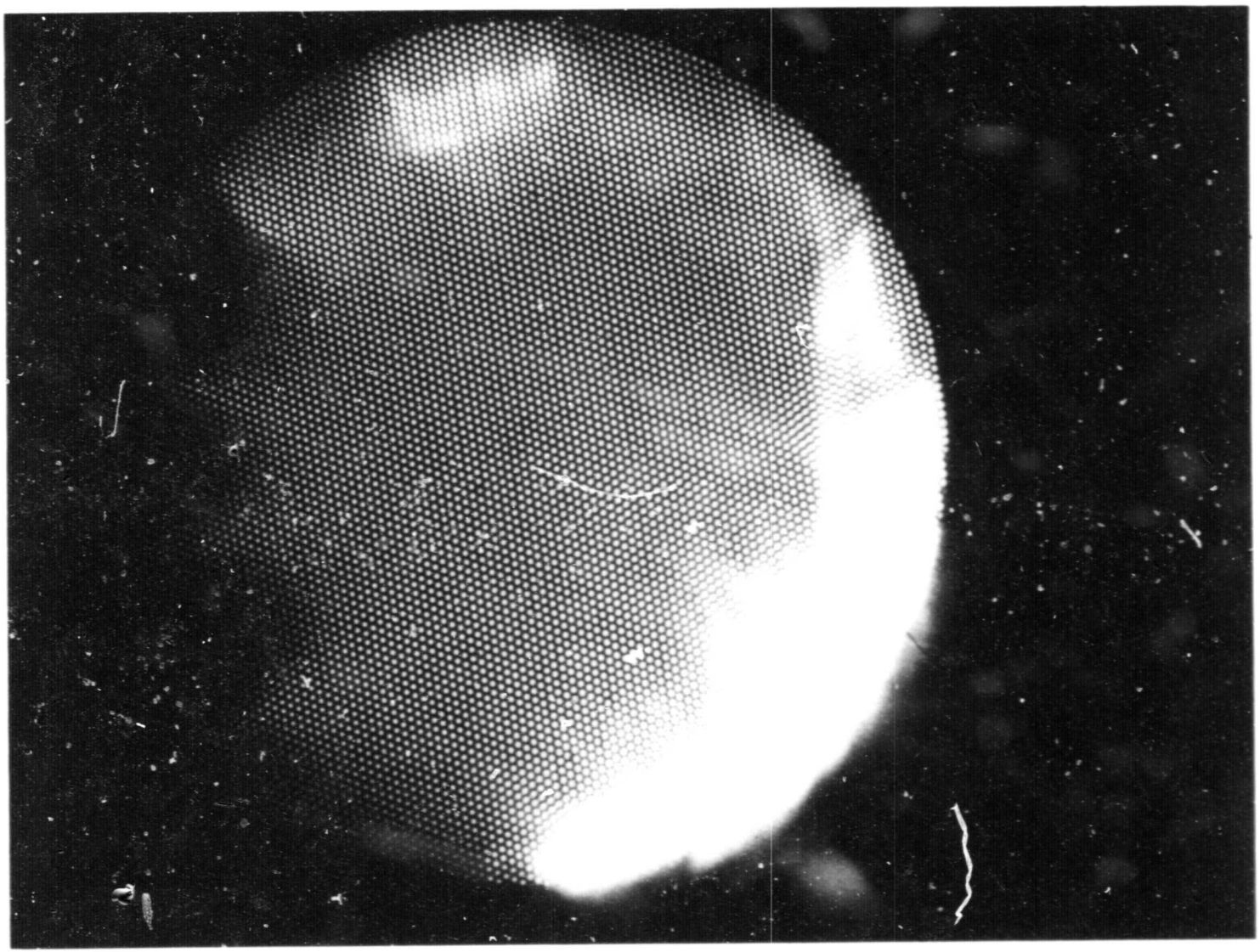

Figure 4.9b Photograph of the ECH discharge with the magnet arrangement indicated in figure 4.9a.

It did become clear from these tests, however, that no matter what the magnet spacing was, the gradient drift of electrons in the plasma production regions is an important factor that should be considered in the ECH thruster geometry. This electron guiding center drift (already mentioned in section 4.2) is in the direction of $\bar{\nabla}B \times \bar{B}$ and can cause electrons to slam into walls before they have a chance to ionize neutral atoms. In an axial line cusp magnetic configuration all of the ∇B drift surfaces terminate at the walls. Assuming perfect mirror confinement of electrons confined to magnetic field lines which pass through the resonance zones, one would like these electrons to make, on the average, at least one ionizing collision before being lost via $\bar{\nabla}B$ drift to the walls. We therefore expect this drift to be important if spatial lengths of roughly

$$\ell(\text{cm}) \gtrsim \frac{V_{\nabla B}}{\nu_c} = \frac{1}{\nu_c} \frac{T_e(\text{eV})}{B(\text{G})} \frac{1}{L_B(\text{cm})} \times 10^8$$

or greater are encountered in the thruster. Here ν_c is the ionizing collision frequency and L_B is the magnetic field gradient scale length. Of course if the $\bar{\nabla}B$ drift surfaces are closed and do not intercept the chamber walls or other obstacles we would expect better energetic electron utilization and hence lower eV/ion values. Such a configuration is described in the following section.

4.4 AZIMUTHAL LINE CUSP CONFIGURATION

The results described here utilized a magnet configuration with 3 line cusps of $SmCo_5$ arranged azimuthally about the 30. cm diameter cylindrical wall as shown in figure 4.10. These magnet rings, which had pole face fields of 4.5kG, were arranged with a center-to-center spacing of 5.5 cm. The downstream magnet ring was placed 2.0 cm from the copper collection plate while the upstream ring was placed 2.0 cm from the edge where the back plate was attached. The discharge chamber length was thus 15. cm, half of the length of the configuration with axial line cusps. The back plate also had mounted to it alternating polarity ring cusps. The central 5. cm diameter disc was samarium cobalt, with pole face field equal to 3.0 kG, while the other two rings on the back plate were of ceramic material with pole face fields of 1.5 kG. This configuration has closed drift surfaces everywhere.

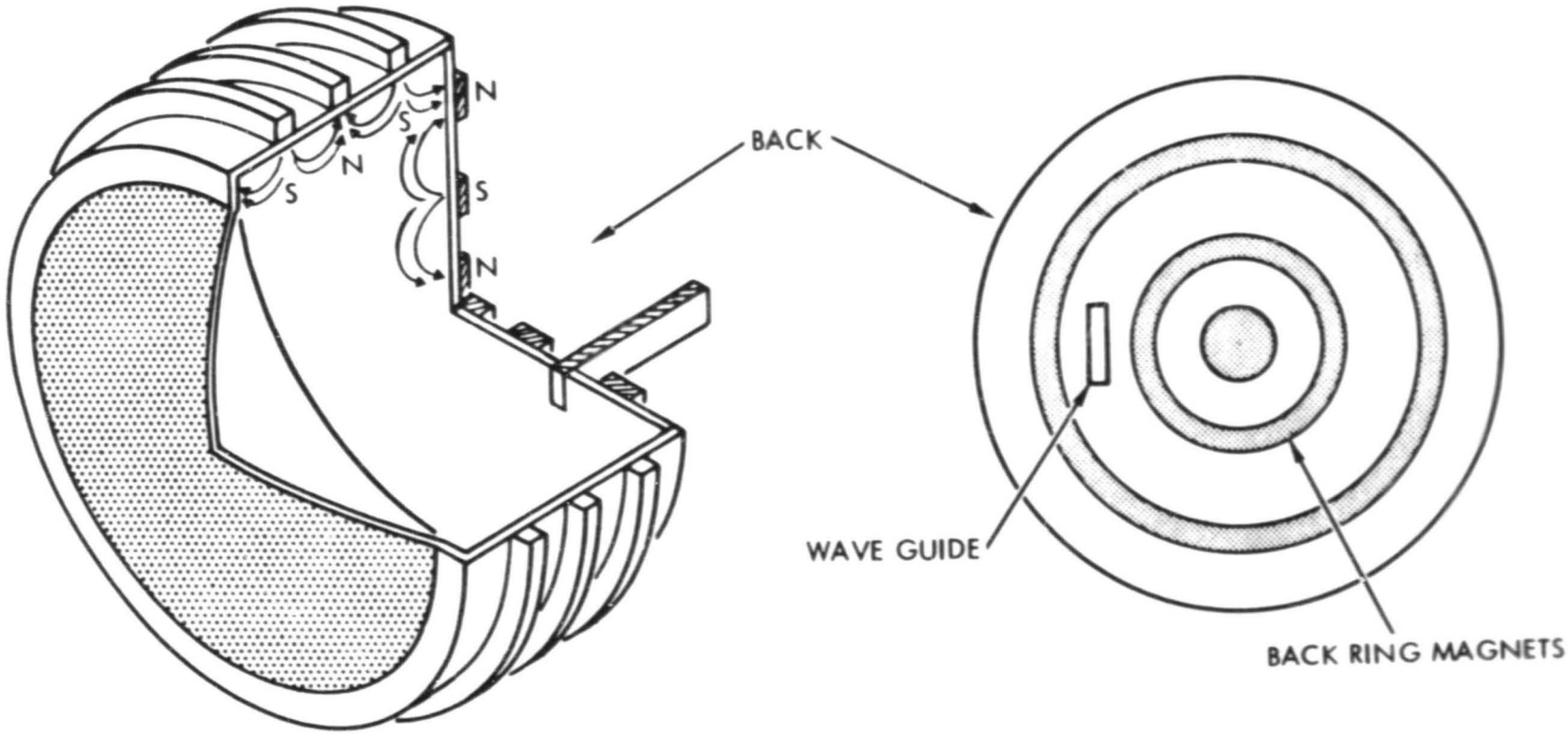

Figure 4.10 Magnet and power feed arrangement for the azimulthal cusp configuration.

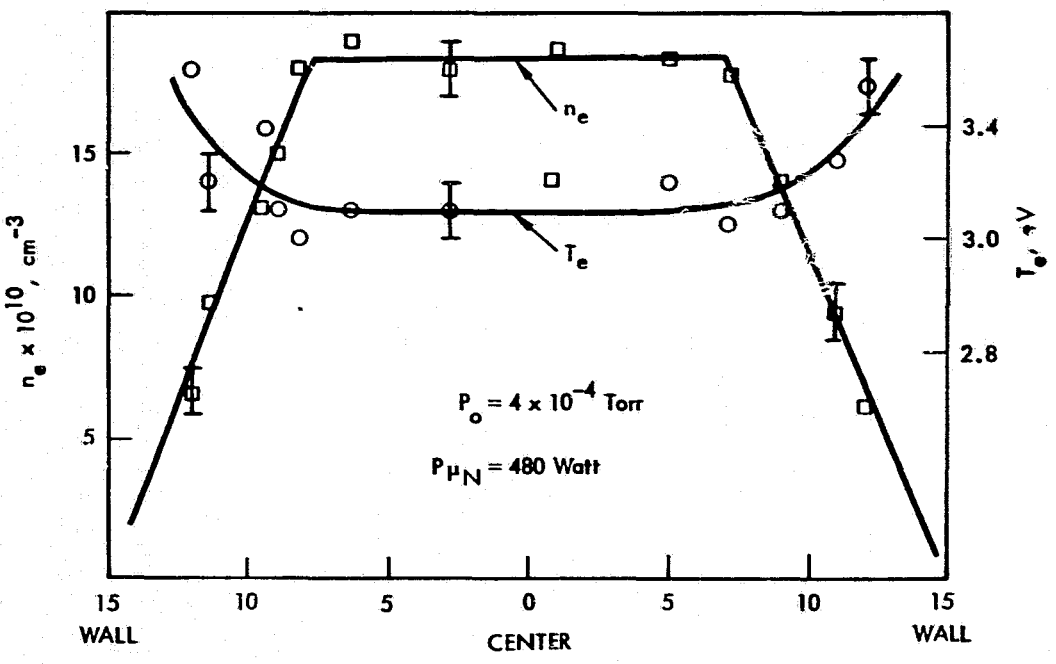

Figure 4.11 Radial profiles of plasma density and electron temperature near the extration grid in the azimuthal geometry.

TABLE 4.2

GRID CURRENT AND eV/ion AS A FUNCTION OF POWER
AND NEUTRAL PRESSURE FOR THE AZIMUTHAL GEOMETRY

$P_o \times 10^{-4}$ Torr	$P_{\mu F}$(Watt)	$P_{\mu R}$(Watt)	$P_{\mu N}$(Watt)	I_G(Amp)	$P_{\mu N}/I_G$
1.6	200.	22.	178.	0.4	445.
1.6	290.	154.	136.	0.8	170.
1.6	400.	70.	330.	1.55	213.
1.6	500.	62.	438.	1.7	258.
1.6	605.	126.	479.	1.8	266.
1.6	710.	214.	496.	1.8	276.
2.4	240.	19.	221.	0.95	232.
2.4	320.	41.	279.	1.5	186.
2.4	410.	69.	341.	1.55	220.
2.4	535.	126.	409.	1.9	215.
2.4	600.	120.	480.	2.4	200.
2.4	700.	164.	536.	2.6	206.
3.6	220.	19.	201.	0.9	223.
3.6	380.	38.	342.	2.0	171.
3.6	520.	114.	406.	2.5	162.
3.6	620.	151.	469.	2.8	168
3.6	730.	183.	547.	3.0	182.
4.8	230.	25.	205.	1.2	171.
4.8	300.	35.	265.	1.25	212.
4.8	420.	100.	320.	2.4	133.
4.8	500.	164.	336.	2.5	134.
4.8	615.	252.	363.	2.5	145.

The microwave feed was again a standard C-band guide soldered to the back plate between the non-resonant ceramic magnet rings to help prevent breakdown directly in front of the feed. Note that in this configuration the feed is approximately such as to launch an ordinary mode wave.

4.4.1 Radial Plasma Profile

The radial plasma density profile, taken with a probe 4. cm from the copper grid, is shown in figure 4.11. Comparison of this profile with the profile of figure 4.5 for the axial line configuration shows that the azimuthal configuration is uniform over a larger extraction area. This will allow greater ion current to be drawn to the copper grid in the azimuthal configuration than in the axial line arrangement. Even flatter profiles than indicated in figure 4.11 may presumably be obtained at the extraction grid by adjusting the axial position of the magnet ring closest to the grid. In theory, with a flatness parameter of one, it should be possible to draw a total of 4.6 amperes of argon to the 700. cm^2 grid even when the plasma density in this ECH source is limited by the cutoff density of 3. x 10^{11} cm^{-2} for 5.0 GHz power and the electron temperature at the grid is only 3.eV. We therefore expect that with proper design one should be able to draw a 3.0 ampere beam from the source using a 65% transparent screen.

We note that the temperature profile, shown also in figure 4.11, while having the same inverted axial line magnets, does not appear to be as steep. The electron temperature in the central regions of the chamber is about 3.eV, the same as in the axial configuration, but increases to only about 3.5eV near the walls. The reason for this is that quite unexpectedly the majority of electron heating appeared to be restricted to the back plate magnetic fields under conditions of high neutral pressure and high microwave power. Very little power appears to be coupled to electrons in the fields of the magnets at the cylindrical walls. This would mean that the major plasma production takes place in regions near the back plate. If this is true, then it may be possible to entirely eliminate the magnets on the cylindrical walls and shorten the thruster to a length of 6. to 8. cm without causing a reduction in performance; on the contrary, the performance may improve over the eV/ion values stated in the following section because cylindrical wall losses would be largely reduced.

C - 2

4.4.2 Source Efficiency

The electrical efficiency of this azimuthal line cusp configuration is summarized in Table 4.2. The ion current (I_G) collected by the copper grid, biased 35. volts negative to the chamber housing, is given as a function of net power ($P_{\mu N}$) at various neutral pressures. The net power divided by the grid current gives the eV per non-extracted ion values. The general trend is that the eV/ion decreases as the neutral pressure increases in a fashion similar to that for the rf thruster. The minimum eV/ion of about 135. volts is comparable to the lowest values so far obtained with the ∿ 1. MHz rf source. (Strictly speaking we should multiply this value by 0.88, as mentioned in section 4.1.1, to obtain a minimum measured eV/ion of about 120 volts.) Whether this reduction by almost a factor of two for this azimuthal geometry ECH source as compared with the axial geometry ECH source is a result of closed drift surfaces has not yet been ascertained. It may be that the improved efficiency is simply a result of reducing the discharge volume by a factor of two. Although these results are encouraging it should be noted that a substantial fraction, 20% to 30%, of the forward power is being reflected back down the feed guide under optimal extraction conditions. An EH tuner installed on the high pressure side of the microwave vacuum window has been unable to reduce the quantity of reflected power substantially. We believe that the key to reducing reflected power lies in the relative geometry between the microwave feed and the magnet configuration; this geometry should be discoverable upon further experimentation.

4.5 SUMMARY

We have described here the initial developement of a thruster ion source based on electron cyclotron heating which utilizes 5. GHz microwave power and magnetic fields of strength up to 4.5 kG. The source is designed to incorporate electrostatic acceleration through the use of physical grids to form the ion beam which provides the thrust. The magnetic geometry is such that low residual magnetic fields of order 10 Gauss are present at the extraction region; these fields should not influence the optical performance of an acceleration system based on magnetic field free theory.

The data obtained to date with the ECH source validates the basic concept. Certain aspects of this source are particularly attractive.

Since the source is electrodeless any lifetime problems associated with cathodes or antenna immersed in the plasma are eliminated. Ion losses to these structures are also absent. The ECH source plasma exhibits a very low maxwellian electron temperature and hence low space potential in the vicinity of the extraction grid. This should lead to greatly reduced screen and discharge chamber sputter rates. The construction of the discharge chamber is simplicity itself, requiring only a metal housing and microwave feed connection.

The discharge chamber losses reported here have been reduced from initial values of order 250. eV/ion to approximately 130. eV/ion. The lower figure translates into about 185.eV per beam ion for the 70.% transparency optical structure used for beam extraction with the 1. MHz rf source.

There are several issues which should be addressed in the future development of the ECH thruster source. Aside from a knowledge of the basic plasma physics involved we have little understanding of the plasma transport processes that occur. We have little understanding of electron confinement in the magnetic mirror-like regions of the source and little knowledge of the extent of ion confinement. It has not been learned how the discreet plasma "modes", in which only a localized region appears to contain heated, ionizing electrons, can be controlled. This "moding" would have serious consequences if it is desired to throttle the engine, as smooth thrust transitions would be difficult to achieve. In addition, one should construct a higher Q cavity than was used in the tests reported here so that values of measured net forward power can, with more certainty, be interpreted as being coupled to plasma electrons. Attempts should be made to reduce the quantity of reflected power, which of course is wasted. Finally, since we have to date been unable to produce an overdense plasma with this type of source geometry, one should be aware of the fact that the maximum beam amperes that can be extracted from this source is limited, for a given extraction area, by the frequency of the microwave power. The microwave frequency chosen will in turn influence the plasma production and confinement properties of the source and hence affect the eV per beam ion that can be obtained.

5.0 SOLENOIDAL B-FIELD CONCEPT

One of the present major objectives of electrostatic ion thruster development is to produce a thruster having high electrical efficiency and high propellant utilization. Within the class of propulsion devices to which ion thrusters belong (i.e. thrusters with a specific impulse in the range of thousands of seconds and thrust in the range of tenths of milli newtons to about one newton), electrostatic acceleration of ions through the use of two and three grid optics systems is electrically very efficient; efficiencies 99.0% and better are not uncommon. Furthermore, the development of optical systems with screen and accelerator grid open area fractions of, for example[1], 0.75 and 0.27, respectively, have allowed considerable improvements in mass utilization and reduction of ion collection by the screen electrode.

In order to achieve further improvements in eV/ion, as well as propellant utilization one must look to improvements in the ion source itself. Indeed, it is source work that concerns much of the present research being performed on ion thrusters. In addition to the concerns of eV/ion and efficient use of mass, the researcher must attempt to develop a source that is both durable and reliable.

The purpose in this section is to examine an ion source concept that may provide an electrical efficiency which is considerably improved over those presently quoted for electron bombardment sources. We briefly discuss the development, over the past two decades, of electron bombardment ion sources for the purpose of gaining insight into the physical processes occurring during their operation; this examination quite naturally leads one to propose a concept which, while not new in its magnetic configuration, is different from electron bombardment sources in its electrical configuration and in the plasma processes that are expected to occur. The conceptual sources we will be discussing will be limited to those in which the electrical energy is supplied by electromagnetic waves rather than by electron injection as in electron bombardment sources.

A survey of the literature on electrostatic ion thrusters will impress upon the reader that the best performance of propellers in terms of electrical efficiency is in the neighborhood of 250. $\pm$ 50. watts of expended

power to produce one ampere of extracted noble gas ions. This efficiency number is about a factor of 2 better than that achieved by early electric thrusters using mercury propellant; this is not meant to imply that a mercury based source is inherently less efficient.

5.1 eV/ion of an Ideal Thruster

Since the objective is to build ion sources having ever decreasing eV per extracted ion values it seems prudent to ask what minimum eV/ion value can be expected for an ideal inert gas thruster. An ideal thruster here is meant to be limited by physical processes rather than engineering constraints.

Figure 5.1 is a sketch of such an ideal thruster. A very strong axial magnetic field permeates a plasma column of length L which is terminated on either end by collection plates of area A_c. Both ions and electrons are well magnetized such that $\rho_e << \rho_i << \sqrt{A_c}$ where ρ_e and ρ_i is respectively the electron and ion cyclotron radius. If the ion transit time $\tau_i \simeq L/2v_{iz}$, where V_{iz} is the mean axial ion velocity, is much less than the time for ions to cross the magnetic field lines, by whatever process, then, of course, the radial plasma losses will be negligible and every ion produced will be collected by the termination plates.

The question of interest is how much energy is required to produce a plasma from which one ampere of ions can be collected. This energy will be the theoretical minimum in eV/ion that can be achieved in <u>any</u> electrostatic ion thruster. It is clear that an actual thruster of the type shown in figure 5.1 would have to be a single ended device in the sense that all ions in the plasma would be extracted by only one collection (or extraction) plate and that the minimum value in eV/ion we obtain would be be degraded by the grid transparency factor.

To obtain a value for the minimum eV/ion in the one dimensional flow geometry of figure 5.1, let us consider a partially ionized plasma with an electron density n_e, an electron temperature T_e and ions, of temperature T_i, which are close to thermal equilibrium with the neutral gas. Electron-ion pairs are created by ionizing collisions between electrons and neutral atoms of density n_o. The rate of production of singly ionized ions is given by

$$\left(\frac{\partial N}{\partial t}\right)_{prod.} = n_o n_e < \sigma v >_i V_{pp} \qquad (1)$$

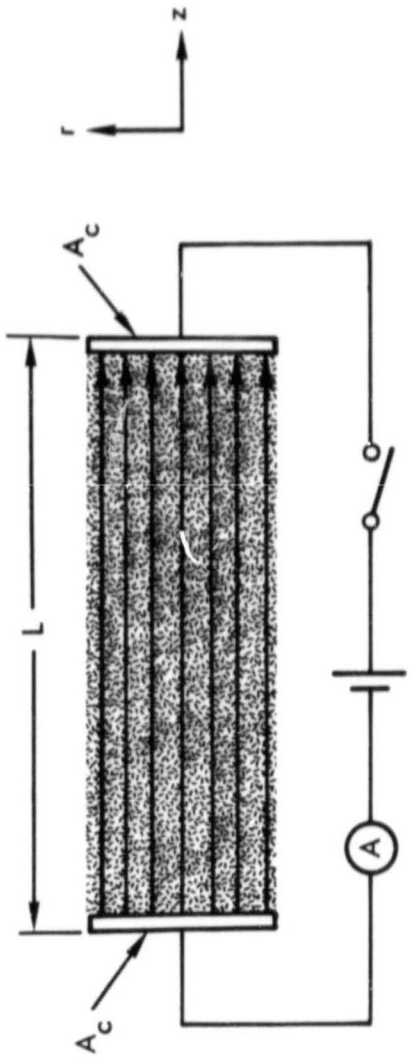

Figure 5.1 The Ideal Solenoidal B Field Source.

where $< \sigma v >_i$ is the rate coefficient for ionization by electron impact of a neutral atom averaged over the electron velocity distribution and V_{pp} is the plasma production volume. In steady state equilibrium this rate of production must equal the ionloss rate given by [2]

$$\left(\frac{\partial N}{\partial t}\right)_{loss} = .5 n_i C_s A_{iL} \qquad (2)$$

where $C_s \equiv (kT_e/M_i)^{1/2}$ and A_{iL} is the ion loss area. Here we have assumed that ion-neutral and ion-ion collisions are low enough so as to not influence the mean axial drift velocity determined by ambipolar flow and further that $T_e > T_i$ by at least a factor of ten. The loss rate given by Eq. (2) has been demonstrated experimentally, for example, in Reference 3. Equating expressions (1) and (2) yields a relationship between the electron temperature and the neutral gas pressure for a device of a given size. In this case $V_{pp}/A_{iL} = L/2$. We illustrate this relationship for L = 50. cm and L = 25 cm in figure 5.2; the rate coefficients[4] shown in figure 5.3 for a maxwellian velocity distribution have been used. Note the strong inverse dependence of T_e on n_o and the existence of a low pressure region below which no equilibrium is possible.

The input power P goes to the plasma in the form of electron thermal energy which in turn will be dissipated by ionization of neutral atoms, by excitation of ions and neutrals and by electron energy flow to the walls. That is, in steady state

$$P = \left[n_e n_o < \sigma v >_i \left(E_i + \frac{< \sigma v >_*}{< \sigma v >_i} E_*\right) + \frac{n_e}{\tau} (2kT_e + e\phi_p) \right] V_{pc} \qquad (3)$$

The first term on the right expresses the energy that goes into ionization, the second term that which goes into excitation and the last two terms represent the average energy dissipated by those electrons that cross the potential barrier between the plasma and the walls. V_{pc} is defined as the plasma containment volume (which may be different from the production volume V_{pp}), τ is the mean energy confinement time and ϕ_p is the plasma potential measured with respect to the electron loss surface. A derivation of the energy lost by electron flow to the walls may be found in Appendix A. The plasma potential for the one dimensional flow case under

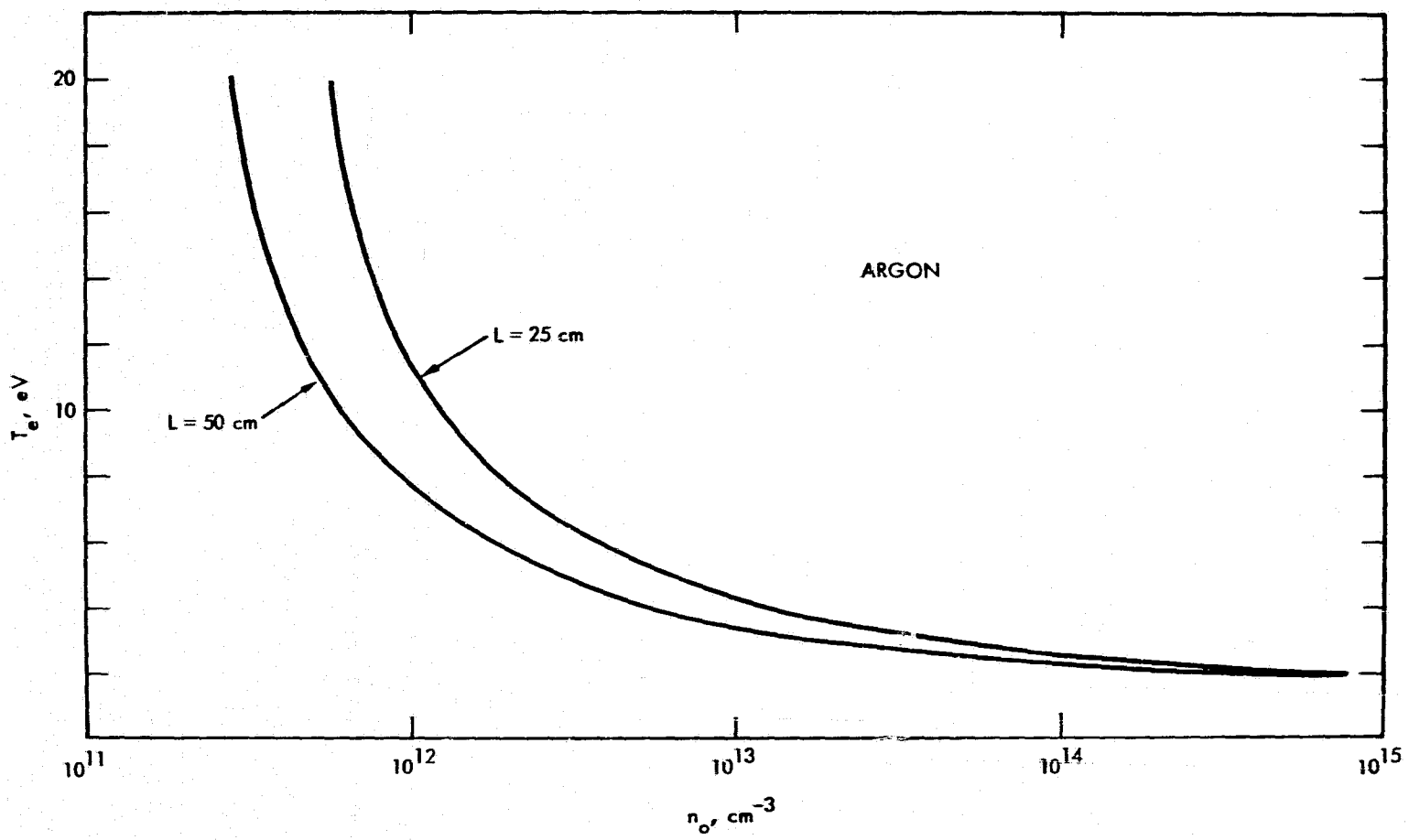

Figure 5.2 Predicted Electron Temperatures as a Function of Neutral Pressure for a Source of Effective Length L.

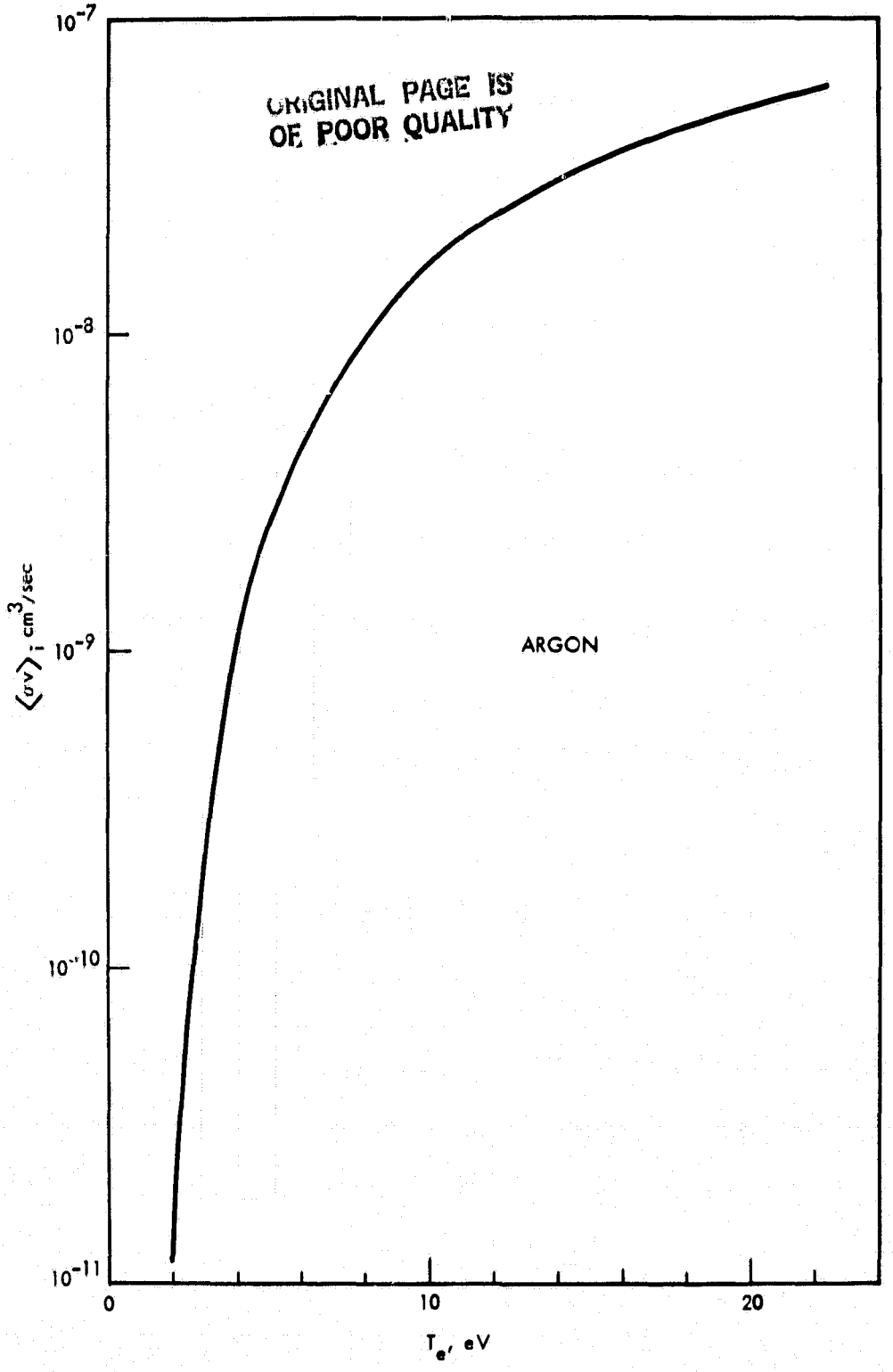

Figure 5.3 Ionization Rate Coefficients for a Maxwellian Electron Velocity Distribution.

consideration is determined from the balance of electron and ion currents to the walls and is given by

$$e\phi_p = kT_e \ln \left(\frac{A_{el}}{A_{il}} \sqrt{\frac{2m_i}{\pi m_e}} \right) \tag{4}$$

where A_{el} is the loss area for electrons and A_{il} is loss area for ions. The mean confinement time we estimate to be

$$\tau = \frac{2V_{pc}}{C_s A_{il}} \tag{5}$$

which is obtained by equating the ion loss rate $.5\, n_i C_s A_{il}$ to $n_i\, V_{pc}/\tau$. From equation (3) we note that the plasma density is directly proportional to the input power as long as the neutral density remains several times larger than the plasma density and the creation of doubly ionized ions can be neglected.

The eV/ion, obtained by dividing the input power P by the ion beam current extracted from an area A_{ib}, is thus given as

$$eV/ion = \frac{P}{.5 n_i C_s A_{ib}} = \frac{A_{iL}}{A_{ib}} \left\{ \frac{V_{pc}}{V_{pp}} \left[E_i + \frac{\langle \sigma v \rangle_*}{\langle \sigma v \rangle_i} E_* \right] + 2kT_e + kT_e \ln \left(\frac{A_{el}}{A_{il}} \sqrt{\frac{2m_i}{\pi m_e}} \right) \right\} \tag{6}$$

To obtain this expression, equations (1), (2), (4) and (5) have been substituted into expressions (3) where appropriate.

In the ideal thruster shown in figure 5.1 the ion loss and ion extraction areas are equal: $A_{il} = A_{ib}$. Furthermore, the plasma containment and plasma production volumes are equal ($V_{pc} = V_{pp}$) since the electron distribution function is assumed to be the same on all field line intercepting the termination plates. Thus, with the reasonable assumption that $T_e >> T_i$, equation (7) reduces to

$$eV/ion = E_i + \frac{\langle \sigma v \rangle_*}{\langle \sigma v \rangle_i} E_* + 2kT_e + kT_e \ln \left(\frac{A_{el}}{A_{il}} \sqrt{\frac{2m_i}{\pi m_e}} \right) \tag{7}$$

Now let us consider some representative values of eV/ion obtained from equation (7). For a monatomic gas it is a good approximation[5] to say that an equal amount of energy goes into excitation and ionization; for argon E_i = 15.7 eV. If we take the case with $A_{el} = A_{il}$, we consequently have the

$$eV/ion = 15.7 + 15.7 + 2T_e + 5.4T_e$$

where T_e is measured in electron volts. For very large ion sources or at high neutral pressures we can expect an electron temperature of about 2eV and a corresponding plasma potential of about 11 volts: The resulting eV/ion = 46. volts. Correcting this value by a grid transparency factor of 0.75 yields a minimum eV/ion = 62. volts for argon. However, with sources operating around the "knee" of the eV/ion versus mass utilization performance curve and where the effective length $L = 2\ V_{pp}/A_{iL}$ can be quite small a temperature of T_e = 5.eV increases the minimum eV/ion to 91. volts for the same grid transparency factor. (We mention that an eV/ion = 80. volts has actually been measured at TRW for an argon plasma in a device 2 meters in length similar to that shown in figure 5.1 employing a magnetic field of about 10. kG.)

Note that according to equation (7) the eV/ion is to some extent dependent upon the relative loss areas for ions (A_{iL}) and electrons (A_{el}). The reason for this is that as the electron loss area becomes smaller (with A_{il} remaining constant) the plasma potential decreases resulting in lower thermal losses of electrons penetrating the potential barrier at the termination sheath.

5.2 Historical Development of Electron Bombardment Thrusters

In order to achieve high electrical efficiency a thruster ion source must accomplish two things. The source must first confine the high energy electrons, either from a monoenergetic, from a maxwellian or from some other arbitrary velocity distribution, for a time sufficient to produce an electron-ion pair. Secondly, the source should confine ions for a time sufficient for them to be drawn from source as a useful beam before they are able to travel to the walls which confine the neutral atoms.

The development over the past two decades of electron bombardment ion sources has focused primarily on the confinement of fast monoenergetic ionizing electrons. Plasma ions appear not to be confined by either electrostatic or magnetic fields in these devices. Thus ions, once created, move in all directions toward the walls, encounter the sheath, are accelerated by the ambipolar field to a speed of order $\sqrt{kT_e/m_i}$ and finally hit the walls where they recombine to once again become neutral atoms.

The basic concept for the confinement of primary electrons in electron bombardment ion sources using electrostatic acceleration has not changed over the years. The early thruster was a simple cylinder over whose volume was imposed a mildly diverging magnetic field[6,7] as shown in Figure 5.4a[8] . A hot filament acting as a cathode produced the ionizing electrons while an anode (or anodes) collected an electron current sufficient to maintain charge neutrality. This concept is essentially that of a Penning[9] or Philips(PIG) discharge. The magnetic field serves two purposes. First, the field causes electrons to execute helical paths about the field lines thus increasing their probability of colliding with and ionizing a neutral atom. Second, by placing the anodes across from field lines directly accessible to these primary electrons and by biasing all other surfaces at or lower than the cathode potential these primaries must suffer collisions, again presumably with neutrals, in order to cross the field lines to reach the anode(s).

Later changes in magnetic field geometry such as the strongly divergent, or radial field or cusped shaped field thrusters shown, respectively, in Figure 5.4b-d, were done primarily to improve the beam profile (i.e. to improve the beam flatness parameter $\equiv \langle J \rangle / J_{max}$) and to increase the volume[10] accessible to injected primary electrons thus increasing the ion production efficiency which results in lowering the eV per beam ion. In all of these configurations the anodes were placed in regions not directly accessible to primary electrons; cross field diffusion of electrons, which may result in turbulence[11] and associated enhanced losses, was relied upon as the electron confinement mechanism. We note that when cusp-shaped magnetic fields, such as the multipole[12] or multi-cusp thruster shown in figure 5.4e , replace the divergent field geometry it should no longer be necessary to place the anodes in a cross field position since the cusp fields can in themselves confine[13,14] primary electrons very efficiently. The non-necessity of cross field anodes

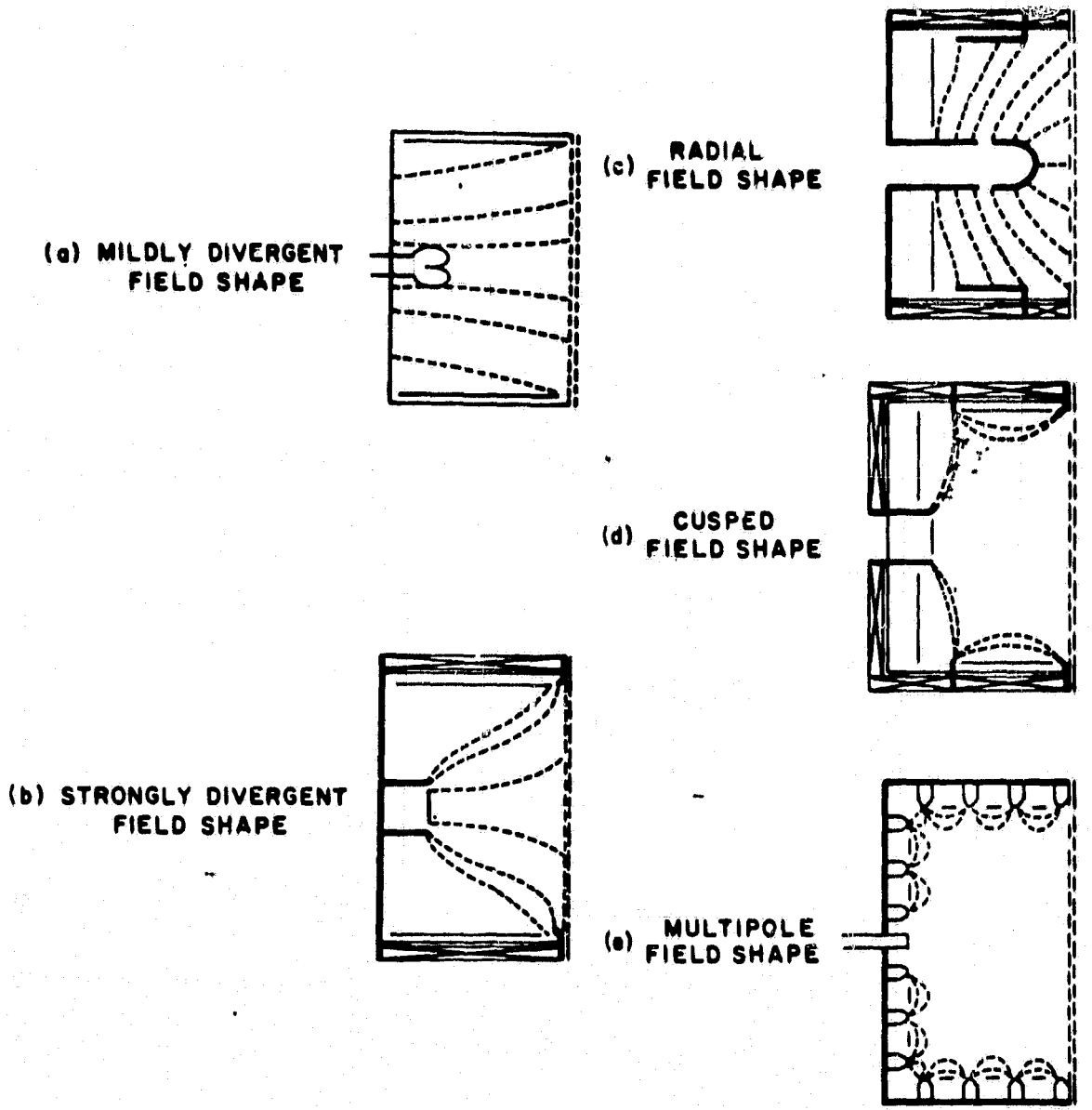

Figure 5.4 Evolution of the Magnetic Geometry for Electron Bombardment Thruster.

in multi-cusped geometries has been demonstrated experimentally by J. Sovey[3]. Sovey found essentially no difference in measured eV per extracted ion between the case with separate cross field anodes and the case where the separate anodes were eliminated and the entire thruster housing served as the anode. In the later case the magnet pole faces were at the anode potential. Since the plasma has direct contact with the pole faces of the magnets we see that cusps must confine primary electrons very well for otherwise the efficiency would have deteriorated.

As stated previously we believe that the eV per beam ion values being measured in the present day electron bombardment ion source, as well as the rf induction source discussed elsewhere in this report, indicate that ionizing electrons in these sources are well confined; well confined, again meaning that they have a high probability of ionizing a neutral before being lost from the system.

From the view of improvement of the source efficiency it is extremely important to be sure that the efficiency improvement of present day electron bombardment sources cannot be provided to a large degree by providing better ionizing-electron confinement but rather must result from increased ion confinement. Therefore, let us consider the simplified source model that allows us to reach this conclusion. We will assume that the production rate of electron-ion pairs in electron bombardment sources is principally due to primary electrons of speed $v_d = (2eV_d/m_e)^{1/2}$ injected into the device. V_d is the discharge voltage. As previously stated the production rate is given by

$$\left(\frac{\partial N}{\partial t}\right)_{prod} = n_o n_p \sigma_i v_p V_p \qquad (8)$$

where n_p is the primary electron density, σ_i the cross section for ionization and V_p the volume accessible to the primary electrons. If I_d is the discharge current, then

$$\frac{I_d}{e} = n_p V_p \sum_j \frac{1}{\tau_j} \qquad (9)$$

where τ_j is the mean time for primary electrons to be lost from the system by the j th process. We consider only two loss mechanisms and these only in their extremes. One extreme is when primaries are lost mostly to the walls (anodes) of the device. This occurs at low neutral gas pressures and/or in devices where there are no confinement magnetic fields. When the losses are principally to the walls

$$\frac{n_p V_p}{\tau_w} = \frac{1}{4} n_p v_p A_{pl} \tag{10}$$

where A_{pl} is the loss area of primaries. Substitution of (9) and (10) into (8) yields in this case

$$\left(\frac{\partial N}{\partial t}\right)_{prod} = 4 n_o \sigma_i \frac{I_d}{e} \frac{V_p}{A_{pl}} \tag{11}$$

In steady state the production rate given by (11) must equal the ion loss rate which we assume is of the form

$$\left(\frac{\partial N}{\partial t}\right)_{loss} = \gamma n_i C_s A_{il} \tag{12}$$

where γ is a numerical factor of order 0.5. Equating (11) and (12) gives

$$\gamma n_i C_s = 4 n_o \sigma_i \frac{I_d}{e} \frac{V_p}{A_{pl}} \frac{1}{A_{il}} \tag{13}$$

Thus, if A_{ib} is the area from which an ion beam is extracted and since $I_d V_d$ is the input power, the eV/ion is given by

$$eV/ion = \frac{I_d V_d}{\gamma_e n_i c_s A_{ib}} = \frac{V_d}{4} \frac{1}{n_o \sigma_i} \frac{A_{il}}{A_{ib}} \frac{A_{pl}}{V_p} \tag{14}$$

Note that in this case the beam efficiency increases with increasing neutral pressure but decreases linearly with effective primary electron anode area A_{pl}. Clearly in this operating regime equation (14) indicates that a hemispherically shaped[15] thruster which presumably has the smallest A_{il}/V_p ratio would be the most efficient geometrical shape.

It is interesting to consider values obtained from equation (14) for a cylindrical source of length L and radius R. Assume a beam is extracted from an area $A_b = \pi R^2$ and, further, that the anode area consists of the entire wall area. Then for V_d = 40. volts and operation at a neutral density of $n_o = 10^{13}$ cm^{-3} equation (15) reduces to

$$eV/ion = \frac{1.3\times10^4}{L(cm)} \left(1+\frac{L}{R}\right)^2 \text{ volts}$$

which for a 30. centimeter thruster of length equal to its radius (the optimum) yields a value of about 3500 eV/ion; rather inefficient!

Now we take the other extreme in which all injected primary electrons go to ionize the gas and none are lost to the walls. In this case the mean free path for ionization $\lambda_m < V_p/A_{pl}$. Thus, with $\lambda_m = 1/n_o\sigma_i$ and defining $V_p/A_{pl} \equiv \beta\,\lambda_m$, the production rate from equation (11) is

$$\left(\frac{dN}{dt}\right)_{prod} = \frac{1}{\lambda_m}\,\frac{I_d}{e}\,\beta\,\lambda_m \simeq \beta\,\frac{I_d}{e} \qquad (15)$$

where β is of order unity. Equating (15) to the loss rate given by (12) we obtain

$$eV/ion = \frac{I_d V_d}{\gamma n_i e C_s A_{ib}} = \frac{V_d}{\beta}\,\frac{A_{il}}{A_{ib}} \qquad (16)$$

Note that this result is substantially the same as equation (6) but with the discharge voltage V_d replacing the sum of ionization, excitation and convection loss energy given by the bracketed {} expression.

For a discharge voltage of 40. volts, typically necessary to maintain the discharge, and with a cylindrically shaped thruster of length equal to radius so $A_{iL}/A_{ib} \simeq 4,/t$ (where t is the grid transparency), expression (16) gives eV/ion $\simeq$ 160./(βt) volts. This value, which assumes that ion are lost to all chamber boundaries, is not inconsistent with presently measured values of eV/ion in the high pressure region past the "knee" of the eV/ion versus mass utilization curve. A correlation of the type indicated by expression (16) may be found in Reference 8.

5.3 DIFFICULTIES WITH A MICROWAVE BASED SOLENOIDAL-B FIELD THRUSTER

As originally proposed the solenoidal B-field concept was to incorporate the use of electromagnetic fields in the frequency range of several gigahertz as the source of power for plasma production. The reasoning behind this choice was that plasma production using microwaves in "mirror" field geometries such as shown in Figure 5.5a is very efficient. Indeed, the 80. eV per extracted ion value mentioned previously to have been measured in the geometry of figure 5.1 was obtained using microwaves as a source of power. The use of microwaves has some distinct systems advantages: a) the discharge is electrodeless b) the microwave source is durable, reliable and can operate at least 10,000 hours without maintenance c) the discharge generally can produce the required plasma density at lower neutral gas pressures thus improving mass efficiency and finally, d) this type of discharge may be an advantage for thrusters mounted on spacecrafts where microwave power is already available.

However, further evaluation of this concept with the use of microwaves showed that considerable obstacles must be overcome in order to make this a viable ion source worthy of an experimental effort. To clarify some of these obstacles let us consider that through some means we are able to produce a field shape resembling one-half of the mirror geometry sketched in figure 5.5b. In a microwave source the background gas is ionized by electrons heated on magnetic field surfaces where the applied microwave frequency ω_μ is equal to the local electron cyclotron frequency $\omega_{ce} = eB/m_e$. Microwaves can readily penetrate a plasma of density $n_e = m_e\omega_{pe}^2 / (4\pi e^2)$ usually only if $\omega_\mu > \omega_{pe}$; if $\omega_\mu < \omega_{pe}$ the waves decay

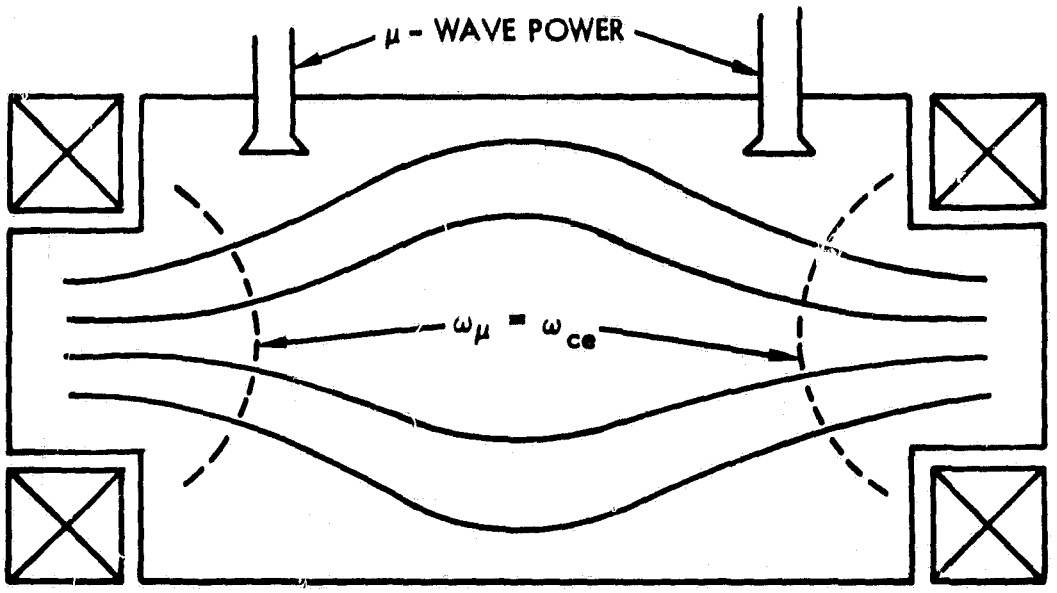

(a)

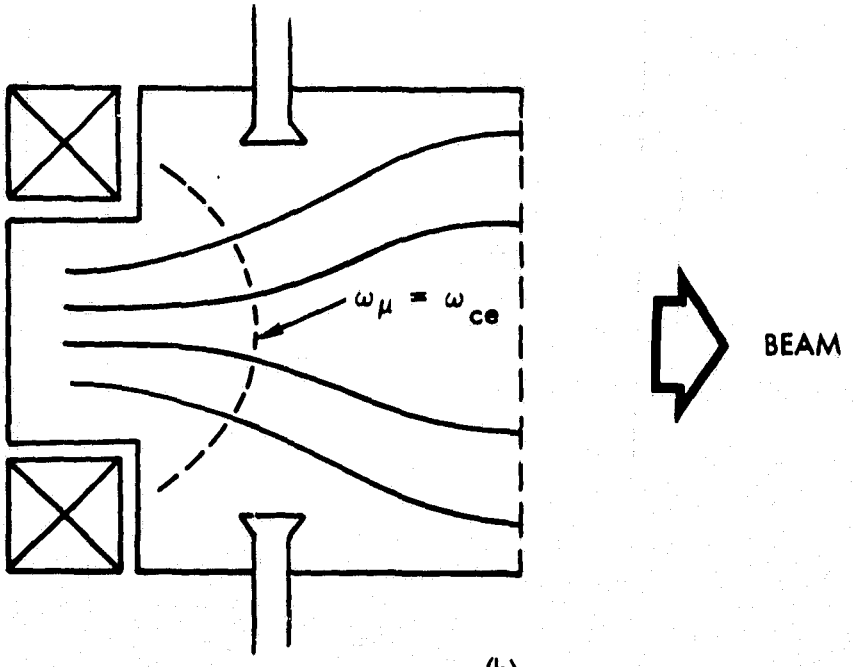

(b)

Figure 5.5 a) Basic Mirror Geometry with ECH Plasma Production.
b) One-Half of a Mirror for Propulsion Applications.

evanescently in the plasma and are reflected. If the plasma density for thruster thruster applications is to be of order $n_e \approx 5.10^{11}$ cm^{-3} this dictates that $f_\mu \approx \omega_\mu/2\pi \gtrsim 6.GHz$. Therefore a magnetic field of order $B \approx \omega_\mu m_e/e \approx 2.KG$ or higher is required for efficient conversion of microwave energy into electron thermal energy.

For a magnetic field configuration of the type shown in figure 5,5b it would be extremely difficult to have a resonance surface of the magnitude of 2,KG within the thruster housing and yet maintain a low level residual magnetic field, say of the order of 10. Gauss at the ion extraction plane. We assume here that a thruster of this type would still utilize electrostatic acceleration[16] and be of reasonable dimensions. Fields of several hundred Gauss at the extractor region would be unacceptable primarily for the following two reasons. First, a field of this magnitude would be likely to have deleterious effects on the ion optics, although we are not aware of any study that has been conducted on this problem. Second, a reasonably high magnetic field would result in the inability to neutralize the ion beam, therefore cause space charge blow up of the beam and reduce the thrust to negligible levels.

One method of overcoming the problem of too high a level of magnetic field at the extractor and yet maintain a resonance surface of order 2.KG within the thruster is to produce configurations where the magnetic field is highly divergent. That is, configurations where an appreciable field is maintained only in small regions of space and does not fill the entire thruster volume. The reader may convince himself that the production of such magnetic fields can only be accomplished through the use of permanent magnets or superconductors. Some results with the use of permanent magnets may be found in section 4 of this report.

Consequently, since we have ruled out the possibility of using strong volume magnet fields in which the ions of the plasma are well magnetized and possibly confined by these magnetic fields, we must look to another confinement mechanism. Nature provides us with only one other type of field which interacts with charged particles.

5.4 ELECTROSTATIC ION CONFINEMENT

Electrostatic containment of ions was credited as the reason for the early success of the MESC[17] ion source developed by Moore, et al., at Electro-Optical Systems. Indeed this cesium source provided a beam at a cost of 100 eV/ion, better than was expected from Moore's theoretical model at that time. Subsequent tests[15] of the MESC source with inert gases gave efficiencies of the order of 225. to 300. eV/ion and higher for a 12. cm thruster.

Aside from the fact that the MESC configuration has a considerable volume of low magnetic field whereas the PIG or divergent field configuration has most of its volume filled with more or less the same strength magnetic field, the basic electrical configuration is very similar. Figure 5.6a is a sketch of a PIG configuration labeled with representative voltages measured with respect to some common. Here the screen and chamber are biased at the cathode potential to electrostatically contain the primary ionizing electrons. These electrons must diffuse across the field to reach the anode which is biased negatively with respect to the plasma potential. Since the magnetic field is very weak ($\sim$ 50 Gauss) the plasma ion larmor radius will be of the order of the chamber dimensions and therefore ions will essentially not be magnetized. Ions are lost to the screen and beam and to the chamber wall in the cathode region. Since electrons must diffuse across the field lines to reach the anode, the ions must follow to preserve local charge neutrality. Kaufman[18] has postulated that turbulence sets in as a result of the necessary cross field diffusion which may lead to ion losses to the radial walls at the Bohm speed. In any case, the rather poor performance in terms of electrical efficiency of the PIG configuration indicates flow of ions to all chamber boundaries and perhaps, in addition, some loss of electrons with energy enough to ionize.

In the MESC configuration indicated in figure 5.6b the screen, chamber walls and magnet poles are all held at the cathode potential to prevent primary electron losses. Again electrons must diffuse across the field lines to reach the anodes which, under optimum conditions, were biased a few volts positive of the plasma potential. (A separate anode, well

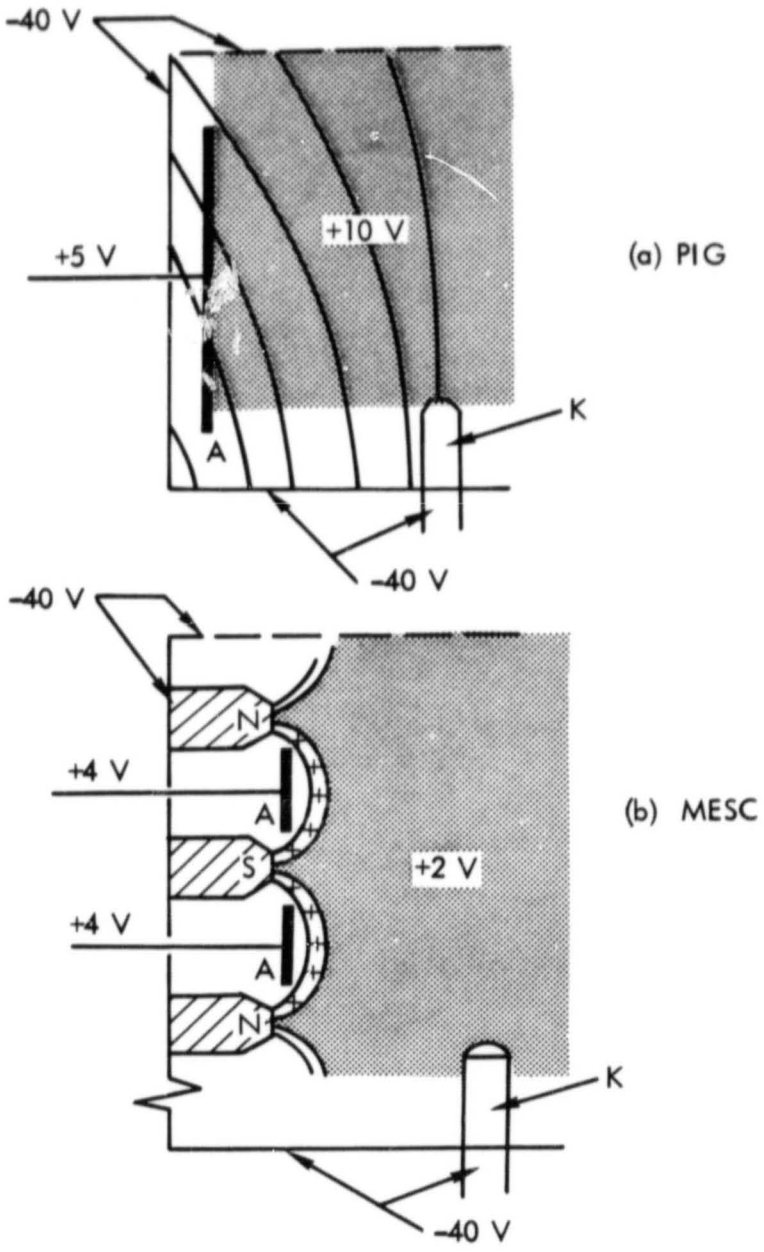

Figure 5.6 Electrode Arrangement and Rerresentation Potentials for a) P.I.G. and b) MESC Discharge.

immersed in the plasma was required to keep the plasma potential negative with respect to the magnet anodes. If this plasma anode was not present the discharge could either not be started or not be maintained.) Improved performance was attributed to electrostatic ion confinement. The field lines cutting the anodes were postulated[17] to be at or slightly positive to the anode potential thus forming a potential barrier for the ions. This presumably occurs because of the high electrical conductivity of the plasma along the field lines although it was not made clear what happens to these positively charged field lines when they intercept the magnet pole faces which are biased negative with respect to the plasma. In any case the ion loss area would be limited to the total magnet pole face area which amounted to about 10% of the total wall area. If this interpretation of electrostatic ion confinement is correct then one is puzzled by J. Sovey's results, mentioned previously, in which cross field anodes were eliminated and magnet pole faces served as anodes. Most investigators[21-23] of ion sources for intense neutral beams operate in this mode with the shell and magnets at the anode potential.

We mention that Moore[17], et al., performed a demonstration experiment whose purpose was to measure the cross field electron current density to the anodes and compare the measurements to a theoretical calculation which was based on classical coulomb collisions and which showed that $J_\perp \alpha 1/B^2$. His measurements gave a dependence of $J_\perp \alpha 1/B^{1.43}$ over a magnetic field variation of 60. to 6000. Gauss. Kaufman, on the other hand, has theorized[19] cross field diffusion to be Bohm like with $J_\perp \alpha 1/B$ but Isaacson and Kaufman[20] experimentally indicate that discharge losses become independent of B at pole face fields of order 50. to 100. Gauss. Such extreme variations in experimental results do not provide much help in understanding the processes occurring in these sources.

Recent attempts to improve the efficiency of electron bombardment sources by creating a negative plasma potential (with respect to the anodes) either by moving the anodes toward stronger magnetic fields or by reducing the anode area indicate little or no decrease in eV/ion. With a negative plasma potential the discharge becomes unstable, fluctuations may increase and performance may be degraded or the discharge may even extinguish.

5.5 A BASIC CONFINEMENT EXPERIMENT

It may be that configurations in which electrons are forced to cross magnetic field lines to maintain the discharge are not conducive to electrostatic ion confinement irrespective of whether or not the plasma potential is negative. In this section we describe a general concept for an rf produced plasma employing radial electrostatic confinement of ions, but not requiring strong cross field electron transport. Since the data base for evaluation of electrostatic confinement is not extensive, we suggest a series of experiments to elucidate the basic plasma transport properties of interest to the concept. The direction of evolution of the experiments parallels to some degree the evolution of present day electrostatic thrusters, from a simple solenoidal magnetic field geometry, which is most conducive to experimental and analytical investigation, to field geometries which are more suitable for thrusters, but more complicated.

The first series of experiments employs a uniform solenoidal magnetic field and is designed to examine the dependence of cross field ion transport on magnetic field and on the magnitude, direction, and spatial distribution of the radial dc (ambipolar) electric field. The configuration is shown schematically in figure 5.7, and can be seen to be identical to the ideal case considered earlier, except that we have removed the requirement $\rho_{ci} << R$ and have designed a great deal of flexibility into the termination plates. The electrons are heated by the electric fields of an rf induction coil, as in RFI Multicusp Thruster. Since most of the heating occurs within a few collisionless skin depths of the antenna wire, and electrons are well confined by the magnetic field, this configuration will produce a radial electron temperature gradient. The radial temperature profile can be controlled to some degree by antenna geometry.** Each conducting termination plate consists of a set of individually biasable concentric annuli, dividing the plasma into a set of nested cyclindrical tubes. The width of each annulus is at least

---

**It should be mentioned that this technique has been used by one of the authors (W. Divergilio) to create a plasma with a strong temperature gradient for basic plasma physics experiments.

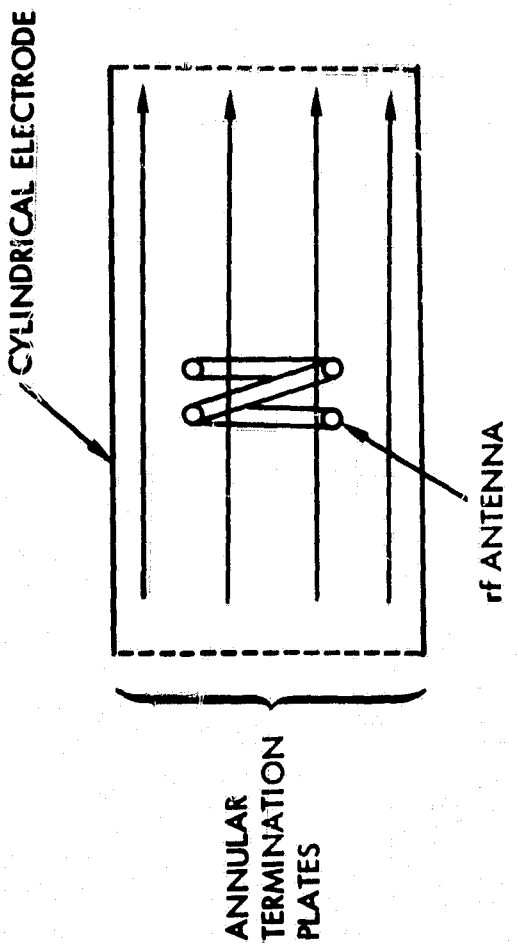

Figure 5.7 Arrangement of an Experiment to Study Confine Properties

several electron gyroradii, so that adjacent plasma tubes are only weakly connected by electron conduction. For a 30 cm diameter source, an annulus with of about 1.5 cm should suffice to meet this condition for magnetic fields as low as 10 Gauss. Under these conditions, and without electrical bias between each pair of termination plate annuli the potential of each plasma tube with respect to its termination annuli will be given by

$$\phi = \frac{kT_e}{e} \ln \left(\frac{A_{el}}{A_{il}} \sqrt{\frac{2m_i}{\pi m_e}} \right)$$

As a diagnostic of the ion end loss rate of each plasma tube a potential $V >> \phi_p$ may be applied between each pair of annuli in the manner of a double Langmuir probe. Of course, it will have to be determined experimentally if this bias effects plasma conditions. It is now possible to impress a radial electrical field on the plasma by applying a bias between adjacent termination annuli. The number of annuli has been kept large so that a significant total radial potential variation could be impressed on the plasma while keeping the potential difference between tubes small compared to kT_e/e. We have also included a cylindrical electrode so that boundary conditions similar to those of a P.I.G. discharge could be created by biasing this electrode very positive with respect to all annuli.

In this configuration, the relative rate of cross field and axial ion transport may be studied as a function of applied electric and magnetic fields, utilizing a combination of diagnostics including measurements of discharge efficiency, plate currents, and direct probing of the plasma. Of particular interest is the relative ion transport rate under conditions of no radial electric field. Under the low density conditions typical of thruster operation, ion heating through electron collisions is negligible, and the true ion temperature is close to the wall (or neutral gas) temperature. Ions, however, gain directed energy from any ambipolar fields that exist in the plasma. The Bohm criterion for a stable sheath, which we may apply at the termination plates, requires that ions enter the sheath with drift energy approximately equal to the electron temperature, implying the existence of an axial potential gradient. In the case of

no radial electric field, we expect the ratio of the total radial to total axial ion losses to be of order $v_i/c_s = \sqrt{T_i/T_e}$ for a system with equal length and radius. Taking a typical value of $T_e \simeq 5eV$, and ion temperature equal to the wall temperature, $T_i \simeq .05$ eV, gives $v_i/c_s \simeq .1$, so that radial ion losses may be negligible even without true electrostatic confinement. The condition of no radial electric field is a desirable one from the standpoint of minimizing turbulence and associated enhanced cross field transport.

The configuration of figure 5.7 is not particularly well suited to thruster applications, even if radial ion losses are negligible, as ions can only be extracted from one end of the source. In this configuration, we estimate the minimum discharge losses as approximately 180 watts per ampere of beam current. However, if this form of electrostatic confinement is successful, the magnetic field geometry may then be modified to reduce ion losses to the axial termination plate opposite the screen or extraction optics.

5.6 A MODIFIED SOLENOIDAL-B FIELD THRUSTER

Such a modified configuration is shown in figure 5.8. The magnetic field geometry is approximately that of one-half a mirror with a magnetic field strength of about 100. Gauss at a conductive termination plate of area A_T and a field value of about 30. Gauss at the thruster screen. The mirror ratio is therefore of order $R_m \equiv B_T/B_{screen} \simeq 3$ or may even be less. The field shape is such that the curvature vector points everywhere toward the plasma interior in order to prevent gross plasma instabilities. The discharge could be produced through gentle heating of electrons by the inductive E fields of an rf antenna placed in the low field strength region near the screen. Proper antenna position and size would limit plasma production to those field lines indicated in figure 5.8. Electron confinement in the axial direction along the field lines is provided at one end by an electrostatic potential which results from biasing the screen sufficiently negative with respect to the plasma and the other direction by mirroring action[24]. The mirror point depends upon the relative magnitudes of the electron velocity components $v_\perp$ and $v_{//}$, respectively perpendicular and parallel to the

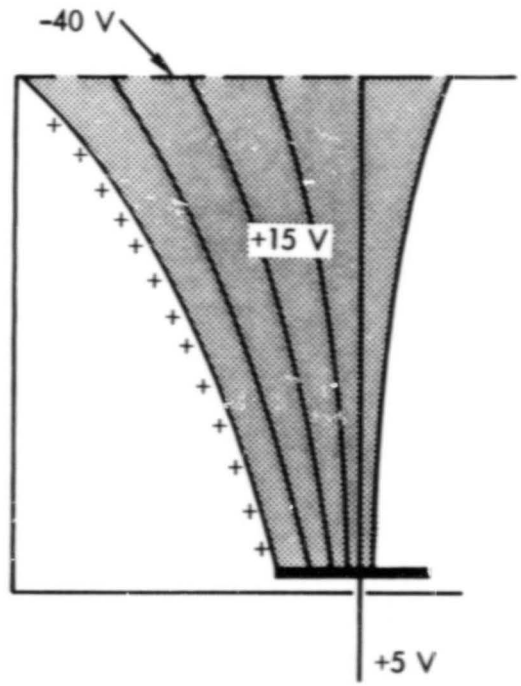

Figure 5.8 Modified Solenoidal B Field Configuration With Radial Electrostatic Ion Confinement. Only One-half of the Thruster is Shown.

field lines. Thus if the inductive field of the antenna is such to favor an increase in $v_{//}$, the mirror point for high energy electrons of the distribution will occur further away from the termination plate. Consequently electrons with sufficient energy to ionize will, with greater probability, create ions near the screen where ion extraction occurs. The electron adiabaticity, $\mu = 1/2\ mv_{\perp}^2 /B$, would be preserved upon reflection at the potential barrier. Electron losses occur principally in the axial direction by those electrons that are scattered into the loss cone and are collected by the biasable termination plate.

Although electrons are well magnetized by the magnetic fields in this device the ions will not be. Ions are lost to the beam, screen and termination plate. Radial ion confinement comes from the radial electric field that occurs as a result of electrons being tied to the magnetic field lines. Simplistically, when an ion moves in the radial direction past the last field line on which electrons reside, a radially inward space charge field will be created which causes the ions to return to the plasma. In essence, there is radial ion confinement from the positive potential barrier at the edge of the plasma as indicated by the + signs in figure 5.8.

Note that since an anode and cathode are not required in an rf discharge there is no need in this configuration to demand cross field electron transport.

The electrical efficiency of the configuration shown in figure 5.8 can be very attractive to the extent that radial ion confinement is present. Although ions free flow to the termination plate this loss is of negligible consequence. For example, with a 30. cm thruster we have a total beam plus screen area of about $A_b + A_s = 700.\ cm^2$ and with a 75% transparency screen a beam area of about 525 cm^2 . If the termination plate has a diameter of 10. cm, corresponding roughly to a mirror ratio of $R_m = 3$, then the eV per extracted ion would be

$$eV/ion = \frac{700 + 78}{525}\ \varepsilon = 1.5\ \varepsilon$$

where ε is energy cost to produce an ion. Without ion losses at the termination plate the eV/ion = 1.35 ε , about 10.% lower.

6. REFERENCES

SECTION 2

1. W. D. Ramsey, J. Spacecraft Rockets 9, 318 (1972).

2. R. Limpaecher and K. Mackenzie, Rev Sci Instr 44, 726 (1973).

3. W. L. Stirling, P. N. Ryan, C. C. Tsai and K. N. Leung, "Magnetic Multipole Line-Cusp Plasma Generator for Neutral Beam Injectors", Rev Sci Instr 50, 102 (1979).

4. W. Hittorf, Ann Physik 21, 137 (1884).

5. G. Francis, "Ionization Phenomena in Gases", Academic, New York (1960).

6. R. J. Sovie and G. R. Seikel, "Radio-Frequency Induction Heating of Low-Pressure Plasmas", NASA Technical Note NASA TND-4206 (1967)

7. H. W. Loeb, "Recent Work on Radio Frequency Ion Thrusters", AIAA Paper No. 70-1102 (1970).

8. T. K. Samec, "Plasma Confinement by Surface Magnetic Fields", UCLA Plasma Physics Group Report PPG-281, (November 1976).

9. H. Goede, "Experimental Investigation of the Anomalous Skin Effect", UCLA Plasma Physics Group Report PPG-487, (April 1980).

10. M. Abramowitz and I. A. Stegun (eds.), "Handbook of Mathematical Functions", (9th printing, Dover Publications, New York).

11. R. A. Dandl, A. C. England, W. B. Ard, H. O. Eason, M. C. Becker, and G. M. Haas, Nuclear Fusion 4, 344 (1964).

12. J. C. Sprott, "Electron Cyclotron Heating in Toroidal Octupoles", Phys Fl 14, 1975 (1971).

13. D. B. Miller and E. F. Gibbons, "Cyclotron Resonance Propulsion System", NASA Contractor Rept., Vol. CR-42336, 1963.

14. B. H. Quon, W. F. DiVergilio and N. H. Lazar, "A Large Volume Plasma Source Produced by Electron Cylcotron Heating", Bull Am Phys Soc Vol. 24, No. 8, October 1979.

15. D. B. Batchelor and R. C. Goldfinger, Oak Ridge National Laboratory Technical Report, ORNL/TM-6992, 1979.

SECTION 3

1. T. D. Masek, "Plasma Properties and Performance of Mercury Ion Thruster", AIAA Paper No. 69-256, 1969.

2. See Section 2 Reference No. 8.

SECTION 5

1. V. K. Rawlin, "Sensitivity of 30cm Mercury Bombardment Ion Thruster Characteristics to Accelerator Grid Design", AIAA Paper 78-668, April 1978.

2. F. F. Chen, Plasma Diagnostic Techniques, R. F. Huddlestone and S. L. Leonard eds., Academic Press, p. 150, (1965).

3. J. S. Sovey, "Performance of a Magnetic Multipole Line-Cusp Argon Ion Thruster", AIAA International Electric Propulsion Conference, April 1981, Paper AIAA-81-0745.

4. W. Lotz, Max Plank Institut für Plasmaphysik, Report No. IPP-1/62, 1967 or H. R. Kaufman, "Inert Gas Thruster", NASA CR-135226.

5. E. Hinnov, A. S. Bishop and F. W. Hoffmann, Princeton University Plasma Physics Report No. MATT-270, (1964).

6. H. R. Kaufman and P. D. Reader, "Experimental Performance of Ion Rockets Employing Electron-Bombardment Ion Sources", American Rocket Society Paper 1374-60, November 1960.

7. H. R. Kaufman, "An Ion Rocket With an Electron-Bombardment Ion Source", NASA TN D-585, January 1961.

8. These figures are reproduced from G. C. Isaacson, NASA CR-135101 June 1977.

9. F. M. Penning, Physica, 4; 71 (1937). R. E. B. Makinson and P. B. Treacy, J. Sci Instr 25, 298 (1948).

10. H. R. Kaufman, "Technology of Electron-Bombardment Ion Thrusters", Advances in Electronics and Electron Physics, Vol 36, p 273 (1974).

11. H. R. Kaufman, "Electron Diffusion in a Turbulent Plasma", NASA TN D-1324.

12. R. D. Moore, "Magneto-Electrostatically Contained Plasma Ion Thruster", AIAA Paper 69-260, March 1969 and W. D. Ramsey, "12-cm Magneto-Electrostatic Containment Mercury Ion Thruster Development", Journal of Spacecraft and Rockets, Vol 9, No. 5, 318-321, May 1972.

13. T. Samec and R. Stenzel, Bull. Am. Phys. Soc. 7, 1017 (1972).

14. K. N. Leung, T. K. Samec and A. Lamm, Phys. Lett. 51A, 490 (1975).

15. W. Ramsey, "Inert Gas Ion Thruster Program", Interim Report No. 1 for NASA Lewis, Xerox Electro-Optical Systems, March 1980.

16. Research has been conducted on electrode-less acceleration utilizing microwave power. See for example: D. B. Miller, G. W. Bethke and G. F. Crimi, "Investigation of Plasma Accelerator (Cyclotron Resonance Propulsion System)", NASA CR-54746. These test, though interesting, had results of low gas utilization, low conversion efficiency (~30%) and problems with the microwave window lifetime.

17. R. D. Moore, R. Vernon, S. Goldner, R. C. Speiser, "Cesium Electron Bombardment Thruster Research", Electro-Optical Systems Report 7240-Final, October 1968; also, R. D. Moore, "Magnetic-Electrostatically Contained Plasma Ion Thruster", AIAA Paper 69-260, March 1969.

18. H. R. Kaufman and R. S. Robinson, "Plasma Processes in Inert Gas Thruster", AIAA International Electric Propulsion Conference, October 1979, Paper AIAA-79-2055.

19. H. R. Kaufman, "Plasma Processes in Inert-Gas Thrusters", J. Spacecraft 18, 470, Sept-Oct 1981.

20. G. C. Isaacson and H. R. Kaufman, "15-cm Multipole Gas Ion Thruster", J. Spacecraft 14, 469, August 1977.

21. A. T. Forrester, D. M. Goebel and J. T. Crow, "A Hollow-Cathode Multipole Boundary Ion Source", Applied Physics Letters, Vol 33, No. 1, July 1978, p. 11-13.

22. W. L. Stirling, P. N. Ryan, C. C. Tsai and K. N. Leung, "Magnetic Multipole Line-Cusp Plasma Generator for Neutral Beam Injectors", Rev. Sci. Instr. 50, Jan 1979.

23. K. W. Ehlers and K. N. Leung, "Characteristics of the Berkeley Multi-Cusp Ion Source", Rev. Sci. Instr., 50, Nov. 1979, p. 1353-1361

24. D. E. Baldwin, "End-Loss Processes from Mirror Machines", Rev. Mod. Phys, 49, 1977.

APPENDIX A

ELECTRON CONVECTIVE ENERGY LOSS

Here we derive an expression for the average energy lost from a plasma as a consequence of electrons penetrating the sheath potential barrier that exists between a plasma and a wall with which the plasma has direct contact. The energy value obtained here is used in the section entitled Solenoidal B-field Concept. The analysis is valid for a magnetic field-free plasma or for a one-dimensional plasma confined by straight field lines where no cross-field or adiabatic effects need be considered. In addition we derive the expression for the potential of the plasma with respect to this wall.

Consider a plasma uniform everywhere except in the sheath region shown in the sketch below.

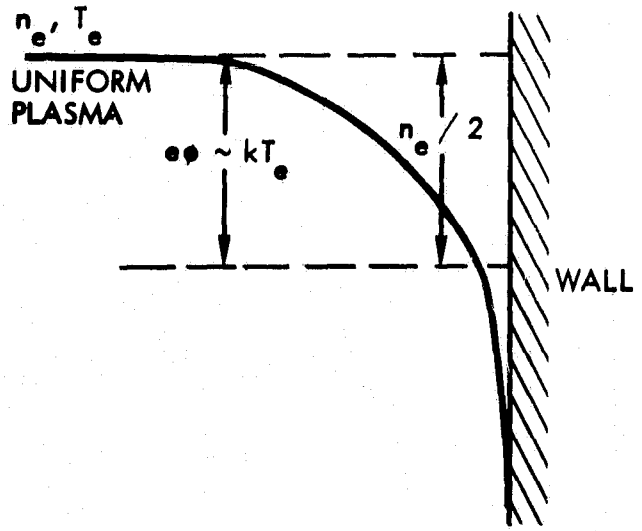

Figure A Plasma Sheath

The uniform region is characterized by a plasma density $n_e \simeq n_i$ and electron distribution function $f(\bar{r},\bar{v}) = n(\bar{r})\hat{f}(\bar{r},\bar{v})$ such that

$$n(\bar{r}) = \int_{-\infty}^{\infty} f(\bar{r},\bar{v})d\bar{v} \quad \text{and} \quad \int_{-\infty}^{\infty} \hat{f}(\bar{r},\bar{v})d\bar{v} = 1 \tag{A1}$$

We take the electrons to be Maxwellian so

$$f(\bar{v}) = \frac{1}{(\sqrt{\pi}u)^3} e^{-(v_x^2+v_y^2+v_z^2)/u^2} \tag{A2}$$

where $u^2 \equiv 2kT_e/m_e$.

The energy dissipation caused by electrons penetrating this sheath is given $\varepsilon = P/\Gamma$ where P is the flux of energy to the wall and Γ is the flux of electrons to the wall. The power per unit area is given by

$$P = \int (\frac{m}{2} v^2) v_z f(\bar{r},\bar{v}) d\bar{v}$$

or

$$P = \frac{m}{2} n(\bar{r}) \int_{-\infty}^{\infty} dv_x \int_{-\infty}^{\infty} dv_y \int_{v_m}^{\infty} dv_z \quad (v_x^2+v_y^2+v_z^2) v_z \frac{1}{(\sqrt{\pi}u)^3} e^{-(v_x^2+v_y^2+v_z^2)/u^2} \tag{A3}$$

where $v_m = (2e\phi/m_e)^{1/2}$ is the minimum electron velocity that can penetrate the potential barrier of height ϕ. Carrying out the integration in equation (A3) yields

$$P = \frac{n(\bar{r})}{2\sqrt{\pi}} \sqrt{\frac{2kT_e}{m_e}} \; [2kT_e+e\phi] e^{-e\phi/kT} \tag{A4}$$

The electron flux to the wall is given by

$$\Gamma = \int v_z f(\bar{r},\bar{v}) d\bar{v}$$

or

$$\Gamma = n(\bar{r}) \int_{-\infty}^{\infty} dv_x \int_{-\infty}^{\infty} dv_y \int_{v_m}^{\infty} dv_z \quad v_z \quad \frac{1}{(\sqrt{\pi}u)^3} e^{-(v_x^2+v_y^2+v_z^2)/u^2} \tag{A5}$$

which after integration results in

$$\Gamma = \frac{n(\bar{r})}{2\sqrt{\pi}} \sqrt{\frac{2kT_e}{m_e}} \; e^{-e\phi/kT_e} \tag{A6}$$

Dividing equation (A4) by (A6) gives the desired result

$$\varepsilon = 2kT_e + e\phi \tag{A7}$$

The plasma potential ϕ is determined from the condition that electron and ion currents exiting the plasma must be of equal magnitude in order to preserve charge neutrality. For a free streaming plasma with no "primary" electron injection the electron current to the walls is given by

$$I_e = n_e \, e \sqrt{\frac{kT_e}{2\pi m_e}} \; e^{-e\phi/kT_e} \; A_{el} \tag{A8}$$

where A_{el} is the area over which electrons are lost to the walls. The ion current is taken to be

$$I_i = .5 n_i e \sqrt{\frac{kT_e}{m_i}} \; A_{il} \tag{A9}$$

where A_{il} is the area over which ions are lost to the walls. From equations (A8) and (A9) we obtain a plasma potential which is positive with respect to the wall and given by

$$\phi = \frac{kT_e}{e} \ln \left(\frac{A_{el}}{A_{il}} \sqrt{\frac{2m_i}{\pi m_e}} \right) \tag{10}$$

Attachment A

This is an Interim Report as designated in Exhibit A-2, Paragraph F, of contract NAS3-22473, Amendment 5. The title page, i, block 13 should specify Type of Report as "Interim".

Specific

Page Number		
2-2		Rewrite equation (2-2) $\vec{V} = -\frac{e\vec{E}}{m(\nu - i\omega)}$
2-3		Equation (2.9) should have an equal sign, P_d=etc. and P_E in the previous line should be P_d
2-7		Page 2-7 is missing
3-7	1	There is a shift of verb tense. Apparatus used should be in past tense
3-7	2	The last two sentences in this paragraph will be more clear if recast as follows: "For such a case the gas was supplied continuously or was pulsed from the ballast. The flowrate through the orifice was thus proportional to the pressure in the ballast which was large enough to maintain a nearly constant flow for several --- etc."
		Note: Other minor corrections as indicated on pages 3-10, 3-12, 4-7, 4-16, 4-18a, 4-22, 5-1, 5-7, 5-12, 5-14, 5-16, 5-17
5-1		Rephrase sentences as indicated for conciseness
5-2		The following pages are largely analytical and many equations used. Please make sure all symbols are defined, and preferably include a symbol list applicable to this section only.